



Durham E-Theses

Traces of Extra Dimensions in Cosmology

O'CALLAGHAN, EIMEAR,EILEEN

How to cite:

O'CALLAGHAN, EIMEAR,EILEEN (2010) *Traces of Extra Dimensions in Cosmology*, Durham theses, Durham University. Available at Durham E-Theses Online: <http://etheses.dur.ac.uk/566/>

Use policy

The full-text may be used and/or reproduced, and given to third parties in any format or medium, without prior permission or charge, for personal research or study, educational, or not-for-profit purposes provided that:

- a full bibliographic reference is made to the original source
- a [link](#) is made to the metadata record in Durham E-Theses
- the full-text is not changed in any way

The full-text must not be sold in any format or medium without the formal permission of the copyright holders.

Please consult the [full Durham E-Theses policy](#) for further details.

Traces of Extra Dimensions in Cosmology

Eimear O'Callaghan

A thesis submitted for the degree of
Doctor of Philosophy



Institute for Particle Physics Phenomenology
Department of Physics
Durham University
September 2010

Traces of Extra Dimensions in Cosmology

Eimear O'Callaghan

Submitted for the degree of Doctor of Philosophy

September 2010

Abstract

In this thesis, we discuss the observational consequences of extra dimensions on cosmological phenomena. We begin with an overview of extra dimensions, from the initial ideas of Kaluza and Klein to the more recent concept of braneworld models and in particular review the cosmological aspects of the DGP braneworld model, which can produce late time acceleration. We then go on to consider the asymmetric brane model, comparing its cosmology to the standard concordance and DGP models and showing how the asymmetric model can be considered a one-parameter extension of the DGP model over a range of relevant physical scales. Using type Ia supernovae data and the cosmic microwave background shift parameter, the effect of this new parameter on the expansion history of the universe is considered. We then turn our attention to cosmic string loops, which emit bursts of gravitational radiation, produced by cusps and kinks on the loops. We investigate the kinematic effect extra dimensions will have on these gravitational wave bursts and find that the effects of the additional dimensions are more pronounced for cusps than for kinks: cusps are rounded off and their probability of formation is reduced, however, the probability of kink formation is unchanged. Finally, we recompute the gravitational wave bursts taking the various factors into account and look at the implications of this recalculation for the LIGO and LISA gravitational wave detectors, find that both signals, and in particular the cusp signal, have a potentially significant damping, and consider the implications for the detection of extra dimensions.

Declaration

This dissertation is based on research carried out at the Institute for Particle Physics Phenomenology, Department of Physics, Durham University, UK. No part of this thesis has been submitted for another qualification to this or any other university and is my own work, unless referenced to the contrary in the text. Chapter 3 is based on original work done in collaboration with my supervisor Ruth Gregory and Alkistis Pourtsidou, [1]. Chapter 4 is a review chapter, while chapter 5 is based on original work done in collaboration with Ruth Gregory, Sarah Chadburn, Ghazal Geshnizjani and Ivonne Zavala, [2, 3], where I made a substantial contribution to the work from section 5.2.2 onwards. In particular I performed the calculation of the gravitational wave amplitude and created all the corresponding plots. Chapter 6 is original work done in collaboration with Ruth Gregory.

Eimear O'Callaghan

Copyright © 2010 by Eimear O'Callaghan.

The copyright of this thesis rests with the author. No quotation from it should be published without the prior written consent and information derived from it should be acknowledged.

Acknowledgements

First of all I would like to thank my supervisor, Ruth Gregory. Thanks for all your help over the years, even if I never did come knocking on your door!

Thanks also go my office mates in OC118, in particular to Aoife, Dave and Tracey for all the random conversations and answering silly LaTeX and Mathematica questions. Thanks also to the rest of the lunch crew - Alison, Jamie, Ciaran, Josie, Andrew, Katy and James. The Ph.D. wouldn't have been the same without you - and how can I mention lunch without mentioning Dave's amazing chocolate brownies! And to Peter and Sam - I'm going to miss our get-togethers!

I gratefully acknowledge the receipt of a Marie Curie EST fellowship and many thanks to Carlton Baugh and Mike Pennington for their help in that regard.

Last but not least, I want to thank my family: my sister, Béibhinn and my grandparents for their regular correspondance and keeping me up to date with all the gossip from home and my cousin Lorna, for providing a mini-break from thesis writing. Finally, to my parents, for all your love and support in whatever I do throughout my life: thank you.

Contents

List of figures	vii
1 Introduction	1
1.1 Kaluza Klein compactification	2
1.2 Large extra dimensions	4
1.3 The Randall Sundrum model	6
1.3.1 RS I	6
1.3.2 RS II	8
1.4 Thesis outline	9
2 The DGP model	11
2.1 Introduction	11
2.2 DGP cosmology	12
2.2.1 Model setup	12
2.2.2 Model regimes	16
2.3 Observational tests of the DGP model	18
2.4 Problems with the DGP model	20
2.5 Conclusions	22
3 The cosmology of asymmetric brane modified gravity	23
3.1 Introduction	23
3.2 Asymmetric braneworld models	24
3.3 Asymmetric cosmology	33
3.4 Conclusions	43
4 Cosmic strings and gravitational wave bursts	44
4.1 Introduction	44
4.2 String motion and cusps	49
4.3 Gravitational waves from cusps	51

5	Gravitational wave bursts from cosmic string cusps in extra dimensions	56
5.1	Introduction	56
5.2	Wave form in extra dimensions	58
5.2.1	String kinematics with extra dimensions	58
5.2.2	The gravitational waveform	60
5.3	Discussion	65
6	Gravitational wave bursts from kinks in extra dimensions	73
6.1	Introduction	73
6.2	Kinks in 3D	74
6.3	Kinks in higher dimensions	78
6.4	Discussion	82
7	Conclusions	86
A	The Damour-Vilenkin interpolating functions	89
	Bibliography	94

List of figures

3.1	The asymmetric warp factor	27
3.2	Variation of the asymmetric effective dark energy equation of state	36
3.3	Plot of magnitude vs. redshift for various models	37
3.4	Parameter space plots from supernova data	39
3.5	Parameter space plots from the shift parameter	41
3.6	Combined parameter space plots	42
5.1	Near cusp event	59
5.2	Amplitudes of gravitational wave bursts from cusp (LIGO)	63
5.3	Amplitudes of gravitational wave bursts from cusp (LISA)	64
5.4	Rates of gravitational wave bursts from cusp (LIGO)	65
5.5	Rates of gravitational wave bursts from cusp (LISA)	66
5.6	Rates of gravitational wave bursts from cusps varying Δ_0	69
5.7	Rates of gravitational wave bursts from cusp varying n	70
5.8	Rate of gravitational wave bursts from cusp varying Δ_0	71
5.9	Gravitational wave bursts from cusp varying n	71
6.1	Amplitudes of gravitational wave bursts from kink (LIGO)	80
6.2	Amplitudes of gravitational wave bursts from kink (LISA)	80
6.3	Rates of gravitational wave bursts from kink (LIGO)	81

6.4	Rates of gravitational wave bursts from kink (LISA)	82
6.5	Kink gravitational wave burst (LIGO)	83
6.6	Kink gravitational wave burst (LISA)	83
6.7	Kink and cusp gravitational wave burst: comparison (LIGO and LISA) .	84

Conventions

Greek indices running over $\mu = 0, 1, 2, 3$ are used to denote 4 dimensional (4D) coordinates, while early Latin indices which run over $a = 0, 1, 2, 3, 4, \dots$ denote higher dimensional coordinates; later Latin indices, $i, j = 1, 2, 3$ are used to denote 3D spatial coordinates.

- Metric signature: $(-, +, \dots, +)$
- Planck mass: $m_{pl}^2 = (8\pi G)^{-1}$
- Riemann tensor: $R_{bcd}^a = \partial_c \Gamma_{db}^a - \partial_d \Gamma_{cb}^a + \Gamma_{ce}^a \Gamma_{db}^e - \Gamma_{de}^a \Gamma_{cb}^e$

“There is a theory which states that if ever anybody discovers exactly what the Universe is for and why it is here, it will instantly disappear and be replaced by something even more bizarre and inexplicable.

There is another theory which states that this has already happenend. ”

— Douglas Adams

The Restaurant at the End of the Universe

Chapter 1

Introduction

At the present point in time, the universe is extremely well described by the concordance model of cosmology, the Λ CDM model, which accounts for most of the increasingly precise cosmological measurements being made today, for instance the cosmic microwave background (CMB), [4, 5], type Ia supernovae (SneIa), [6, 7, 8, 9, 10, 11], and large scale structure surveys (LSS), [12, 13]. However, $\sim 72\%$, [4], of the contents of the universe are unaccounted for in the Λ CDM model. This contribution to the overall energy density is commonly thought to be some negative pressure fluid or ‘dark energy’ necessitated by the present observed accelerated expansion of the universe, [6, 7, 8]. Furthermore we find that $\sim 24\%$ of the remaining (matter) content is not the usual baryonic matter which makes up everything we see around us, but is instead unknown (and invisible) ‘dark matter’. While there are plenty of dark matter candidates, the lightest supersymmetric particle (LSP), axions, or sterile neutrinos, [14], to name but a few, there is still little consensus on its exact form. However, with the prospect of advances being made by the LHC in constraining supersymmetry and other beyond the standard model (BSM) theories, along with present direct detection experiments such as DAMA, [15], CDMS, [16], XENON, [17] and COGENT, [18] and the results from the bullet cluster, [19], it is hoped that dark matter will become more tightly constrained in the near future.

More poorly understood, however, is the remaining $\sim 72\%$ made up of dark energy. The concordance model of cosmology takes it to be vacuum energy in the form of a small positive cosmological constant, Λ , but a difference of ~ 120 orders of magnitude is found to exist between observations and the theoretical expectation. In consequence, many alternative theories have been developed in order to explain the phenomena observed in our universe, despite the obvious success of the Λ CDM model in describing the experimental data. These alternative models can be split into distinct groups: those that

modify the matter content of the universe (e.g. quintessence, [20]), those that modify its geometry, such as $f(R)$ theories, [21, 22, 23], MOND, [24, 25], and extra dimensional models of gravity (e.g. braneworld models) and finally models that take a purely phenomenological approach, such as the Cardassian, [26], and Hobbitt, [27], models which modify the Friedmann equation of motion for the universe.

The notion that extra dimensions exist in our universe and could have an effect on what we see around us, is not a new idea in physics: Kaluza first advocated the existence of a fifth dimension in order to unify the gravitational and electromagnetic forces in 1921. The idea has gained more widespread popularity in recent years with the advent of string theory, [28], where the one dimensional strings, which replace point particles as the most elementary ‘building blocks’, are found to live naturally in 10 dimensions. However, the world we observe around us seems only to have 3 spatial dimensions and we must therefore find some way to hide any extra dimensions in a theory. One of the most common ways of doing this is via the mechanism of compactification, which compactifies the extra dimensions on very small (and hence unobservable) scales, as suggested originally by Klein, [29]. More recently, another method of hiding extra dimensions has been suggested, through confinement. These models, known as braneworld models, assume that our four dimensional (4D) universe is confined on a sheet or ‘brane’ embedded in a higher dimensional bulk spacetime, allowing much larger, or indeed infinite extra dimensions to exist.

1.1 Kaluza Klein compactification

Kaluza, [30], considered the vacuum Einstein equations in 5 dimensions in order to obtain the 4D gravity and electromagnetism equations, in such a way that 4D matter could be considered a manifestation of a pure higher dimensional geometry. The 5D vacuum Einstein equations can be obtained from a 5D version of the usual Einstein-Hilbert action:

$$S = -\frac{1}{16\pi G^{(5)}} \int \sqrt{-g^{(5)}} R^{(5)} d^4x dy , \quad (1.1)$$

where $x^a = (x^\mu, y)$, $R^{(5)}$ and $g_{\mu\nu}^{(5)}$ are the 5D Ricci scalar and metric and $G^{(5)}$ is the 5D analogue of Newton’s gravitational constant, while the 5D metric can be written in the

form, [31]:

$$g_{ab}^{(5)} = \phi^{-1/3} \begin{pmatrix} g_{\alpha\beta} + \kappa^2 \phi A_\alpha A_\beta & \kappa \phi A_\alpha \\ \kappa \phi A_\beta & \phi \end{pmatrix}. \quad (1.2)$$

Using this metric in the action (1.1) along with the condition that all derivatives with respect to the fifth coordinate, y , vanish, (this is known as Kaluza's cylinder condition, which removed the need to account for the lack of an observed extra dimension), the action becomes

$$S = - \int d^4x \sqrt{-g} \left(\frac{R}{16\pi G} + \frac{1}{4} \phi F_{\alpha\beta} F^{\alpha\beta} + \frac{1}{6\kappa^2 \phi^2} \partial_\alpha \phi \partial^\alpha \phi \right), \quad (1.3)$$

which yields 4D gravity and electromagnetism along with a scalar field ϕ , where $F_{\alpha\beta} = \partial_\alpha A_\beta - \partial_\beta A_\alpha$, $\kappa \equiv 4\sqrt{\pi G}$ and $G \equiv G^{(5)}/\int dy$ is the 4D gravitational constant.

However, assuming the cylinder condition in order to get rid of derivatives with respect to y is an unsatisfactory method of dealing with the extra dimension. In 1926, Klein, [29], conceived of a mechanism which would hide the extra dimension in a realistic manner, while still retaining the remarkable results Kaluza had achieved. He considered the extra dimension to have a circular (S^1) topology so that any quantity $f(x^\mu, y) = f(x^\mu, y + 2\pi r)$, where r was the radius of the circle (i.e. the 'size' of the extra dimension). This periodic dependence on the extra dimension meant that the fields $g_{\mu\nu}$, A_μ and ϕ could all be Fourier expanded in y :

$$\phi(x^\mu, y) = \sum_n \phi_n(x^\mu) e^{iny/R}. \quad (1.4)$$

If the fields then satisfied the 5D massless wave equation, $\square^{(5)}\phi = 0$, the Fourier modes $\phi_n(x^\mu)$ were found to satisfy

$$\square \phi_n = \left(\frac{n}{r}\right)^2 \phi_n, \quad (1.5)$$

where the righthand side could be looked on as an effective mass term: $m_n^2 = (n/r)^2$. Klein then noted that if the size of the extra dimension was extremely small, the masses of even the lowest Fourier modes would be too heavy to be seen and so the only observed quantities would be the zero modes, removing the dependence on the extra dimensions and replicating Kaluza's cylinder condition. Present limits from high energy colliders,

[32], (due to the fact that no Kaluza-Klein particles have been observed), place an upper bound on r of $\sim 10^{-18}$ m.

However, compactification is not the only possible method of hiding extra dimensions. Braneworld models are models which demand that our 4D universe lives on a sheet or ‘brane’ embedded in a higher dimensional spacetime in which only gravity is allowed to propagate. This allows the extra dimensions to be of much larger size. As the remaining fundamental forces are confined to the brane, it is unsurprising that the effects of higher dimensions are not observed.

One of the first models to explore these braneworlds was the large extra dimension (LED) model of Arkani-Hamed, Dimopoulos and Dvali (ADD), who originally proposed the idea to solve the gauge hierarchy problem in particle physics, [33, 34, 35].

1.2 Large extra dimensions

The hierarchy problem in fundamental physics describes the disparity between two fundamental scales: the electroweak scale ($m_{EW} \sim 10^3$ GeV) and the Planck scale ($m_{pl} \sim 10^{19}$ GeV). While electroweak interactions have been probed at distances $\sim m_{EW}^{-1}$, [32], gravity is only well tested down to sub-mm scales, nowhere near the 10^{-33} cm corresponding to m_{pl}^{-1} , [36, 37, 38], and the treatment of m_{pl} as a fundamental scale requires that we assume gravity remains unmodified over the ~ 30 orders of magnitude in between. In an attempt to overcome the hierarchy problem, Arkani-Hamed, Dimopoulos and Dvali, [33, 34, 35], proposed that in fact there was only one fundamental mass scale, the electroweak scale, and the observed size of m_{pl} arose from the existence of n compact extra spatial dimensions of radius $\sim R$.

If we consider two test masses m_1 and m_2 placed within a distance r of each other in $4 + n$ dimensions, the force they feel will depend on their relative distance compared to the size of the extra dimensions, R . If $r \ll R$, the masses will see all $4 + n$ dimensions and will feel a force given by the $(4 + n)$ dimensional generalisation of Newton’s law:

$$F(r) \sim \frac{m_1 m_2}{M_{pl(4+n)}^{n+2} r^{n+2}}, \quad (1.6)$$

where we take $M_{pl(4+n)}$ to be the fundamental mass scale of the full higher dimensional theory. If on the other hand $r \gg R$, the masses cannot see the extra dimensions and

this time the force law is found to be, [33, 34]:

$$F(r) \sim \frac{m_1 m_2}{M_{pl(4+n)}^{n+2} R^n r^2}, \quad (1.7)$$

and the more usual 4D $1/r^2$ dependence is obtained. If we now compare the latter result to the usual 4 dimensional force, $m_1 m_2 / m_{pl}^2 r^2$, we can obtain an expression for the effective 4D Planck mass as, [33]:

$$m_{pl}^2 = M_{pl(4+n)}^{n+2} R^n. \quad (1.8)$$

Following [33] in setting $M_{pl(4+n)} \sim m_{EW}$, as the one fundamental scale in this theory but taking $m_{pl} \sim 10^{-19}$ GeV, eqn. (1.8) yields

$$R^n \sim \frac{m_{pl}^2}{m_{EW}^{2+n}} \sim \frac{10^{32} \text{ TeV}^2}{m_{EW}^{2+n}}, \quad (1.9)$$

and so,

$$\begin{aligned} R &\sim 10^{\frac{32}{n}} \left(\frac{1 \text{ TeV}}{m_{EW}} \right)^{1+\frac{2}{n}} \text{ TeV}^{-1} \\ &\sim 10^{(32/n)-17} \text{ cm} \left(\frac{1 \text{ TeV}}{m_{EW}} \right)^{1+\frac{2}{n}}. \end{aligned} \quad (1.10)$$

The case of one extra dimension ($n = 1$) has already been ruled out, as $R \sim 10^{13}$ m would imply that deviations from Newtonian gravity would have been observed on solar system scales for this to be true. However any $n \geq 2$ is still a possibility, although recent results, [36, 38], suggest that $n = 2$ (i.e. $R \sim 10^{-3}$ m) could also be ruled out. Nonetheless, $n > 2$ extra dimensions are still allowed by the current constraints.

As mentioned at the beginning of this section, unlike gravity, the standard model (SM) gauge forces (the electroweak and strong forces) have been accurately measured down to the electroweak scale, [32]. Therefore, in order to be compatible with the size of the extra dimensions as derived in eqn. (1.10), the SM forces cannot propagate freely in the extra dimensions, but must be confined to a 4 dimensional submanifold, or ‘brane’, in the higher dimensional spacetime. The small size of m_{pl} is then explained by the large size of the extra dimensions compared to the weak scale, so that effective 4D gravity is weakly coupled, [33]. This large difference between the size of the extra dimensions and the weak scale led to alternative ideas being proposed: models which contained large

extra dimensions which did not necessarily need to be compactified, such as the warped extra dimensions model of Randall and Sundrum.

1.3 The Randall Sundrum model

Not long after the emergence of the ADD model, Randall and Sundrum (RS) proposed an alternative method of tackling the hierarchy problem, [39, 40]. They maintained that in postulating the existence of only one fundamental scale in their extradimensional theory, ADD had simply shifted the hierarchy problem: it was now necessary to explain why the size of the (compactified) extra dimensions was so much greater than the fundamental scale in the theory rather than explaining the discrepancy between the weak and Planck scales. As an alternative to the ADD setup, where the full spacetime could be factorised as a product of a 4D spacetime with a compactified n dimensional space, [33], they suggested a model with just one extra dimension and a non-factorisable metric of the form

$$ds^2 = a(y)^2 \eta_{\mu\nu} dx^\mu dx^\nu + dy^2 . \quad (1.11)$$

The coordinates are given by $x^a = (x^\mu, y)$, where x^μ are the usual 4D coordinates and y represents the extra dimension; $a(y)$ is known as the warp factor and is usually a rapidly varying function of the extra dimension multiplying the 4D metric, [39, 41]. The use of the warp factor in the metric can result in the creation of a large hierarchy without requiring the size of the extra dimension to be large with respect to the fundamental scale. As in the ADD model, 4D subspaces are known as ‘branes’, while the full higher dimensional spacetime is known as the ‘bulk’.

1.3.1 RS I

In their original paper, [39], RS took a finite interval of the extra dimension of size $y = r_c \phi$, where $-\pi \leq \phi \leq \pi$ and r_c can be thought of as a ‘compactification radius’ relating ϕ to the proper distance in the extra dimension, (even though the extra dimension is not in fact compactified). They furthermore took ϕ to be periodic and imposed an orbifold (\mathbb{Z}_2) symmetry condition, $(x, \phi) = (x, -\phi)$, so that the metric was in fact completely specified by values in the range $0 \leq \phi \leq \pi$. The extent of the extra dimension was then

bounded by two 3-branes (i.e. 4D subspaces, as in ADD) situated at the orbifold fixed points, $\phi = 0, \pi$.

The action for this setup is given by, [39]:

$$S = \int d^4x \int_{\pi}^{\pi} d\phi \sqrt{-G} (-\Lambda + 2M^3 R) + \int d^4x \sqrt{-g_{vis}} (\mathcal{L}_{vis} - V_{vis}) + \int d^4x \sqrt{-g_{hid}} (\mathcal{L}_{hid} - V_{hid}), \quad (1.12)$$

where \mathcal{L} is the matter Lagrangian and V the vacuum energy (or tension) of each 3-brane, Λ is the bulk cosmological constant (i.e. the cosmological constant of the 5D spacetime), M is the 5 dimensional fundamental mass scale, G_{MN} is the 5D metric and the 4D projected metrics on each brane are given by

$$g_{\mu\nu}^{vis}(x^\mu) \equiv G_{\mu\nu}(x^\mu, \phi = \pi), \quad g_{\mu\nu}^{hid}(x^\mu) \equiv G_{\mu\nu}(x^\mu, \phi = 0). \quad (1.13)$$

RS then chose a metric ansatz respecting 4D Poincaré invariance in the x^μ directions:

$$ds^2 = e^{-2\sigma(\phi)} \eta_{\mu\nu} dx^\mu dx^\nu + r_c^2 d\phi^2. \quad (1.14)$$

Using this metric with the equations of motion coming from eqn. (1.12), they found that the bulk and boundary vacuum energies had to be related by a single scale for a solution to be valid:

$$V_{hid} = -V_{vis} = 24M^3 k, \quad \Lambda = -24M^3 k^2, \quad (1.15)$$

where k , the bulk curvature, is of order the Planck scale, [39]. They thus obtained a metric of the form

$$ds^2 = e^{-2kr_c|\phi|} \eta_{\mu\nu} dx^\mu dx^\nu + r_c^2 d\phi^2, \quad (1.16)$$

which decays from the brane situated at $\phi = 0$ to the $\phi = \pi$ brane. We can also see from eqn. (1.15) that the bulk cosmological constant, Λ , is negative, and so the bulk spacetime must be AdS_5 - 5D anti de Sitter - where an anti de Sitter spacetime is a spacetime with a constant negative curvature.

As we discussed in the previous section, gravity has been well tested down to sub-mm scales, [37, 36, 38], without any deviations from the expected results. RS therefore took r_c to be small and considered the effective 4 dimensional theory. They found that, while

the 4D effective Planck mass is only weakly dependent on r_c , [39]:

$$m_{pl}^2 = \frac{M^3}{k}(1 - e^{-2kr_c\pi}), \quad (1.17)$$

the SM masses on the $\phi = \pi$ brane are given by

$$m = e^{-kr_c\pi} m_0, \quad (1.18)$$

which can produce TeV scale physical masses from fundamental mass parameters of order the Planck scale without requiring kr_c to be very large, i.e. without a large hierarchy between the ‘compactification radius’ and the fundamental scale. This result led to the two branes being labelled as in the action (1.12): the SM fields with TeV scale masses on the $\phi = \pi$ brane were said to be living on the visible brane, while the fundamental mass parameters were said to belong on the hidden brane at $\phi = 0$.

However, if we look at eqn. (1.15), we can see that the visible brane on which our SM fields live has a negative tension. In [42], Shiromizu, Maeda and Sasaki derived the effective 4D Einstein equations for the brane, defining the 4D Newtonian constant, G_N , in terms of the 4D brane tension λ . However, they found that the presence of a negative tension brane (i.e. $\lambda < 0$) led to an ambiguity between the vacuum and matter energy densities, making it impossible to define the gravitational constant. Furthermore, a negative brane tension would result in $G_N < 0$. In [43], it was realised that the presence of a negative tension brane would lead to the equations of motion derived from the braneworld model changing sign relative to the standard cosmological equations. This would cause the universe to collapse on a timescale of a few thousand years if it possessed an energy density, ρ , and pressure, p , related by the standard equation of state, $p = w\rho$, for any $w < \frac{1}{3}$. The radiation era would therefore be well-behaved as in standard cosmology, but a matter (or dark energy) dominated phase would collapse, an occurrence which could be only be averted by the use of non-standard big-bang nucleosynthesis, or modification of the RS I model. For these reasons, the RS I model which suggests that we live on a negative tension brane, cannot be a physical model of our universe.

1.3.2 RS II

In [40], Randall and Sundrum considered a one brane version of the above model. The initial setup was as in the RS I model, but the locations of the hidden and visible branes

were reversed, so that our universe was situated on a positive tension brane, and the brane situated at $\phi = \pi$ could be removed from the physical setup by taking it to infinity. It is easy to see that the expression derived for the 4D effective Planck mass in the RS I model, eqn. (1.17), is still well defined even if we take r_c to infinity. However, due to the exchange of the branes, while this theory can now model a physical universe (as the SM fields live on a positive tension brane), it no longer solves the hierarchy problem, as the warp factor is simply 1 on the $y = 0$ (visible) brane.

This infinite extra dimension meant that the model gave rise to a continuum of Kaluza-Klein (KK) excitations rather than the discrete spectrum of the RS I model, [44]. These were studied by considering the linearised tensor perturbations about the metric, $h_{\mu\nu}(x, y)$, and separating the 4D and extra dimensional components, writing $h(x, y) = \psi(y)e^{ip \cdot x}$, where $p^2 = m^2$. RS found that the spectrum contained a single normalisable bound state mode corresponding to the massless 4D graviton wavefunction, and a continuum of massive states, [40], and computed the non-relativistic gravitational potential between two particles, m_1 and m_2 , separated by a distance r to be, [40]:

$$V(r) = G_N \frac{m_1 m_2}{r} \left(1 + \frac{1}{k^2 r^2} \right). \quad (1.19)$$

We can clearly see that this is the 4D Newtonian potential with a correction term added. Since as before, the bulk curvature term is of order the Planck scale, the correction to the potential is highly suppressed. RS therefore found that despite the addition of an infinite extra dimension, the model could still produce an effective 4D theory of gravity, arising from the inclusion of the warp factor in the metric, which effectively ‘trapped’ the gravitational force close to the brane.

1.4 Thesis outline

As we have said, one of the present motivations for studying modified models of gravity is explaining the apparent late time acceleration of our universe and it makes sense therefore to consider phenomena at cosmological distances (of order today’s horizon size H_0^{-1}), where we are once more entering a region where gravity has not been well tested. However, all of the extra dimensional models discussed above modify gravity on extremely small scales, evading the experimental bounds of [36, 37, 38], while reproducing Einstein gravity on large scales.

In chapter 2 we will therefore review the well-known braneworld model of Dvali, Gabadadze and Porrati (DGP), [45], which can produce modifications of gravity at large distances. We concentrate in particular on the cosmological equations derived from this model. In chapter 3, we consider the observational effects of a relative of the DGP model: the asymmetric brane model, [46, 47]. This model allows the bulk mass scale and cosmological constant to vary from one side of the brane to the other, which can result in a widening of the DGP parameter space. We explore the cosmological consequences of this increase in the parameter space.

We then switch focus and consider the early universe consequences of braneworld-type models in string theory. These models can produce inflation in the early universe through a mechanism known as brane inflation, [48, 49], where an attractive potential between two branes allows slow-roll inflation to take place; this cuts off before the branes collide and annihilate, reheating the universe. Cosmic strings, topological defects which possess features that can produce large bursts of gravitational radiation, can be produced as a byproduct of the brane inflation mechanism, possibly giving rise to a network of cosmic strings throughout the universe. We give a brief review of cosmic strings and the calculation of gravitational radiation from cusps on cosmic string loops, [50, 51], in chapter 4, before going on to consider the effect extra dimensions could have on the gravitational wave bursts produced by cusps in chapter 5 and kinks in chapter 6. Finally, we conclude in chapter 7.

Chapter 2

The DGP model

2.1 Introduction

The modified gravity model of Dvali, Gabadadze and Porrati (DGP), [45], is a five dimensional theory, thus possessing one extra dimension (although the model has been extended to $D > 5$ dimensions, [52, 53]). It was one of the first braneworld models to consider the effects of extra dimensions which were not constrained by either compactification or warping. Unlike the ADD and RS models, the DGP model modifies gravity at cosmological (rather than sub-mm) distances, where the crossover between Einstein gravity and the modified theory is set by the fundamental mass scales in the model. A number of other models have also explored the possibility of modifying gravity on large scales, [54, 55, 56], in particular the GRS model, [57, 58], the stealth model of Charmousis, Gregory and Padilla, [59] and the asymmetric brane model, [46, 47].

The DGP model was originally introduced as a mechanism to produce 4D Newtonian gravity on the brane in a model with infinite extra dimensions, [45]. However, it has excited considerable interest among cosmologists, as it can produce late time acceleration without the aid of dark energy. Indeed extensive tests of the model with observational data, [60, 61, 62, 63, 64, 65, 66], have been performed, which show that while it is not as good a fit to the data as the concordance model, it is nonetheless acceptable.

2.2 DGP cosmology

2.2.1 Model setup

We are interested in the production of late time acceleration without a cosmological constant and therefore wish to look at the cosmology of the model. The DGP model consists of a tensionless 3-brane embedded in a 5D Minkowski spacetime with a \mathbb{Z}_2 symmetry around the brane. We write the action in the form

$$S = S_{bulk} + S_{brane} . \quad (2.1)$$

Following the method used in [67] and [68], (although a different definition of the fundamental mass scales means some factors of 2 have changed), the bulk action can be written as

$$S_{bulk} = M^3 \int_{\mathcal{M}} d^5x \sqrt{-g^{(5)}} (R^{(5)} - 2\Lambda) + 2M^3 \int_{brane} d^4x \sqrt{-\gamma} K . \quad (2.2)$$

This setup includes the Gibbons-Hawking boundary term containing the extrinsic curvature, a term which did not appear in the RS action, (1.12). It arises due to a subtlety in the manner in which the gravitational action can be written: whether we consider the brane to be a genuine zero-thickness object acting as a boundary between two spacetimes, or as a zero-thickness approximation of a finite width domain wall as is the case in early braneworld models, [69, 70, 71]; these two approaches have long been found to be equivalent, [72]. In using this form of the action, we consider the brane as a common boundary between two spacetimes, \mathcal{M}_1 and \mathcal{M}_2 , which because of the \mathbb{Z}_2 symmetry of the DGP model, are in fact identical. The full spacetime, $\mathcal{M} = \mathcal{M}_1 \cup \mathcal{M}_2$.

In the action (2.2), $g_{ab}^{(5)}$ and $R^{(5)}$ represent the 5D metric and Ricci scalar respectively, while M is the 5D fundamental mass scale and Λ is a bulk cosmological constant. The factor of γ in the second term of (2.2) is related to the induced metric on the brane given by

$$\gamma_{ab} = g_{ab} - n_a n_b , \quad (2.3)$$

where n^a is the unit normal to the brane in \mathcal{M}_i pointing out of \mathcal{M}_i ¹, while the extrinsic curvature of the brane is

$$K_{ab} = \gamma_a^c \gamma_b^d \nabla_{(c} n_{d)} , \quad (2.4)$$

where $K_{ab} = K_{ab}^{(1)} = K_{ab}^{(2)}$.

The brane action is given by

$$S_{brane} = \int_{brane} d^4x \left(\frac{m_{pl}^2}{2} \sqrt{-\gamma} R + \mathcal{L}_{matter} \right) . \quad (2.5)$$

\mathcal{L}_m represents the matter Lagrangian, $\gamma_{\mu\nu}$ and R , the 4D induced metric and corresponding (brane) intrinsic curvature, while m_{pl} is the 4D fundamental mass scale.

The bulk equations of motion are found from the bulk action to be the 5D Einstein equations:

$$R_{ab}^{(5)} - \frac{1}{2} R^{(5)} g_{ab} = -\Lambda g_{ab} , \quad (2.6)$$

while the brane equations of motion, found from the Israel conditions, [72], are given by

$$M^3 K_{ab} + \frac{m_{pl}^2}{2} (R_{ab} - \frac{1}{6} R \gamma_{ab}) = \frac{1}{2} (T_{ab} - \frac{1}{3} T \gamma_{ab}) , \quad (2.7)$$

obtained by varying (2.1) with respect to the induced brane metric, γ_{ab} ; the energy momentum tensor for the additional matter on the brane is

$$T_{ab} = -\frac{2}{\sqrt{-\gamma}} \frac{\partial \mathcal{L}_m}{\partial \gamma^{ab}} . \quad (2.8)$$

We now wish to consider the cosmological implications of the model. In order to study this, since we have Einstein gravity in the bulk, we know that each (identical) bulk is completely specified by the AdS-Schwarzschild metric, [74]:

$$-h(r) dt^2 + \frac{dr^2}{h(r)} + r^2 d\mathbf{x}_\kappa^2 , \quad (2.9)$$

¹This convention for the normal vectors, n_a , is the opposite to that used in [67], [68]: see [73].

where

$$h(r) = r^2 k^2 + \kappa - \frac{\mu}{r^2}. \quad (2.10)$$

The k^2 term is a general bulk curvature term (related to Λ), while κ encodes the brane curvature and μ is the mass of a bulk black hole.

In order to construct the brane, we glue two copies of the solution in the bulk space-time together, where the brane will form the common boundary situated at $r = a(\tau)$. Then, the boundary, $\partial\mathcal{M} = \partial\mathcal{M}_1 = \partial\mathcal{M}_2$, is given by the section $(t(\tau), a(\tau), \mathbf{x}^\mu)$ of the bulk metric (2.9), where τ is the proper time of an observer comoving with the boundary, so that

$$-h(a)\dot{t}^2 + \frac{\dot{a}^2}{h(a)} = -1, \quad (2.11)$$

where the differentiation is with respect to τ . The unit normal to $\partial\mathcal{M}$ is now given by

$$n_a = \epsilon(-\dot{a}(\tau), \dot{t}(\tau), \mathbf{0}), \quad (2.12)$$

where $\epsilon = \pm 1$. If $\epsilon = 1$, the bulk spacetime, \mathcal{M} , corresponds to $a(\tau) < a < \infty$, while for $\epsilon = -1$, \mathcal{M} corresponds to $0 \leq a < a(\tau)$, [67]. The induced metric on $\partial\mathcal{M}$ is that of a FRW universe,

$$ds^2 = -d\tau^2 + a^2 d\mathbf{x}_\kappa^2, \quad (2.13)$$

while the induced Ricci tensor and scalar, evaluated using this metric, are found to be

$$R_{ij} = \left(\frac{\ddot{a}}{a} + 2\left(\frac{\dot{a}}{a}\right)^2 + 2\frac{\kappa}{a^2} \right) \gamma_{ij} \quad (2.14)$$

and

$$R = 6 \left(\frac{\ddot{a}}{a} + \left(\frac{\dot{a}}{a}\right)^2 + \frac{\kappa}{a^2} \right). \quad (2.15)$$

We define the Hubble parameter as $H = \frac{\dot{a}}{a}$ on the boundary and introduce a homogeneous, isotropic fluid on the brane, whose energy momentum tensor is, [46]:

$$T_{ab} = (\rho + p)\tau_a\tau_b + p\gamma_{ab} , \quad (2.16)$$

with energy density ρ , pressure p and τ^a , the velocity of a comoving observer (which in \mathcal{M} is $\tau^a = (\dot{t}(\tau), \dot{a}(\tau), \mathbf{0})$); we can now evaluate the spatial components of (2.7) and find

$$\begin{aligned} M^3 K_{ij} + \frac{m_{pl}^2}{2}(R_{ab} - \frac{1}{6}R\gamma_{ab}) &= \frac{1}{2}\left(T_{ij} - \frac{1}{3}T\gamma_{ij}\right) \\ \implies M^3 \frac{h}{a} \dot{t}\gamma_{ij} + \frac{m_{pl}^2}{2}(R_{ab} - \frac{1}{6}R\gamma_{ab}) &= \frac{1}{2}\left(T_{ij} - \frac{1}{3}T\gamma_{ij}\right) . \end{aligned} \quad (2.17)$$

Using eqn. (2.16), the velocity τ^a and eqn. (2.3) to calculate the induced metric components, we find the spatial components of the energy momentum tensor to be

$$T_{ij} = p\gamma_{ij} , \quad (2.18)$$

while the trace is given by

$$T = g^{ab}T_{ab} = -\rho + 3p , \quad (2.19)$$

and therefore using eqns. (2.14) and (2.15) for the induced intrinsic curvature terms, the spatial components of the Israel equation become

$$M^3 \frac{h}{a} \dot{t}\gamma_{ij} + \frac{m_{pl}^2}{2} \left(\left(\frac{\dot{a}}{a} \right)^2 + \frac{\kappa}{a^2} \right) \gamma_{ij} = \frac{\rho}{6} \gamma_{ij} , \quad (2.20)$$

which if we use eqn. (2.11) to substitute for \dot{t} gives

$$\frac{m_{pl}^2}{2} \left(H^2 + \frac{k}{a^2} \right) - \epsilon M_5^3 \sqrt{H^2 + \frac{h}{a^2}} = \frac{\rho}{6} . \quad (2.21)$$

Finally, if we substitute for $h(a)$ using (2.10), the modified DGP Friedmann equation is

$$\rho = 3m_{pl}^2 \left(H^2 + \frac{\kappa}{a^2} \right) - 6M^3 \epsilon \sqrt{H^2 + k^2 + \frac{\kappa}{a^2} - \frac{\mu}{a^4}} . \quad (2.22)$$

2.2.2 Model regimes

We now wish to consider the cosmological evolution of this model using the expressions calculated in the previous section. We rewrite eqn. (2.22), setting the bulk curvature, $k = 0$, along with the cosmological constant, since as mentioned earlier, the model setup assumes a 5D Minkowski bulk spacetime. We neglect the black hole mass term, μ , also. The equation then becomes

$$\rho = 3m_{pl}^2 \left(H^2 + \frac{\kappa}{a^2} \right) - 6M^3 \epsilon \sqrt{H^2 + \frac{\kappa}{a^2}} . \quad (2.23)$$

Looking at this equation, it is easy to see that the usual 4D Friedmann equation (derived from General Relativity),

$$\rho = 3m_{pl}^2 H^2 , \quad (2.24)$$

is recovered whenever the square root term on the RHS is subdominant. This occurs if

$$\sqrt{H^2 + \frac{\kappa}{a^2}} \gg 2\epsilon \frac{M^3}{m_{pl}^2} , \quad (2.25)$$

or, if the spatial curvature terms are neglected, [75]:

$$H^{-1} \ll \frac{m_{pl}^2}{2M^3} \equiv r_{DGP} . \quad (2.26)$$

If, on the other hand, the square root is the dominant term on the RHS, we can write the Friedmann equation as

$$H^2 + \frac{\kappa}{a^2} \simeq \frac{\rho^2}{36M^6} , \quad (2.27)$$

and we say that the model has entered the fully 5D regime.

The scale r_{DGP} , defined in eqn. (2.26), is known as the crossover scale between the 4D and 5D regimes of the model: for distances smaller than r_{DGP} , 4D cosmology is recovered, while at distances large compared to r_{DGP} , the extra dimension has an effect and must be taken into account. Dvali, Gabadadze and Porrati, [45], obtained this scale when considering the potential mediated by a (5D) scalar field on the 4D brane worldvolume, finding $V \sim 1/r$ below this distance and $V \sim 1/r^2$ at larger distances. Setting the size of r_{DGP} is extremely important, as it is the change in the behaviour of

the model around this scale which allows us to keep well-tested (4D) results from General Relativity while attempting to explain large distance effects with the extra dimension. For this reason, r_{DGP} is generally chosen to be of order the current horizon size.

Along with the effects of the crossover scale, the behaviour of the modified Friedmann equation (2.22) is heavily dependent on the value of the parameter ϵ . The scale factor, a , diverges at late times on the brane, [75], (i.e. the times in which we are interested) and so we neglect the spatial curvature term. We first consider the case where $\epsilon = -1$ and allow the energy density $\rho \rightarrow 0$ in order to study the vacuum solutions of the model. It is easily seen if we rewrite eqn. (2.23) as

$$\sqrt{H^2 + \frac{\kappa}{a^2}} = -\frac{M^3}{m_{pl}^2} + \sqrt{\frac{\rho}{3m_{pl}^2} + \frac{M^6}{m_{pl}^4}}, \quad (2.28)$$

that $H \rightarrow 0$ as $\rho \rightarrow 0$, the usual Minkowski vacuum. Since we are allowing $\rho \rightarrow 0$, there will be a point where it is small in comparison with M^6/m_{pl}^4 and we can expand the square root, obtaining eqn. (2.27). The $\epsilon = -1$ branch of the solution thus results in a transition to the full 5D regime at late times.

The $\epsilon = 1$ branch on the other hand, exhibits markedly different behaviour. If we consider eqn. (2.28) with $\epsilon = 1$ we find, letting $\rho \rightarrow 0$, that instead of $H \rightarrow 0$ it has a minimum value of, [75]:

$$H_{self} = \frac{2M^3}{m_{pl}^2}. \quad (2.29)$$

Therefore at late times, as ρ becomes small, this branch of the solution will not enter the full 5D regime unlike the $\epsilon = -1$ case, but will have a transition from the usual 4D equation to an inflationary solution where $H \sim H_{self}$.

The DGP model is thus able to follow a period of radiation and matter dominated cosmology, expressed in the 4D regime of the generalised Friedmann equation, by a period of late time acceleration without the aid of a cosmological constant term, provided we choose the $\epsilon = 1$ or self-accelerating branch of the model. This self-acceleration arises due to the inclusion of the intrinsic curvature of the brane in the action (2.5), which behaves as a negative cosmological constant on the brane, causing acceleration, [75]. The $\epsilon = -1$ solution (known as the FRW branch), mimics the evolution of the usual FRW cosmology of the Λ CDM model in producing late time acceleration only with the inclusion of vacuum energy on the brane and is therefore not usually considered further if

an alternative to dark energy is sought. However, since the crossover scale must be tuned to match observations, we have not managed to remove the tuning problem entirely.

The self-accelerating solution of the DGP model can be rewritten in terms of cosmological densities as, [76]:

$$H^2(z) = H_0^2 \left\{ \Omega_k (1+z)^2 + \left(\sqrt{\Omega_{r_{DGP}}} + \sqrt{\Omega_{r_{DGP}} + \Omega_i (1+z)^{3(1+w_i)}} \right)^2 \right\}, \quad (2.30)$$

where there is an implicit sum over the (usual) contributions to the energy density with equations of state $p_i = w_i \rho_i$, the other contributions are defined as

$$\Omega_k \equiv \frac{-k}{H_0^2 a^2}, \quad \Omega_{r_{DGP}} \equiv \frac{1}{4r_{DGP}^2 H_0^2}, \quad (2.31)$$

where $\Omega_{r_{DGP}}$ is an effective cosmological density related to the crossover scale, and the normalisation condition becomes

$$\Omega_k = 1 - \left(\sqrt{\Omega_{r_{DGP}}} + \sqrt{\Omega_{r_{DGP}} + \Omega_m} \right)^2, \quad (2.32)$$

where in this case we have ignored the radiation component, which will be negligible at late times.

2.3 Observational tests of the DGP model

The fact that the DGP model could explain the late time acceleration of the universe without a cosmological constant, combined with a relatively simple modified Friedmann equation (2.22) encoding its cosmological evolution, has ensured that it has become one of the most popular and widely studied modified gravity alternatives to the Λ CDM model. As well as providing a mechanism for late time acceleration, the DGP model does not have a large number of new parameters. Indeed it has the same number of parameters as Λ CDM, simply replacing the cosmological constant term, Ω_Λ , with a term $\Omega_{r_{DGP}}$, related to the crossover scale as defined in eqn. (2.30), which is analogous to the cosmological density terms. A number of authors, [60, 61, 62, 63, 77], have compared the DGP model to the available observational data, primarily various type Ia supernova data sets, CMB anisotropy data from WMAP (through the CMB shift parameter R) and the baryon acoustic oscillation peak obtained from the SDSS survey.

The unprecedented success of the Λ CDM model is not that it can fit one data set, but that it can simultaneously satisfy multiple sets of data at different redshifts. If the DGP model is to be a serious challenger to the concordance model, then it must do at least as well at this aspect.

Type Ia supernovae are relatively reliable standard candles and their magnitude-redshift relation is the most easily satisfied of the above tests. This relation relies on the luminosity distance, d_L , the distance at which an object would lie based on its luminosity:

$$d_L(z) = \frac{(1+z)}{H_0 \sqrt{|\Omega_k|}} \mathcal{S} \left(\sqrt{|\Omega_k|} \int_0^z \frac{dz'}{E(z')} \right), \quad (2.33)$$

where $\mathcal{S}(X) = (X, \sin X, \sinh X)$ for a flat, closed or open universe respectively, $E = H/H_0$ and $H(z)$ is the Hubble parameter whose current value is denoted as H_0 ; the magnitudes are then calculated using $\mu = 5 \text{Log}_{10} d_L(z)$.

Another obvious test involves the WMAP observations of the CMB anisotropies, [4, 78, 79, 80]. This is not a simple task in a modified gravity model such as DGP, whose linear density perturbations are not well understood, [65]. Deffayet et al. looked at the CMB anisotropies in [81], but changed the background equation of motion only (using the modified Friedmann equation (2.22) calculated above), leaving the 4D perturbations in place. However, they state that this is not particularly well justified for large scales (late times), where the effect of the extra dimension begins to be felt.

Instead, we consider the CMB shift parameter, [82], which encodes much of the information about the CMB without the need for model perturbations. The shift parameter

$$R(z_*) = \frac{\sqrt{\Omega_m}}{\sqrt{|\Omega_k|}} \mathcal{S} \left(\sqrt{|\Omega_k|} \int_0^{z_*} \frac{dz'}{E(z')} \right), \quad (2.34)$$

is related to the position of the first acoustic peak in the temperature anisotropy spectrum, which is in turn related to the angular diameter distance to and the comoving size of the sound horizon at the last scattering surface; the function $\mathcal{S}(x)$ is defined as for the luminosity distance and z_* is the redshift at decoupling. It is measured by WMAP, [4, 83], and is a relatively model independent quantity, as it does not depend on H_0 , [66, 62]; it is therefore typically used to constrain dark energy models, [83]. Some pitfalls of using this parameter rather than the full CMB dataset have been discussed in [65].

The final primary observation usually considered is the baryon acoustic oscillation (BAO) peak measured from the SDSS survey, [84, 85]. However, while analyses including this distance measure have been performed, doubts have been raised over how appropriate it is to use as a constraint on models which do not behave as constant equation of state dark energy, such as braneworld models, [86, 63, 87]. The data from SDSS used to find the BAO measurement were analysed using a fiducial Λ CDM model where they were compressed to give a constraint at a single redshift and a single scaling relation was used for the best fit; this is found to be accurate to within a few percent for Λ CDM-type models, [84]. However, the DGP model (and other modified gravity models without constant w evolution) could evolve in a very different manner and it is possible that the errors in applying this measurement could be much more significant, [86, 62].

The overall results of these investigations suggest that in general, the Λ CDM model is still a better fit to the data than DGP, although in many cases DGP is almost as good a fit and is certainly not ruled out definitively. However, one point to note is the significant tension between datasets, particularly for the flat DGP model. While this is improved somewhat by the addition of curvature to the modified gravity model, as [60] points out, there is the added complication of tension between the CMB constraint on $\Omega_m h^2$ and the Hubble Key Project value for h , [88], ($H_0 = 100h \text{ km s}^{-1} \text{ Mpc}^{-1}$). Nonetheless, despite these difficulties, the DGP model is still a viable option from an observational viewpoint.

Finally we note that that the DGP model can be rewritten in the form of a quintessence or dark energy model with an effective equation of state dependent on redshift. These two models cannot be distinguished using the methods just outlined above. Instead, the quantity $\delta = \delta\rho_m/\rho_m$, known as the growth function, [89, 90], which behaves differently in modified gravity and dark energy models, must be studied in order to distinguish between them. However this will not be discussed further.

2.4 Problems with the DGP model

Ever since the appearance of the DGP model as a theory of modified gravity, it has become increasingly clear that, while the cosmological results are promising (as discussed in the previous section), there are serious underlying issues with the model, in particular with the self-accelerating branch of the solution. Any or all of these problems would render the model fundamentally flawed as a realistic model of the universe.

The most well-known issue with the self-accelerating branch of the DGP model is the existence of ghosts. Ghosts are states with a wrong sign kinetic term and violate unitarity, which can lead to catastrophic consequences if they couple to normal matter. They were originally thought not to be present in the DGP model (unlike the earlier GRS model, [57, 58]). Indeed it is true to say that the normal branch of the DGP solution is ghost free. Unfortunately the self-accelerating branch is not.

Ghosts appear in the 4D perturbation spectrum (tensor and scalar modes) of the self-accelerating branch whether or not tension is included in the model. The action (2.1) is generalised by the addition of a tension term σ to the 4D integral and the background metric is given by, [67]

$$ds^2 = a^2(y)(dy^2 + \bar{\gamma}_{\mu\nu}dx^\mu dx^\nu) , \quad (2.35)$$

where

$$\bar{\gamma}_{\mu\nu}dx^\mu dx^\nu = -dt^2 + e^{2Ht}d\mathbf{x}^2 , \quad (2.36)$$

and the warp factor, $a(y) = \exp(\epsilon Hy)$, where $\epsilon = \pm 1$. Perturbing this background metric and splitting the fluctuations, $h_{\mu\nu}$, into their scalar, vector and tensor components, it was found that the perturbation spectrum of the DGP accelerating branch consists of a continuum of massive states and 2 discrete modes with smaller masses, [67, 91]: the spin-0 (scalar) perturbation with $m^2 = 2H^2$ and the helicity-0 state of the spin-2 (tensor) perturbation. This last mode has a mass in the range $0 < m^2 < 2H^2$, which was found to be forbidden by Higuchi, [92], as it yields a state with a negative norm, and so is in fact a ghost. This is the case when the DGP brane is given a positive tension, whereas the negative tension brane has a scalar ghost, [67, 93]. If the brane is tensionless (the standard DGP setup) then these modes mix and the model yet again contains a ghost, [67]. However, the authors of the model argue that the inclusion of strong coupling in the model could solve the ghost problem, [94, 95].

If interactions in a model become strongly coupled at some energy scale, perturbation theory breaks down above this scale and the predictivity of the model is lost. In order for the model to be of any use, the ultraviolet (UV) completion of the theory is needed so that calculations can be moved beyond the perturbative level. A number of authors have found that strong interactions occur at very low energy scales in the DGP model, [96, 97, 98]. Luty, Porrati and Rattazzi, [96] found this scale (in terms of wavelength

rather than energy) to be

$$\lambda_3 \sim \left(\frac{r_{DGP}^2}{m_{pl}^2} \right)^{1/3}. \quad (2.37)$$

If r_{DGP} is of order the current horizon size (in order to explain present late time acceleration), then this length scale is of order 1000 km and the model is strongly coupled at distances below this scale. As yet, the high energy (UV) behaviour of the DGP model is unknown.

However, even if we allow for UV completion of the model and presume this solves the problem of ghosts on the self-accelerating branch as proposed in [94, 95], there are still issues in the model which are not purely a result of perturbation theory. Some of these problems, for instance, pressure singularities at a finite radius, tunnelling instabilities and issues with black holes in the bulk, are discussed further in [68].

2.5 Conclusions

As we have seen, the DGP model, [45], can produce cosmological evolution which admits the possibility of late time acceleration without the use of dark energy or a cosmological constant, primarily through the inclusion of an induced intrinsic curvature term in the action (2.5). This self-accelerating branch of the solution has been found to fit observational data reasonably well, although there is more tension between the various data sets than is the case with the standard concordance model. However, the appearance of ghosts in the perturbative spectrum, and, even if they were eventually found to be caused by the lack of a UV-complete model, the existence of other more intransigent instabilities, has cast doubts on the ability of the model to realistically represent the universe. In this case, it would seem sensible to consider other similar braneworld models which can produce late time acceleration (e.g. [59, 46, 47]) and using these, perform the same extensive tests and analysis as have been done in the case of the DGP model. In this way it is possible that the same self-accelerating effects could provide an answer to the question of late time acceleration, while possibly mitigating some of the problems encountered by the DGP model. Even if these models are also found to contain similar problems, the broadening of the focus to include braneworld models which produce large scale modifications of gravity outside of the DGP model can only be of benefit.

Chapter 3

The cosmology of asymmetric brane modified gravity

3.1 Introduction

As we have seen in the last chapter, the DGP model offers a plausible and (cosmologically) simple alternative to the concordance model in attempting to explain late time acceleration, but suffers from a number of serious problems which rule it out as a realistic model of the universe. We therefore wish to consider the behaviour of other braneworld models which could offer alternatives to Λ CDM: in particular, we consider the asymmetric brane model of Padilla, [46, 47].

The asymmetric (AC) model has more in common with the Randall Sundrum rather than the DGP model in its setup, consisting of a 3-brane with non-zero tension acting as a boundary between two bulk anti de Sitter (AdS) spacetimes, while lacking the characteristic brane induced curvature term of the DGP model. It relaxes the \mathbb{Z}_2 symmetry around the brane possessed by the DGP and RS models, but is still able to produce infrared modifications of gravity. The main implication of relaxing this symmetry is an increase in the parameter space of the model: the cosmological constant and Planck masses can vary from one side of the brane to the other. This allows more freedom in the AC metric's warp factor, $a(y)$, allowing large scale modifications of gravity which, as we have discussed in chapter 1, are not present in the RS model. The asymmetric model also possesses a strong hierarchy between the Planck masses and the AdS curvature scales on each side of the brane. If on one side of the brane, the Planck mass and cosmological constant are large, it leads to a localising effect on braneworld gravity

(similar to that in the RS model). If on the other hand, the cosmological constant and the Planck mass are both taken to be small, the opposite effect is achieved and gravity is modified in the infrared, [99]. Choosing appropriate scales, it is therefore possible to have an effectively 4D regime giving way to 5D behaviour at very large scales in a similar manner to the DGP model.

In this chapter, we explore the cosmology of the asymmetric model, focusing in particular on the type Ia supernova data, [100, 9, 10], and the expansion parameters from WMAP, [78, 83], tests which have already been performed for the DGP model. We first show how the AC model can be viewed as a one parameter extension of the DGP model over a wide range of scales. We then explore the effect of this additional parameter on the expansion history of the universe, comparing in particular with the DGP model. We finally discuss the effect of this parameter on the observational constraints.

3.2 Asymmetric braneworld models

We begin by reviewing the asymmetric model, [47], and deriving the cosmological equations. The action can be written as a combination of a bulk and brane action as in chapter 2, where the ‘bulk’ action contains the gravitational field dynamics, and is given by the Einstein-Hilbert and Gibbons-Hawking terms:

$$S_{bulk} = \sum_{i=1,2} M_i^3 \int_{\mathcal{M}_i} d^5x \sqrt{-g} (R - 2\Lambda_i) + 2M_i^3 \int_{brane} d^4x \sqrt{-\gamma} K^{(i)}. \quad (3.1)$$

Here, g_{ab} is the bulk metric with corresponding Ricci scalar, R and the sum ensures that the bulk spacetimes on either side of the brane are included. The metric induced on the brane is given as before by eqn. (2.3), while the extrinsic curvature is given by eqn. (2.4). The brane action for the AC model is written as

$$S_{brane} = \int_{brane} d^4x (-\sigma \sqrt{-\gamma} + \mathcal{L}_{matter}), \quad (3.2)$$

where σ is the brane tension and \mathcal{L}_{matter} describes the matter content on the brane.

Again we have written the action in a form which includes the Gibbons-Hawking boundary term containing the extrinsic curvature, as we did in the last chapter. Due to the asymmetric nature of the AC model, the boundary approach, typified by the inclusion of this term, is a somewhat more natural method of representing the model than the

δ -function used to denote a purely mathematical boundary, making the equations of motion easier to obtain.

The equations of motion for each bulk are given by the 5D Einstein equations (2.6) used in the last chapter, while the brane equations of motion are found once again from the Israel conditions, [72], and in this model are given by

$$2\langle M^3 K_{ab} \rangle - \frac{\sigma}{6}\gamma_{ab} = \frac{1}{2}\left(T_{ab} - \frac{1}{3}T\gamma_{ab}\right), \quad (3.3)$$

obtained by varying the AC action with respect to the induced brane metric, γ_{ab} , where $\langle Z \rangle = (Z_1 + Z_2)/2$ and $\Delta Z = Z_1 - Z_2$ for a quantity Z_i differing across the brane¹. We use the same expression for the energy momentum tensor of the additional matter on the brane, eqn. (2.8).

The background metric, \bar{g}_{ab} , is found by solving the equations of motion with $T_{ab} = 0$, and may be written as

$$ds^2 = \bar{g}_{ab}dx^a dx^b = a^2(y)\eta_{\mu\nu}dx^\mu dx^\nu + dy^2, \quad (3.4)$$

where $x^a = (x^\mu, y)$, the brane is situated at $y = 0$, and $a(y)$ is the warp factor. The bulk equations of motion (2.6) can be solved to give

$$\left(\frac{a'}{a}\right)^2 = -\frac{\Lambda}{6}, \quad \frac{a''}{a} = -\frac{\Lambda}{6}, \quad (3.5)$$

thus, the warp factor has the general form

$$a_i(y) = e^{-\theta_i k_i |y|}, \quad (3.6)$$

where $\theta_i = \pm 1$, the subscript $i = 1, 2$ refers to the two sides of the brane ($i = 1$ being $y < 0$), and $\Lambda_i = -6k_i^2$ defines the AdS curvature scale on each side.

If we now consider the 00 component of the brane equations of motion (3.3) (again with $T_{ab} = 0$) and the metric (3.4), we find

$$K_{00} = a' a, \quad (3.7)$$

¹The appearance of the average of the extrinsic curvature, $\langle K_{ab} \rangle$, rather than the more usual ΔK_{ab} in eqn. (3.3) is a result of the manner in which the unit normal to the brane is defined, [73], as mentioned in the last chapter.

which imposes a condition on the brane tension:

$$2\langle M^3\theta_k \rangle = \frac{\sigma}{6}. \quad (3.8)$$

Three separate cases of this model were considered in [47] for different θ_i values (see figure 3.1): (i) the Randall Sundrum (RS) case, $\theta_1 = \theta_2 = 1$, (ii) the inverse Randall Sundrum (IRS) case, $\theta_2 = \theta_1 = -1$, and (iii) the mixed case, where $\theta_1 = -\theta_2 = 1$. If θ_1 corresponds to the lefthand side of the brane ($y < 0$) and θ_2 corresponds to the righthand side of the brane ($y > 0$), then the RS case has the warp factor decaying away from the brane on both sides, while the inverse RS case has the warp factor growing on both sides. In the mixed case, the warp factor decays away from the brane on the left, whilst growing on the right. As explained in detail in [47, 99], (see also the discussion below about the scales where the model exhibits 4D behaviour), whereas 4 dimensional Einstein gravity cannot be reproduced at any scale in the inverse RS case, it can be achieved in the RS and mixed cases, along with infrared modifications. However, only the mixed case will approach a de Sitter state at late times, leading to exponential late time acceleration without an effective cosmological constant, [46], (as we discussed in chapter 1, the RS II model produces effectively 4D gravity despite the presence of an infinite extra dimension). Therefore, only the mixed case where $\theta_1 = -\theta_2 = 1$ is considered from now on.

Turning to cosmological solutions, since we have Einstein gravity in the bulk, as in the DGP model, we know that once again, the bulk is completely specified by the AdS-Schwarzschild metric specified by eqns. (2.9) and (2.10), [74]. For simplicity, we will take the case where there is no black hole in either bulk, $\mu_i = 0$.

Following the same procedure as in chapter 2, the brane is constructed by glueing a solution in \mathcal{M}_1 to a solution in \mathcal{M}_2 , where the brane will form the common boundary. Then, in \mathcal{M}_i , the boundary $\partial\mathcal{M}_i$ is given by the section $(t_i(\tau), a_i(\tau), \mathbf{x}^\mu)$ of the bulk metric (2.9), where τ is the proper time of an observer comoving with the boundary and eqn. (2.11) applies as before, while the outward pointing unit normal in each spacetime is still given by eqn. (2.12). We evaluate the spatial components of (3.3) in the same manner as we did in chapter 2, (though without the inclusion of the intrinsic curvature terms now), and find

$$2\left\langle M^3 \frac{\dot{h}}{a} t \gamma_{ij} \right\rangle - \frac{\sigma}{6} \gamma_{ij} = \frac{1}{2} \left(T_{ij} - \frac{1}{3} T \gamma_{ij} \right). \quad (3.9)$$

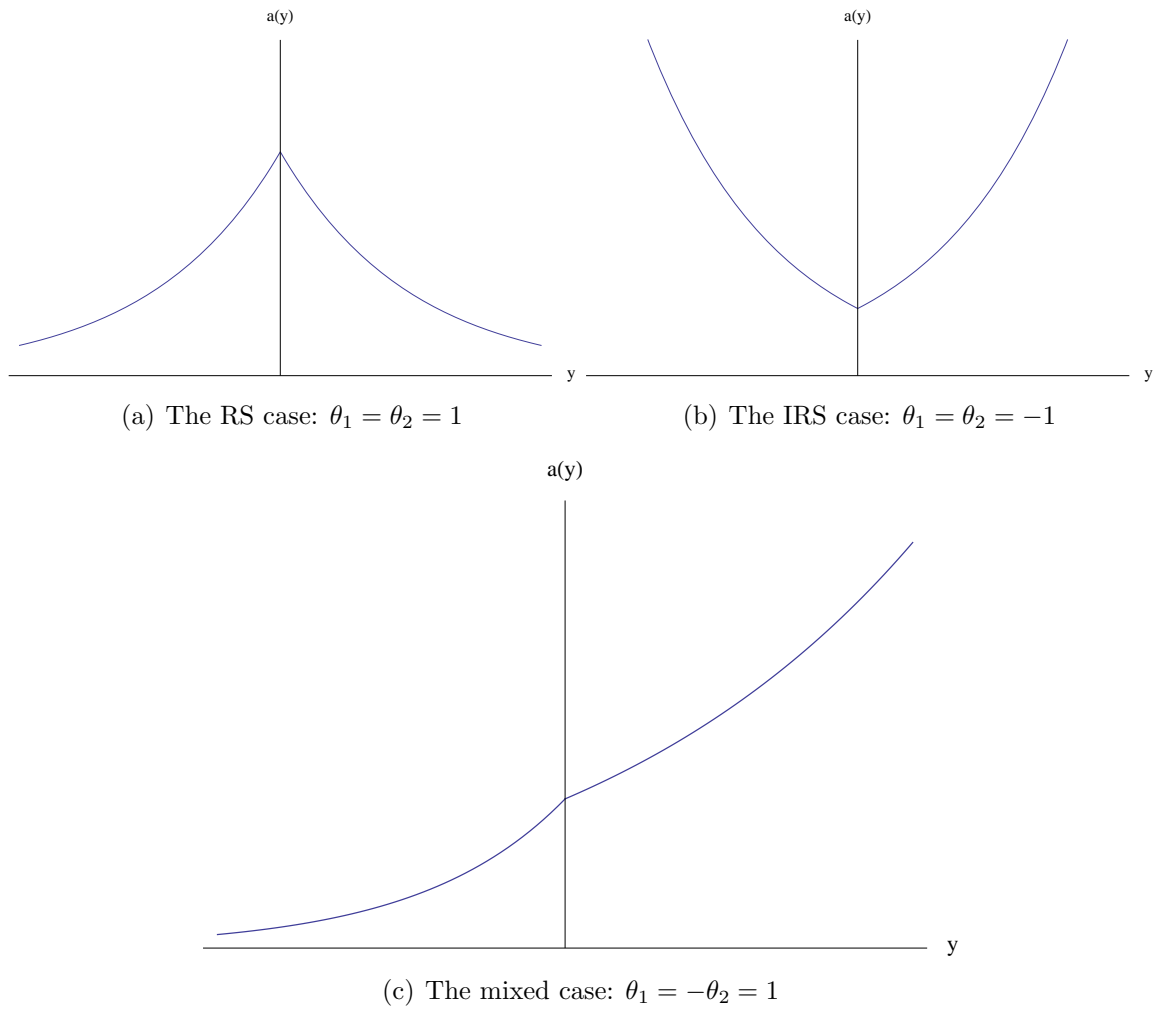


Figure 3.1: Representation of the 3 combinations of warp factor allowed in the asymmetric brane model

Finally, taking account of the extra brane tension term in the AC model, we substitute for σ using (3.8), and $h(a)$ using (2.10) with $\mu_i = 0$, and find that the modified Friedmann equation for the mixed case is

$$\rho = 6 \left[M_1^3 \left(\sqrt{H^2 + \frac{\kappa}{a^2} + k_1^2} - k_1 \right) - M_2^3 \left(\sqrt{H^2 + \frac{\kappa}{a^2} + k_2^2} - k_2 \right) \right]. \quad (3.10)$$

As we said at the beginning of the chapter, the AC model can produce 4D behaviour at certain scales, before gravity is modified in the infrared, producing 5D behaviour. We would like to know the range of scales over which these behaviours are obtained. We therefore follow the method of [47] and consider the linearised equations of motion. If we write the perturbed metric as $g_{ab} = \bar{g}_{ab} + h_{ab}$ and work in Gaussian normal coordinates ($h_{\mu z} = h_{zz} = 0$) and the transverse-traceless (TT) gauge ($\partial_\nu h_\mu^\nu = h_\mu^\mu = 0$), the linearised bulk equations of motion (2.6) are given by

$$\left[\frac{\partial^2}{a^2} + \frac{\partial^2}{\partial z^2} - 4k^2 \right] h_{\mu\nu}(x, y) = 0. \quad (3.11)$$

However, as explained in [44], the presence of matter on the brane causes it to bend, leading to problems in applying the Israel equations. Therefore a gauge transformation that yields new coordinates, which are also Gaussian normal, and positions the brane at $y = 0$ is needed, [47]:

$$y \rightarrow y - f(x), \quad x^\mu \rightarrow x^\mu - Q^\mu(x) + \frac{\theta}{2k}(1 - a^{-2})\partial^\mu f, \quad (3.12)$$

where $f(x)$ and $Q^\mu(x)$ are bulk quantities which can vary on either side of the brane. The metric perturbation can be recalculated in terms of these new coordinates using $h_{ab} = 2\nabla_{(a}\xi_{b)}$, where $x^a \rightarrow x^a + \xi^a$, and is found to be

$$h_{\mu\nu}^{new} = h_{\mu\nu}(x, y) + 2a^2 Q_{(\mu,\nu)} + k^{-2}(1 - a^2)\partial_\mu\partial_\nu F + 2F\bar{g}_{\mu\nu}, \quad (3.13)$$

where $F = \theta f k$ and $h_{\mu\nu}^{new}$ is the perturbation in the new coordinates. The linearised Israel equations can also be written in this coordinate system, varying eqn. (3.3) and using eqn. (3.8) to give

$$\Delta[M^3 h'_{\mu\nu}(x, 0)] - \frac{\sigma}{3} h_{\mu\nu}^{br} = \Sigma_{\mu\nu}(x), \quad (3.14)$$

where

$$\Sigma_{\mu\nu}(x) = T_{\mu\nu} - \frac{1}{3}T\eta_{\mu\nu} + 4\left\langle \frac{M^3\theta}{k} \right\rangle \partial_\mu \partial_\nu F . \quad (3.15)$$

$h_{\mu\nu}^{br}$ is the perturbation of the metric on the brane in the original coordinates, while a prime denotes differentiation with respect to the extra dimension.

If we now transform the linearised equations into momentum space (a tilde representing a Fourier transformed quantity), the general solution to the bulk equations of motion (3.11) is

$$\tilde{h}_{\mu\nu}(p, y) = A_{\mu\nu}(p)I_2\left(\frac{p}{ak}\right) + B_{\mu\nu}(p)K_2\left(\frac{p}{ak}\right) , \quad (3.16)$$

where I_2 and K_2 are modified Bessel functions of order n and $A_{\mu\nu}$ and $B_{\mu\nu}$ are unknown functions independent of the extra dimension; we also require that $\tilde{h}_{\mu\nu} \rightarrow 0$ as $|y| \rightarrow \infty$. For the three different cases of this model (RS, IRS and mixed), this results in the solution being written as

$$\tilde{h}_{\mu\nu}(p, y) = \frac{C_2(p/ak)}{C_2(p/k)} \tilde{h}_{\mu\nu}^{br} , \quad (3.17)$$

where we have used the properties of the modified Bessel functions, [101]:

$$I_2(z) \rightarrow 0, \quad K_2(z) \rightarrow \infty \quad \text{as } z \rightarrow 0 \quad (3.18)$$

$$I_2(z) \rightarrow \infty, \quad K_2(z) \rightarrow 0 \quad \text{as } z \rightarrow \infty , \quad (3.19)$$

(for some arbitrary z), to find that

$$C_2 = \begin{cases} K_2 & \text{for RS case} \\ I_2 & \text{for IRS case} , \end{cases} \quad (3.20)$$

and $C_2^{(1)} = K_2$, $C_2^{(2)} = I_2$ for the mixed case. If we insert this solution, (3.16), into the Fourier transform of the linearised Israel equation (3.14), we find the solution for the (Fourier transformed) brane metric as, [47]:

$$\tilde{h}_{\mu\nu} = \frac{\tilde{\Sigma}_{\mu\nu}(p)}{R(p)} , \quad (3.21)$$

where

$$R(p) = -2p \left\langle M^3 \theta \frac{C_1(p/k)}{C_2(p/k)} \right\rangle, \quad (3.22)$$

and we have used another property of Bessel functions, [101]:

$$zI_2'(z) + 2I_2(z) = zI_1(z) \quad zK_2'(z) + 2K_2(z) = -zK_1(z). \quad (3.23)$$

C_2 is given by eqn. (3.20) as before and in a similar manner,

$$C_1 = \begin{cases} -K_1 & \text{for RS case} \\ I_1 & \text{for IRS case,} \end{cases} \quad (3.24)$$

with $C_1^{(1)} = -K_1$, $C_1^{(2)} = I_1$ for the mixed case. If we now consider the brane metric in the new coordinates (which can be found by setting $y = 0$ in eqn. (3.13)) and transform it to momentum space:

$$\tilde{h}_{\mu\nu}^{br(new)} = \tilde{h}_{\mu\nu}^{br} + 2ip_{(\mu} \tilde{Q}_{\nu)} + 2\tilde{F} \tilde{\eta}_{\mu\nu} \quad (3.25)$$

we can rewrite it using eqn. (3.21), provided we choose our gauge term, $\tilde{Q}_\mu(p)$, to cancel the $p_\mu p_\nu$ term arising from $\tilde{\Sigma}_{\mu\nu}$. We also note that \tilde{F} is related to the transformed energy momentum tensor, \tilde{T} , which follows from the fact that $\Sigma_\mu^\mu = 0$ due to the metric perturbation being traceless, and finally obtain

$$\tilde{h}_{\mu\nu}^{br} = \frac{1}{R(p)} \left[\tilde{T}_{\mu\nu} - \frac{1}{3} \tilde{T} \tilde{\eta}_{\mu\nu} \right] - \frac{1}{6\alpha p^2} \tilde{T} \tilde{\eta}_{\mu\nu}, \quad (3.26)$$

where

$$\alpha = \left\langle \frac{M^3 \theta}{k} \right\rangle. \quad (3.27)$$

In order to find the scales at which the AC model exhibits 4D behaviour, we compare eqn. (3.26) to its 4D counterpart, [47]:

$$\tilde{h}_{\mu\nu} = \frac{1}{m_{pl}^2 p^2} \left[\tilde{T}_{\mu\nu} - \frac{1}{2} \tilde{T} \tilde{\eta}_{\mu\nu} \right]. \quad (3.28)$$

Comparing these two equations, we can see that for a 4D regime to exist, we require $R(p) \sim \alpha p^2$ and $\alpha = m_{pl}^2$. On calculating $R(p)$ (using Bessel function approximations

for small and large arguments) for the RS and IRS cases, the IRS case is found never to produce Einstein gravity, as it is never proportional to p^2 , whereas the RS case can in certain regimes, [47]. For the mixed case (on which we are concentrating), we can see that

$$R(p) = p \left[M_1^3 \frac{K_1(p/k_1)}{K_2(p/k_1)} + M_2^3 \frac{I_1(p/k_2)}{I_2(p/k_2)} \right]. \quad (3.29)$$

Introducing a new length scale, which can be seen as an analogue of the DGP crossover scale,

$$r_c = \frac{M_1^3}{M_2^3 k_1}, \quad (3.30)$$

Padilla, [47], found that

$$R(p) \sim \begin{cases} M_2^3 p & \text{for } k_2 \ll p \ll 1/r_c \\ \frac{1}{2} \frac{M_1^3}{k_1} p^2 & \text{for } 1/r_c \ll p \ll k_1 \\ M_1^3 p & \text{for } p \gg k_1. \end{cases} \quad (3.31)$$

Returning to coordinate space, we therefore find the range of scales over which gravity is four dimensional (i.e. where $R \sim p^2$) to be

$$k_1^{-1} \ll r \ll r_c, \quad (3.32)$$

which clearly requires $M_1 \gg M_2$. For this model to be phenomenologically viable, this range of scales must be appropriate. Since we are looking at r_c as representing the scale at which late time acceleration sets in and gravity is modified, we expect the crossover scale to be of order the current horizon size, $r_c \sim H_0^{-1}$, much as we discussed in chapter 2 for the DGP crossover scale, r_{DGP} . On the other hand, as mentioned in chapter 1, table-top tests of General Relativity, [36, 37], have confirmed its validity down to sub-mm scales, which fixes our largest frequency scale, k_1 (the UV cut-off of the theory), so that $k_1^{-1} \sim 0.1$ mm. These constraints give us a large hierarchy of scales, and, as already noted, require a large hierarchy in the parameters.

It is interesting to see these scales emerge from an analysis of the Friedmann equation (3.10). Obviously (3.10) looks nothing like the standard Friedmann equation, and so can only reduce to such in certain asymptotic limits. Setting $\kappa = 0$ for simplicity, and

using

$$\sqrt{H^2 + k^2} \simeq \begin{cases} k + \frac{H^2}{2k} & \text{for } H \ll k \\ H & \text{for } H \gg k \end{cases}, \quad (3.33)$$

we see that we can only get the H^2 behaviour required if $k_1 \gg k_2$, and we take $H \ll k_1$. In this regime, the Friedmann equation can be written as

$$\rho \simeq 3 \frac{M_1^3}{k_1} H^2 - 6M_2^3 \left(\sqrt{H^2 + k_2^2} - k_2 \right). \quad (3.34)$$

We therefore see the existence of an accelerating vacuum whenever

$$H_A^2 = 4k_1 \frac{M_2^3}{M_1^3} \left(k_1 \frac{M_2^3}{M_1^3} - k_2 \right) > 0. \quad (3.35)$$

We can also read off the 4D Planck mass by comparing with the standard 4D Friedmann equation, (2.24):

$$m_{pl}^2 \simeq \frac{M_1^3}{k_1} > 0. \quad (3.36)$$

This agrees with the expression derived in [47], and also with a direct computation of the propagator, (see appendix A of [1]).

As we said in section 3.1, we would like to compare (3.34) with the cosmological equations from the DGP model discussed in chapter 2. If we assume the model is flat or has very small non-zero curvature, the DGP brane cosmological equations (2.23) can be rewritten as

$$\rho = 3m_{pl}^2 H^2 - 6\epsilon M^3 H. \quad (3.37)$$

The choice of sign in the linear Hubble term is due to the choice of which part of the bulk is kept: the minus sign ($\epsilon = 1$), corresponding to the exterior being kept, is the self-accelerating branch as before, which has late time cosmological acceleration as discussed in chapter 2. The crossover scale r_{DGP} is defined as in eqn. (2.26).

To compare the asymmetric and DGP models, note that if we take $H \gg k_2$, then we may approximate the second bracket in (3.34), and obtain

$$\rho \simeq 3 \frac{M_1^3}{k_1} H^2 - 6M_2^3 H, \quad (3.38)$$

which is of course (3.37) after suitable substitution.

Over a large range of scales therefore, AC cosmology can be viewed as a generalisation of DGP cosmology. To parameterise this in a simple way for our analysis, we set

$$\alpha = \frac{k_1}{H_0} \frac{M_2^3}{M_1^3} \quad \beta = \frac{k_2}{H_0} \quad E = \frac{H}{H_0}, \quad (3.39)$$

where H_0 is the current value of the Hubble parameter. (3.10) then becomes:

$$\rho = 3m_{pl}^2 H_0^2 \left[E^2 + \frac{\kappa}{a^2 H_0^2} - 2\alpha \left(\sqrt{E^2 + \frac{\kappa}{a^2 H_0^2} + \beta^2} - \beta \right) \right]. \quad (3.40)$$

Here, $\alpha = (2H_0 r_{DGP})^{-1}$ is essentially the same as the DGP crossover scale, (2.26), and β is the new parameter coming from the asymmetric physics. It is precisely the effect of this new parameter which we seek to explore.

3.3 Asymmetric cosmology

In order to explore the effects of the AC model, it is useful to rewrite the Friedmann equation in an Einstein form by solving (3.40) for $E = H/H_0$:

$$E(z)^2 = \Omega_k (1+z)^2 + \Omega_i (1+z)^{3(1+w_i)} + 2\alpha(\alpha - \beta) + 2\alpha \sqrt{(\alpha - \beta)^2 + \Omega_i (1+z)^{3(1+w_i)}}. \quad (3.41)$$

Here, an implicit sum over the various contributions to the energy density with equations of state $p_i = w_i \rho_i$ is understood and $\Omega_k = -\kappa/a_0^2 H_0^2$ as before. Note that the + root of the quadratic is required to get the correct $\Omega \rightarrow 0$ limit of the Israel equations. We can now readily compare the AC model with Λ CDM and DGP, which are implicitly contained in (3.41): $\alpha = 0$ and we include an Ω_Λ for Λ CDM, and $\beta = 0$ for DGP (see eqn. (2.30), using $\alpha^2 = \Omega_{r_{DGP}}$). Since the DGP model has been carefully analysed with cosmological expansion data (see chapter 2 and references therein), here we focus qualitatively on the additional features the β term brings relative to DGP.

The aim of gravitationally driven late time acceleration is to avoid using a cosmological constant, (Ω_Λ) , therefore evaluating (3.41) at the current time gives a constraint between the model parameters α, β and the current matter and curvature densities:

$$\Omega_m = 1 - \Omega_k - 2\alpha(\sqrt{1 - \Omega_k + \beta^2} - \beta), \quad (3.42)$$

(ignoring the relatively insignificant radiation component). This means that once Ω_m and Ω_k are fixed, the asymmetric cosmology forms a one parameter family of solutions (note that DGP is entirely constrained by fixing Ω_m and Ω_k : see eqn. (2.32)). From (3.39), we see that both α and β are positive, and in addition self-acceleration requires $\beta < \alpha$ from (3.35). Thus our additional parametric degree of freedom in the asymmetric model has a fairly limited range.

The modified Friedmann equation (3.41) shows clearly the effect of β over the range $[0, \alpha]$. As already noted, $\beta = 0$ corresponds to the DGP model, with $\alpha^2 = \Omega_{r_{DGP}}$ in the usual notation of encoding the DGP crossover scale as an effective DGP Ω contribution. The other limit, $\beta = \alpha$, corresponds to an $n = 1/2$ Cardassian model, [26], or alternatively, a dark energy fluid with (constant) equation of state $w = -1/2$.

As with DGP, relaxing the constraint of flatness leads to a wider range of parameter choice:

$$\frac{(1 - \Omega_k - \Omega_m)}{2\sqrt{\Omega_m}} \geq \alpha \geq \frac{(1 - \Omega_k - \Omega_m)}{2\sqrt{1 - \Omega_k}}, \quad (3.43)$$

and the cosmological models now form a three parameter family, which can be labelled using $\{\Omega_m, \Omega_k, \alpha^2\}$ (or by trading one of the Ω parameters for β). In order to more readily compare with DGP results, we will use the former parameterisation, and compare results in the $\{\Omega_m, \alpha^2\}$ plane (recall $\alpha^2 = \Omega_{r_{DGP}}$ in DGP) either for various fixed β values with Ω_k varying, or fixed Ω_k values with β varying. In spite of the enlarged parameter space, the asymmetric cosmology turns out to be under more cosmological tension than DGP.

A nice way to encode this information is to consider the effective dark energy which is the difference between the square of the Hubble parameter and the matter content, [102, 103, 104]:

$$\Omega_{DE}(z) = 2\alpha(\alpha - \beta) + 2\alpha\sqrt{(\alpha - \beta)^2 + \Omega_i(1+z)^{3(1+w_i)}}, \quad (3.44)$$

where we have taken $\Omega_k = 0$ for simplicity. The effective dark energy pressure is then the discrepancy between the Einstein pressure and the actual pressure. The pressure is calculated using, [103]:

$$p = \frac{H^2}{4\pi G} \left(q - \frac{1}{2} \right), \quad (3.45)$$

where the deceleration parameter q is given by

$$q = \frac{H'(z)}{H(z)}(1+z) - 1. \quad (3.46)$$

For the full asymmetric model, using eqn. (3.41), we calculate the pressure to be

$$\frac{p_{ASY}}{3m_{pl}^2 H_0^2} = (1+w_i)\Omega_i(1+z)^{3(1+w_i)} + \frac{\alpha(1+w_i)\Omega_i(1+z)^{3(1+w_i)}}{\sqrt{(\alpha-\beta)^2 + \Omega_i(1+z)^{3(1+w_i)}}} - E(z)^2, \quad (3.47)$$

while the Einstein pressure is found to be

$$\frac{p_E}{3m_{pl}^2 H_0^2} = (1+w_i)\Omega_i(1+z)^{3(1+w_i)} - \Omega_i(1+z)^{3(1+w_i)}; \quad (3.48)$$

taking the difference between them, the effective dark energy pressure is

$$\Pi_{DE}(z) = -\alpha \left[2(\alpha-\beta) + \frac{2(\alpha-\beta)^2 + (1-w_i)\Omega_i(1+z)^{3(1+w_i)}}{\sqrt{(\alpha-\beta)^2 + \Omega_i(1+z)^{3(1+w_i)}}} \right]. \quad (3.49)$$

If we now use (3.44) and (3.49), we can find an effective equation of state,

$$w_{DE}(z) = -1 + \frac{(1+w_i)\Omega_i(1+z)^{3(1+w_i)}}{2[(\alpha-\beta)\sqrt{(\alpha-\beta)^2 + \Omega_i(1+z)^{3(1+w_i)}} + (\alpha-\beta)^2 + \Omega_i(1+z)^{3(1+w_i)}]}. \quad (3.50)$$

This shows how the equation of state always has $w \geq -1$ for $\alpha \geq \beta$, and thus the model can never enter a phantom regime. We also see how for $\beta > 0$, w is raised from its DGP ($\beta = 0$) value (see figure 3.2). Overall therefore, we expect that expansion data will favour a lower Ω_m , offsetting the increased value of w , in both DGP and AC models.

In order to see this explicitly, we look qualitatively at the effect of the AC model compared to DGP on various tests of the cosmological expansion history at the different epochs discussed in chapter 2, concentrating on type Ia supernovae, [100, 9, 10] and the cosmic microwave background, [78, 83].

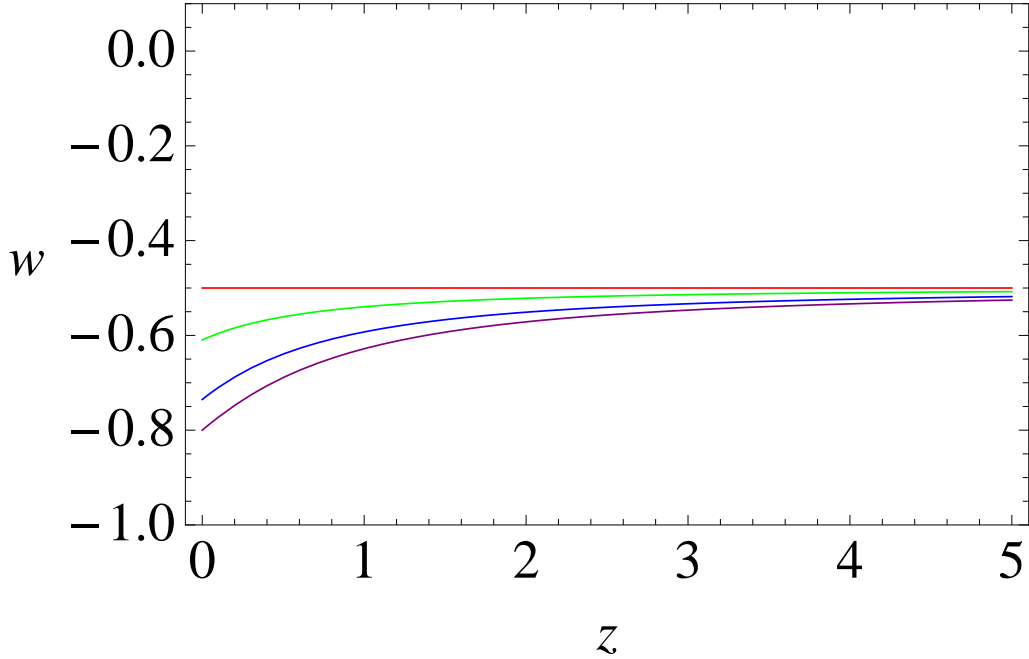


Figure 3.2: Variation of the effective dark energy equation of state taking $\Omega_m = 0.25$. The values of α run from the minimum allowed ($\beta = 0$, the DGP value) in purple, to the maximum value, $\alpha = \beta$, shown in red. These clearly show how increasing β neutralises acceleration in asymmetric cosmology.

We first look at the type Ia supernovae redshift-luminosity relation based on the luminosity distance, d_L , which is given by eqn. (2.33), as discussed in chapter 2. Since the Hubble parameter is higher in AC cosmologies (at fixed Ω_m) and increases with increasing β , (2.33) shows that this results in a lessening of the luminosity distance and hence a lower magnitude. Figure 3.3 demonstrates this with a direct redshift-magnitude plot.

A more conventional visualisation of the effect of the AC model is given by plotting the preferred regions of $\{\Omega_m, \alpha^2\}$ parameter space at different values of Ω_k , β . Figure 3.4 shows the projection on the $\{\Omega_m, \alpha^2\}$ plane at fixed β and fixed Ω_k values respectively: α^2 is plotted against Ω_m as this more readily compares with the $\Omega_{r_{DGP}}$ parameter conventionally used in the analysis of DGP models. We calculate an expression for χ^2 using the ESSENCE supernova dataset, [100, 9, 10], containing 192 datapoints:

$$\chi_{red}^2 = \frac{1}{192} \sum \frac{(\mu_{obs} - 5\text{Log}_{10}d_L(z) - 43.3)^2}{\mu_{err}^2} \quad (3.51)$$

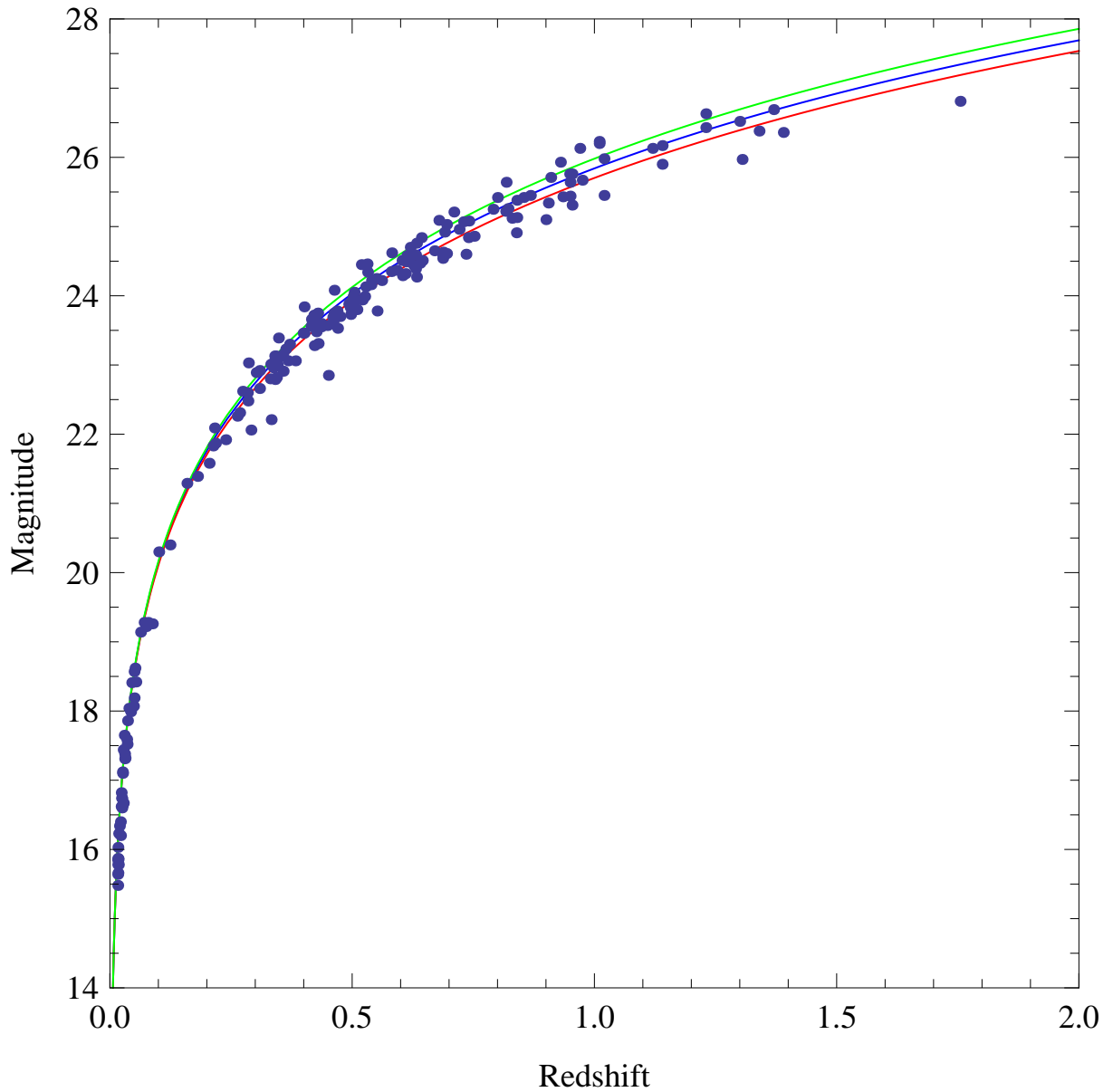


Figure 3.3: Plot of magnitude vs. redshift for (from top to bottom curve) Λ CDM (green), DGP (blue) and the AC model (with $\alpha = 0.702$, $\beta = 0.702$) (red), along with the ESSENCE supernova redshift data. $\Omega_m = 0.27$.

where we calculate $d_L(z)$ from (2.33), using (3.41) for $E(z)$. The contours plotted in figure 3.4 are then 1σ contours, found using $\chi_{min}^2 + \Delta\chi^2$, where $\Delta\chi^2$ is a standard value and we minimise (3.51) over the model parameters α and Ω_m .

The lefthand figure indicates how the preferred region of parameter space reacts to the β parameter (two values, $\beta = 0, \alpha/2$ are shown), and the righthand figure how the parameter space reacts to Ω_k for general β . In each case the figure shows that α increases in response to increasing β , and although the effect on Ω_m is less marked, it decreases slightly. Inspection of (3.41) shows why this is so. In effect, fitting the data is accomplished by keeping $E(z)$ relatively unchanged. If we increase β , we can see that this can be mostly counterbalanced by an increase in α , with possible sub-leading changes in the other parameters. It is interesting to note that the projection at fixed Ω_k is relatively insensitive to that value of Ω_k , as can be seen from the large overlap between the bands, despite the rather large value of Ω_k chosen for clarity of the plot. The flat universe band is much broader than the $\Omega_k = 0.1$ band because the effect of the geometry (via the sinh function in the luminosity distance (2.33)) tends to magnify any variations in the comoving distance due to variations in the parameters.

It is clearly not difficult to reproduce the supernova redshift-luminosity relation in isolation, particularly if the possibility of an open universe is included. However, as already discussed, the real tension for DGP (and even more so for the asymmetric model) is in combining the supernova constraints with the constraints from other cosmological data, [62, 60, 61].

The CMB shift parameter, as in chapter 2, is given by

$$R(z_*) = \frac{\sqrt{\Omega_m} H_0}{c} (1 + z_*) D_A(z_*) = \frac{\sqrt{\Omega_m}}{\sqrt{|\Omega_k|}} \mathcal{S} \left(\sqrt{|\Omega_k|} \int_0^{z_*} \frac{dz'}{E(z')} \right) \quad (3.52)$$

where $z_* = 1090.51 \pm 0.95$ is the redshift at decoupling, [78], (and c has been temporarily reintroduced for reference). The problem with lowering Ω_m now becomes more apparent. While we can ensure that the comoving distance is maintained by dropping Ω_m , the shift parameter is also lowered by this process. Indeed, flat DGP requires $\Omega_m \simeq 0.35$ to match the WMAP 5 year value $R = 1.71 \pm 0.02$, [78, 83]. However, one feature revealed by the β parameter is that for sufficiently large Ω_k (or small Ω_m), the angular diameter actually increases sufficiently with decreasing Ω_m to outweigh this effect, and the shift parameter thus increases with decreasing Ω_m .

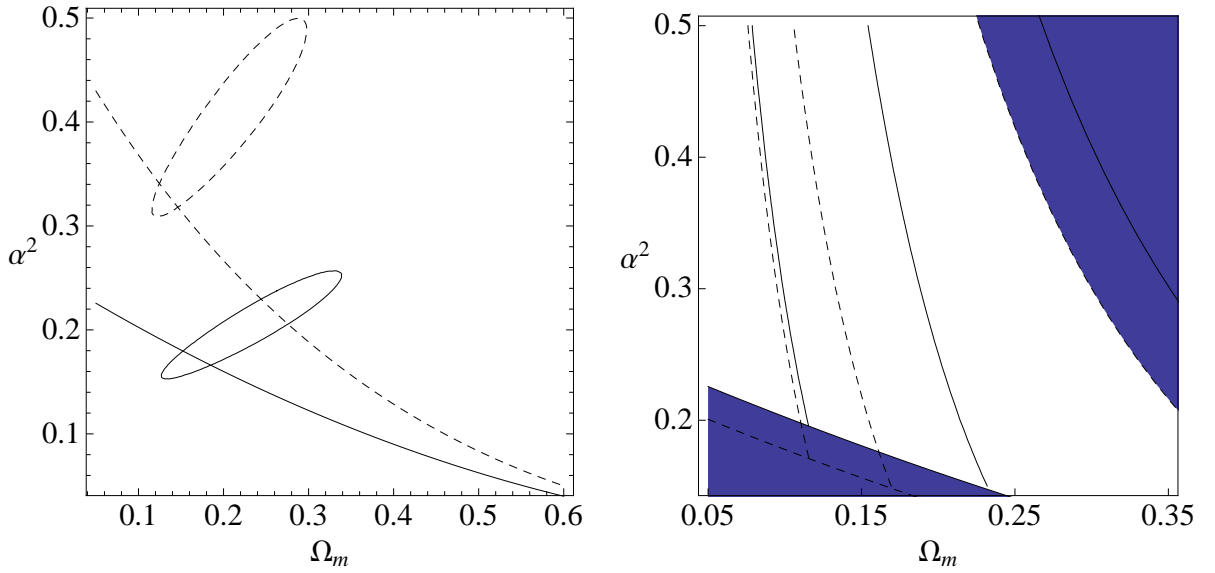


Figure 3.4: An illustration of the constraints on parameter space due to the supernova data. 1σ contours are plotted in all cases. On the left, two fixed values of β are shown: $\beta = 0$ is the solid contour, and $\beta = \alpha/2$ the dashed contour (the separate lines indicate $\Omega_k = 0$ for each β value). In the righthand figure, β now varies freely and the bands indicate two fixed values of Ω_k : the dashed contour, $\Omega_k = 0.1$, and the solid contour $\Omega_k = 0$. The upper and lower bounding values of β are also shown.

In order to compare the shift parameter constraint on the AC model to the situation with the DGP model, [62, 60, 61], we allow for open, flat and closed cosmologies, and test the parameter space compatible with the given shift parameter using the stated WMAP range above. Figure 3.5 shows allowed regions of $\{\Omega_m, \alpha^2\}$ parameter space projecting onto fixed β and fixed Ω_k subspaces.

The lefthand figure in figure 3.5 shows three different β values ranging from the DGP to the Cardassian limit. These show that as β is increased, preferred values of Ω_m become higher. The righthand figure shows three different Ω_k values. We chose three indicative values of Ω_k , the flat universe, $\Omega_k = 0.03$ (the best fit value for the open DGP model according to the analysis of Song, Sawicki and Hu in [60]) and 0.06 to illustrate the appearance of a minimum in the allowed region. The minimum appears because decreasing Ω_m decreases $E(z)$ over the redshift range, which, together with the magnifying effect of the sinh function, overwhelms the decrease in the prefactor of the shift parameter and results in an overall increase of R_* . In this plot, the limiting values of β are shown, and increasing β corresponds to moving roughly diagonally upwards across the plot. Once again, this indicates that the preferred value of Ω_m generally increases as β is increased.

We can now see how even just these two constraints on parameter space are problematic by combining them, since increasing β tends to prefer a decreased Ω_m to fit the supernova data, yet an increased Ω_m to fit the CMB shift parameter. Increasing Ω_k in general causes the two ranges for Ω_m and α to move together, but unfortunately this pushes Ω_m to an unacceptably small value. In figure 3.6 we combine the plots, and include for reference an indication of the constraint coming from the baryon acoustic oscillation peak detected by the SDSS survey, [84, 85]. This is usually represented as a dimensionless constant

$$A = D_V(z_1) \frac{\sqrt{\Omega_m} H_0}{cz_1} = \frac{\sqrt{\Omega_m}}{E(z_1)^{1/3}} \left[\frac{1}{z_1 \sqrt{|\Omega_k|}} \mathcal{S} \left(\sqrt{|\Omega_k|} \int_0^{z_1} \frac{dz'}{E(z')} \right) \right]^{2/3} = 0.469 \pm 0.017, \quad (3.53)$$

where $z_1 = 0.35$, and D_V is the geometric average dilation scale, [84, 85]. As mentioned in chapter 2, there is some debate as to whether this measure should be used for models which do not behave as a constant equation of state dark energy, [86, 63, 87], and in particular where growth of perturbations may differ significantly from the Einstein case. The perturbation theory as presented in appendix A of [1] indicates that the AC model is much the same as DGP, and we do not propose to add to this debate here. Nonetheless,

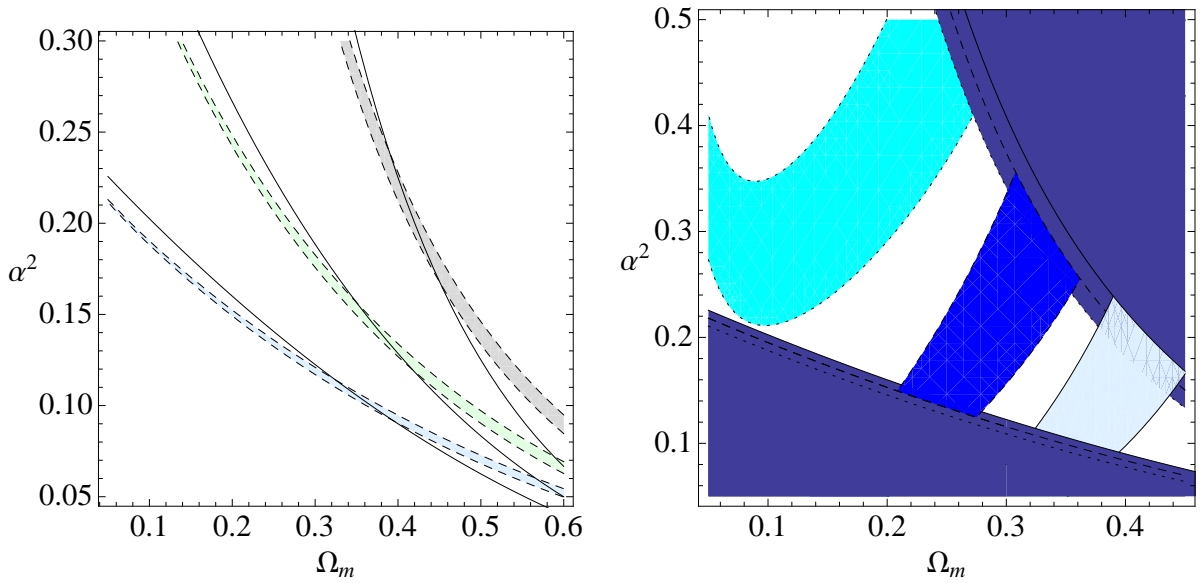


Figure 3.5: A depiction of the region of asymmetric cosmology parameter space consistent with the shift parameter. On the left, Ω_k varies freely, and three fixed values of β are shown: $\beta = 0$, or the DGP limit, is the lowest (blue) band, the green band an intermediate value of β , and the grey band the maximal value of β . The solid lines indicate $\Omega_k = 0$. On the right, β now varies freely and the bands indicate three fixed values of Ω_k : the lightest band on the right is a flat universe, the middle dark band is $\Omega_k = 0.03$, and the left hand (cyan) band is $\Omega_k = 0.06$, with the bounding values of β indicated in each case. The allowed regions in the plots are obtained using WMAP 5 year values.

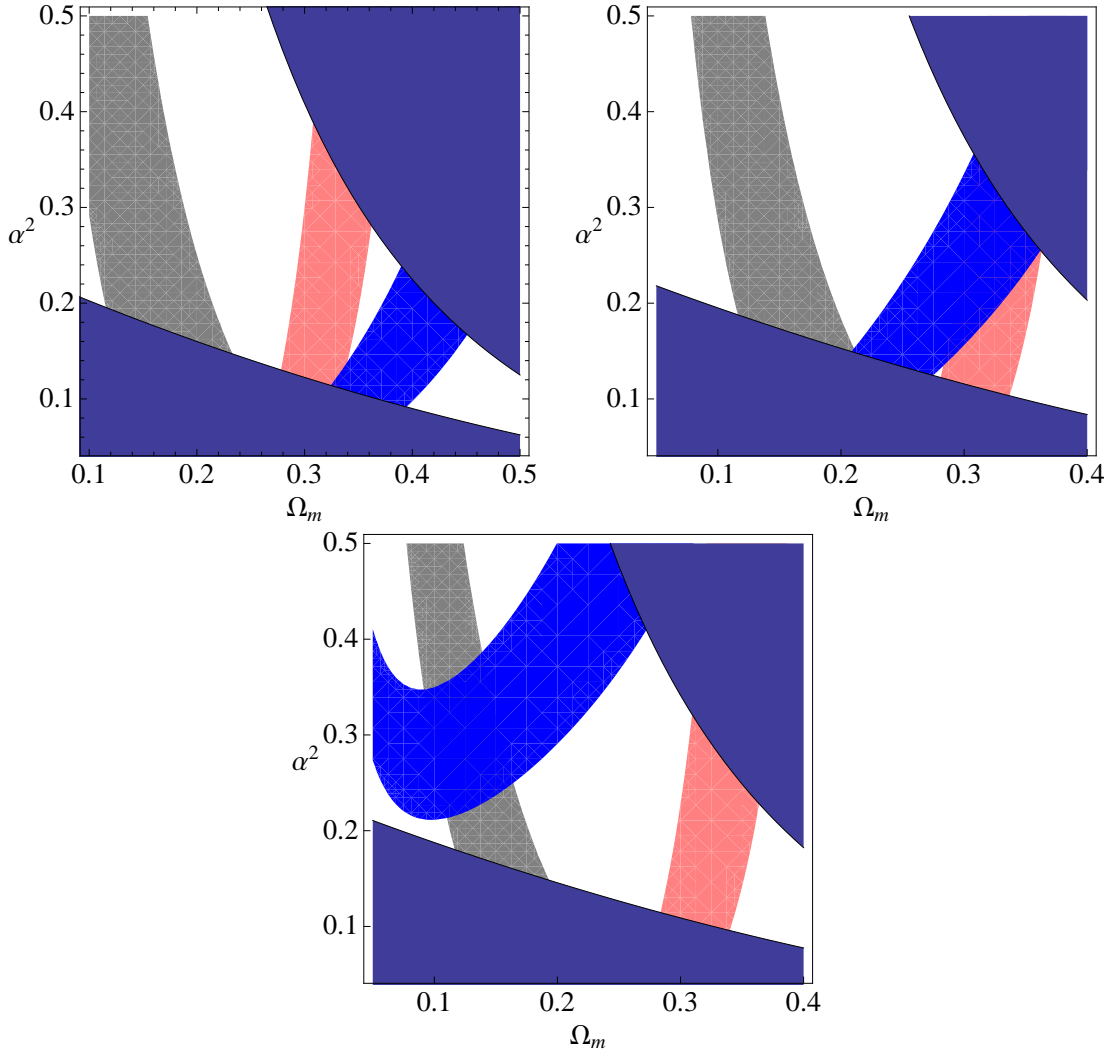


Figure 3.6: A look at the combined effect on the parameter space of asymmetric cosmology fixing Ω_k (0, 0.03, and 0.06 respectively) and allowing β to vary between its two limits as indicated. The dark (blue) band shows the shift parameter preferred range of Ω_m and α^2 , the lighter (grey) band from the supernova data, and the lightest (pink) band that from the BAO constraint.

we include this band of parameter space as it is indicative of how serious a problem structure formation presents. We do not however use it to constrain our parameters. For example, in the $\Omega_k = 0, 0.03$ plots, the BAO strip suggests that while these models might be a significantly poorer fit to the data than Λ CDM, structure formation is not a particular problem; the main issue in these plots is the way the other bands respond to increasing β .

Figure 3.6 shows explicitly the problem of increasing β on the parameter space. For $\Omega_k = 0, 0.03$, increasing β causes the allowed regions of parameter space to diverge.

For the relatively large value of $\Omega_k = 0.06$, the supernova and shift parameter regions do overlap, centred around $\alpha^2 \sim 0.28$, $\Omega_m \sim 0.13$ (with $\beta \sim 0.4\alpha$). However, even ignoring the discrepancy with the BAO strip (which is severe) this overlap occurs at an unacceptably low value of Ω_m . WMAP constrains $\Omega_m h^2 = 0.1326 \pm 0.0063$, [78], meanwhile the Hubble Key Project finds $h = 0.72 \pm 0.08$, [88]. Therefore, taking the largest allowable value of Ω_m as indicated in the final plot of figure 3.6, $\Omega_m \simeq 0.17$, requires a h value of $0.86 - 0.9$, well above the Hubble Key Project range.

Thus our results show that increasing β increases the tension in fitting the data relative to the DGP model. In spite of the enlarged parameter space, the asymmetric cosmology turns out to be under more cosmological tension. This is because for a given matter content, (3.41) shows that the Hubble parameter increases with redshift more rapidly than in DGP (which itself is more rapid than Λ CDM) as the β parameter increases. This means that for a given Ω_m , the comoving distance out to a particular redshift is lower in asymmetric gravity than DGP, which is correspondingly lower than Λ CDM. Unfortunately, this means that AC cosmologies are therefore not a good description of our universe.

3.4 Conclusions

In this chapter, we have examined the asymmetric brane model, [46, 47], a braneworld theory of modified gravity, with a view to exploring how well it can explain the late time acceleration of the universe. Above a Hubble distance of order 1 mm, the effective evolution of this model is a one-parameter generalisation of the DGP model and the additional parameter is found to impede the expansion of the universe, lowering it relative to DGP. As such, it turns out that the asymmetric model has more problems fitting the cosmological expansion data than DGP. In addition, recent work on ghosts in the stealth model, [73], suggests that any model with a self-accelerating branch in its solution will contain ghosts. This description encompasses the AC model and unfortunately it seems that, like DGP, pure AC models are not viable cosmological models for late time acceleration. Nonetheless, as we stated earlier, the analysis is a valuable exercise in checking the behaviour of all possible modified gravity models available in order to either identify or rule out alternatives to Λ CDM.

Chapter 4

Cosmic strings and gravitational wave bursts

4.1 Introduction

In the rest of this thesis, we turn our attention from the late time behaviour to one of the early universe consequences of braneworld models - cosmic strings - and consider the effects that extra dimensions can have on them.

It has been realised in recent decades that phase transitions could occur in the early universe, as they do in condensed matter systems, resulting in the formation of topological defects, which could still be in existence today, [105]. Topological defects are a generic prediction of grand unification theories: theories which predict the unification of the strong and electroweak forces at very high energy scales (the SM and Minimal Supersymmetric Standard Model (MSSM) suggest that this occurs at $\sim 10^{16}$ GeV, [106]). The different forces we observe today, along with the well-known standard model gauge group, $SU(3) \times SU(2) \times U(1)$, then appear when the original gauge symmetry is broken as the early universe cools with expansion. If they exist, topological defects could provide an invaluable method of studying the behaviour of the very early universe. Unfortunately energies at this scale are far beyond those accessible by (even the most energetic) accelerator experiments today, however their possible effects on astrophysical phenomena could provide an alternative testing ground.

The formation of the various types of topological defect - domain walls, cosmic strings, monopoles and other hybrid structures - depends on the structure of the vacuum manifold, [107]. However it has been found, [105], that the existence of domain walls or

monopoles would be cosmologically disastrous for our universe, as the topological defects come to dominate at late times. A network of cosmic strings, on the other hand, has been shown to be cosmologically benign, [108]. The majority of research into the astrophysical and cosmological effects of topological defects has therefore concentrated on cosmic strings.

If we consider the simplest model of spontaneous symmetry breaking, the Goldstone model, [105, 109, 110], we can write down a Lagrangian of the form

$$\mathcal{L} = (\partial_\mu \phi^\dagger)(\partial^\mu \phi) - \frac{1}{4}\lambda(\phi^\dagger \phi - \eta^2)^2, \quad (4.1)$$

where λ and η are positive constants and ϕ is a complex scalar field. This Lagrangian is invariant under a global $U(1)$ transformation:

$$\phi(x) \rightarrow e^{i\alpha} \phi(x). \quad (4.2)$$

The last term in eqn. (4.1) is the potential, $V(\phi)$, whose minima, it can easily be seen, lie on a circle of radius $|\phi| = \eta$, meaning that the vacuum state of the theory can be written as a non-zero expectation value:

$$\langle 0|\phi|0\rangle = \eta e^{i\theta}, \quad (4.3)$$

where θ is an arbitrary phase. If we now consider the effect of the $U(1)$ transformation on the phase, we find that $\theta \rightarrow \theta + \alpha$: while the Lagrangian is invariant, the vacuum state is not and we say that the symmetry is spontaneously broken. The values the field ϕ takes at different points in the vacuum are independent of each other if the regions are separated by a distance greater than some correlation length, ξ , [107, 111]. As the field cannot travel faster than the speed of light, this correlation length will always be smaller than the horizon, [105].

A cosmic string is formed if the vacuum manifold is not simply connected, i.e. it contains holes around which loops can get trapped. As the path of a closed loop is traced out in physical space, it is possible for the field, ϕ , to wrap around the hole formed by the minima of the potential in the vacuum. As the field wraps around the hole in the vacuum manifold, it develops a non-trivial winding, since the phase jumps in value (e.g. from 0 to 2π) when the field completes a full turn of the hole in the manifold. This phase jump can only be continuously resolved if the field takes the value of $\phi = 0$, which is situated at the top of the potential, V . This state is therefore energetically

disfavoured and so the winding of the string will remain. The structure ‘trapped’ inside this winding is a cosmic string. These strings must be infinite or form closed loops, [109], as it is otherwise possible to continuously resolve the winding, causing the defect to collapse.

Cosmic strings have a finite width, typically comparable to the Compton wavelength of a particle whose mass is of the order of the symmetry breaking scale. In the case of the GUT scale this corresponds to a thickness of $\sim 10^{-29}$ cm, [112, 113]. Given that this distance is so much smaller than astrophysical or cosmological scales, it is acceptable to view cosmic strings as idealised zero-width objects. In this case, the action of the cosmic string can be approximated using the Nambu-Goto action, [114]:

$$S = -\mu \int d^2\sigma \sqrt{\gamma}. \quad (4.4)$$

Strings which intersect each other (or themselves) intercommute, or exchange partners rather than passing through one another and classical strings which intersect almost always intercommute, [115, 116, 117]. This process leads to the formation of cosmic string loops in the case of a self-intersection, as a portion of the string is cut off.

Cosmic strings loops were originally studied in the context of structure formation and loops were thought to be ideal seeds for galactic formation, [118, 119, 120, 121]. Cosmic strings were also considered as a possible candidate to source the temperature fluctuations observed in the cosmic microwave background (CMB). They were ruled out as the primary source of the fluctuations, as the angular power spectrum of the cosmic strings was found to be rather featureless, most notably lacking the distinctive series of acoustic peaks observed by the WMAP experiment at small angular scales, [122, 123], however, it is still possible that they could contribute at a subdominant level, [124]. Nevertheless, while these original motivations have not stood the test of time, cosmic strings are still of interest today, as they could provide possible explanations of various astrophysical phenomena such as gamma-ray bursts, [125, 126, 127], and high energy cosmic rays, [128, 129], while straight strings produce a conical deficit in spacetime, which can lead to gravitational lensing, [112, 130, 131]. Finally, cosmic string loops emit gravitational waves as they oscillate under their own tension, losing energy at a rate of

$$\dot{E} \sim \Gamma G\mu^2, \quad (4.5)$$

found using the quadrupole formula, [132], where μ is the string tension, G is Newton's gravitational constant and Γ is a constant of proportionality. The production of cosmic string loops through intercommutation fragments straight strings, and the decay of these loops following their formation is an important energy loss mechanism for a network of cosmic strings, diluting the density of strings in the network, thus preventing strings from coming to dominate the universe, [119, 115]. We focus on this gravitational radiation from cosmic string loops for the rest of the chapter.

Gravitational waves, [133], are an important prediction of General Relativity which can be thought of as 'ripples' in the geometry of spacetime, propagating at the speed of light. However, despite significant efforts and various experiments and detectors, they have yet to be observed. The main reason for the lack of direct detections so far is that the deformation of objects due to the passage of a gravitational wave from a distant source (as any promising source is likely to be) is expected to be extremely small. The usual method of computing the expected amplitude of a wave from such a source uses the linearised form of the Einstein equations, which take the form

$$\square \bar{h}_{\mu\nu} = -16\pi G T_{\mu\nu} , \quad (4.6)$$

where $h_{\mu\nu}$ is the metric perturbation generated by the source, $\bar{h}_{\mu\nu} \equiv h_{\mu\nu} - \frac{1}{2}h\eta_{\mu\nu}$ is the trace-reversed metric perturbation and the harmonic gauge ($\partial^\nu \bar{h}_{\mu\nu} = 0$) is used. Indeed the only indirect evidence for the existence of gravitational waves comes from the observations of a binary pulsar discovered by Hulse and Taylor, [134, 135], in 1974, where it was found that the changes in the pulsar rotation period agreed with the predictions made by Einstein for energy being lost to gravitational radiation. Pulsar timing experiments are ongoing today, allowing for the possibility that extremely low (nHz) frequency gravitational waves will be detected, [136, 137].

The main focus for the direct detection of gravitational waves is on experiments using interferometric methods. The current interferometer experiments searching for a gravitational wave signal are Virgo, [138, 139], in Italy, GEO 600, [140, 141], in Germany and LIGO (the Laser Interferometer Gravitational-Wave Observatory), [142], in the US. In these experiments, a laser beam is split and passed into two orthogonal arms, where it travels back and forth a number of times, reflecting off mirrors suspended at either end of each arm, before being recombined. Any variation in the path length arising from changes in the distances between the mirrors due to perturbations from gravitational waves, corresponds to a shift in the relative phase of the beams, which can be used to

measure the amplitude of the gravitational waves. A number of science runs have taken place at all of these detectors (indeed LIGO has performed searches for gravitational wave bursts from cosmic strings, [143]), but as yet, no gravitational wave has been observed. The frequency sensitivity of all ground-based interferometers is constrained by a number of factors. In particular, the lowest frequency cutoff (of ~ 10 Hz) is determined by environmental noise. For this reason, a space-based interferometer mission, known as LISA, [144], (the Laser Interferometer Space Antenna) is also planned, which it is hoped will be sensitive to gravitational waves at lower frequencies.

However, interferometers are not the only detectors where it is hoped gravitational radiation will be discovered. Another class of experiments hoping to perform a direct detection of gravitational waves are resonant or bar detectors, [145]. These experiments were the original way in which attempts at detecting gravitational waves were carried out and were pioneered by Weber, [146, 147]. They look for deviations from a resonant frequency of vibration of a metal bar which would occur if the bar were to be deformed by a gravitational wave. While they have less flexibility than interferometers, being able to detect disturbances around their resonant frequency only, they do have the advantage of being able to run in a more continuous manner without detector upgrades. Finally, the recent papers of Cruise et al., [148, 149], describe a prototype experiment for detecting very high frequency gravitational radiation based on interactions between electromagnetic and gravitational waves.

While all cosmic string loops emit gravitational radiation as they oscillate, there are two cases in which the radiation emitted has a peculiarly strong and distinctive signal. Cosmic string cusps and kinks are phenomena which will always appear when cosmic string loops are considered. A cusp is formed when a point on the loop is moving at the speed of light, while kinks arise from a discontinuity in the tangent vector to the loop which occurs at any string intercommutation. The details of their formation cause cusps and kinks to emit high frequency, highly directed bursts of gravitational radiation which produce an easily recognisable signal. These gravitational waves bursts (GWB's) have been discussed in detail in the papers of Damour and Vilenkin, [50, 150, 51]. In the rest of this chapter, we review the formation of cosmic string cusps and the calculation of the cusp gravitational wave burst signal performed by Damour and Vilenkin, [50], in anticipation of the inclusion of extra dimensions.

4.2 String motion and cusps

In order to consider cosmic string loops in higher dimensions, we begin by briefly reviewing the kinematics of cosmic strings in 4 spacetime dimensions, deriving the general form of a string solution and showing how cusps are generic. This formulation was largely developed by Kibble and Turok, [151, 121], and is the standard method for finding loop trajectories.

Cosmic strings are usually studied using a worldsheet formalism, where the worldsheet is the 2D manifold traced out by the string loop as it moves through the usual 4D spacetime. Let $X^\mu(\sigma^A)$ be the spacetime coordinates of the string worldsheet, where $\sigma^A = \{\tau, \sigma\}$ are intrinsic coordinates on the worldsheet: τ is the worldsheet time coordinate and σ represents motion along the string. For the closed loops considered in this chapter, $\sigma \in [0, L]$, where L is the length of the loop. The induced metric on the worldsheet appearing in the Nambu-Goto action, (4.4), is then:

$$\gamma_{AB} = \frac{\partial X^\mu}{\partial \sigma^A} \frac{\partial X^\nu}{\partial \sigma^B} g_{\mu\nu}, \quad (4.7)$$

where $g_{\mu\nu}$ is the spacetime metric. The action (4.4) is therefore proportional to the area of the string worldsheet, where the constant of proportionality μ , is the tension, or mass per unit length of the string, as in eqn. (4.5). Note that cosmic strings have a tension along their length equal to their energy density.

Because we are dealing with a two dimensional metric, we can always choose a gauge in which γ is conformally flat:

$$\dot{X}^\mu X'^\nu g_{\mu\nu} = 0 \quad (4.8)$$

$$\left(\dot{X}^\mu \dot{X}^\nu + X'^\mu X'^\nu \right) g_{\mu\nu} = 0, \quad (4.9)$$

where a dot denotes $\partial/\partial\tau$ and a prime $\partial/\partial\sigma$. Kibble and Turok then chose the spacetime coordinates to coincide with the centre of mass frame of the string, and the worldsheet time coordinate to correspond with the spacetime time (temporal gauge). Thus writing $X^\mu = (\tau, \mathbf{r}(\tau, \sigma))$, we have:

$$\dot{\mathbf{r}} \cdot \mathbf{r}' = 0 \quad (4.10)$$

$$\dot{\mathbf{r}}^2 + \mathbf{r}'^2 = 1 \quad (4.11)$$

$$\ddot{\mathbf{r}} - \mathbf{r}'' = 0, \quad (4.12)$$

where the first two equations correspond to the gauge constraints, and the final equation is the wave equation of motion for the string. It is conventional to use lightcone coordinates:

$$\sigma_{\pm} = \tau \pm \sigma , \quad (4.13)$$

in which the solutions to the equation of motion (4.12) take the form of left and right moving waves, conventionally written in the form

$$\mathbf{r} = \frac{1}{2}[\mathbf{a}(\sigma_-) + \mathbf{b}(\sigma_+)] , \quad (4.14)$$

where the gauge conditions constrain \mathbf{a}' and \mathbf{b}' to lie on a unit sphere, commonly dubbed the ‘Kibble-Turok’ sphere:

$$\mathbf{a}'^2 = \mathbf{b}'^2 = 1 . \quad (4.15)$$

Notice that while the periodicity of \mathbf{a} and \mathbf{b} is L , the periodicity of the actual motion of the string is $L/2$, since $\mathbf{r}(\sigma + L/2, \tau + L/2) = \mathbf{r}(\sigma, \tau)$.

There is an additional constraint that must be satisfied by both \mathbf{a}' and \mathbf{b}' , for consistency with the facts that the loop is closed, and that we are in the centre of mass frame. The former condition requires that $\mathbf{r}(\tau, 0) = \mathbf{r}(\tau, L)$, hence

$$\int_0^L \mathbf{r}' d\sigma = \int_0^L (\mathbf{b}' - \mathbf{a}') d\sigma = 0 . \quad (4.16)$$

The latter condition requires the average momentum integrated along the string to vanish, i.e.:

$$\int_0^L \dot{\mathbf{r}} d\sigma = \int_0^L (\mathbf{b}' + \mathbf{a}') d\sigma = 0 , \quad (4.17)$$

thus

$$\int_0^L \mathbf{b}' d\sigma = \int_0^L \mathbf{a}' d\sigma = 0 . \quad (4.18)$$

Hence \mathbf{a}' and \mathbf{b}' follow trajectories on a unit sphere with zero weight – their average position is the origin. Since they both define curves on a two dimensional manifold which must cover both halves of the sphere equally, they will in general cross. Inserting

the expression for \mathbf{r} into the intrinsic metric, (4.7), gives:

$$\gamma_{AB} = \frac{1}{2}(1 - \mathbf{a}' \cdot \mathbf{b}')\eta_{AB}, \quad (4.19)$$

thus when \mathbf{a}' and \mathbf{b}' are collinear, the metric becomes degenerate and a point of the worldsheet instantaneously reaches the speed of light. Strictly speaking the mass concentration on the string is infinite at this point, however as it has zero area the total energy is finite. However, since the vicinity of this point is highly relativistic, this rapidly moving part of the worldsheet will have high momentum, and hence we expect some significant gravitational interaction. Due to the extreme behaviour of the worldsheet at these points, there has been some question as to whether the Nambu action (4.4) is still valid near cusps. This issue was discussed in appendix A of [3], where the use of the uncorrected Nambu action, eqn. (4.4), is justified with the use of a lower bound on the lightcone coordinates: $\sigma_{min} \sim (wL)^{1/2}$, where w is the string width. Due to the size of the string width, this quantity is small enough that the cusp is very well approximated by the uncorrected action. Cusps are thus transient but powerful events; moreover, they are generic on string trajectories (notwithstanding the effect of small scale structure, [152]). We now turn to a summary of the gravitational effects of cusps.

4.3 Gravitational waves from cusps

It is worth reviewing the Damour-Vilenkin argument, [50], as the derivation of the gravitational wave signal is quite involved and lengthy. Damour and Vilenkin (DV) first computed the linearised metric perturbation arising from a single cusp event on a cosmic string loop of length L in flat spacetime. The waveform of the cusp was found to have a power law behaviour of $f^{-4/3}$ (or $f^{-1/3}$ in their logarithmic Fourier representation) at large frequencies, f , of the gravitational wave. They then used this flat spacetime waveform to infer the cosmological waveform behaviour in the geometric optics limit, thus deriving a gravitational wave amplitude of a single cusp event which decays quite strongly with redshift. Finally, by considering a one scale model for the string network, they computed an event rate for observing cusp GWB's which increased rapidly with redshift z . By choosing a physically reasonable event rate, and picking a fiducial experimentally motivated (detector based) frequency, they determined the typical redshift contributing to the GWB and calculated the amplitude of the cusp signal, presenting the results as a function of $G\mu$.

In order to present an analytic argument, DV introduced various interpolating functions in redshift space, and approximated at various stages the exact expressions in the waveform. As we review their argument, we will keep these exact expressions until the final stage of the calculation. When, in the next chapter, we add in the effect of the extra dimensions, we will first follow the same method as DV, introducing the same interpolating functions so that a direct comparison can be made. For interest however, we will also include an exact numerical redshift integration.

The first step is to calculate the gravitational wave sourced by a cosmic string loop in flat spacetime, which requires us to solve the linearised Einstein equations (4.6), whose solution in the far field approximation is given by

$$\bar{h}_{\mu\nu} \simeq \frac{4G}{r} \sum_{\omega} e^{-i\omega(t-r)} T_{\mu\nu}(\mathbf{k}, \omega), \quad (4.20)$$

where $T_{\mu\nu}(\mathbf{k}, \omega)$ is the Fourier transformed energy momentum tensors.

The energy momentum of the cosmic string is

$$T^{\mu\nu} = \mu \int d^2\sigma (\dot{X}^\mu \dot{X}^\nu - X'^\mu X'^\nu) \delta^{(4)}(x^\mu - X^\mu(\sigma, \tau)), \quad (4.21)$$

which means the gravitational wave is determined by the Fourier transform

$$T^{\mu\nu}(\mathbf{k}, \omega) = \frac{\mu}{T_L} \int_0^{T_L} d\tau \int_0^L d\sigma \dot{X}_+^{(\mu} \dot{X}_-^{\nu)} e^{-\frac{i}{2}(k \cdot X_+ + k \cdot X_-)}, \quad (4.22)$$

where $X_+^\mu = (\sigma_+, \mathbf{b}(\sigma_+))$, $X_-^\mu = (\sigma_-, \mathbf{a}(\sigma_-))$, and a dot now denotes a derivative with respect to the argument of X_\pm^μ ; $k^\mu = \frac{4\pi m}{L}(1, \mathbf{n}) = m\omega_L(1, \mathbf{n})$ is the null wave vector. Here, ω_L is the frequency of the fundamental mode of the string loop.

A cusp corresponds to a lining up of the momenta of the left and right moving modes on the string loop: $\dot{X}_+^\mu = \dot{X}_-^\mu = \ell^\mu = (1, \mathbf{n}')$. Choosing the coordinate origins, we may write

$$X_\pm^\mu(\sigma_\pm) = \ell^\mu \sigma_\pm + \frac{1}{2} \ddot{X}_{0\pm}^\mu \sigma_\pm^2 + \frac{1}{6} \ddot{\ddot{X}}_{0\pm}^\mu \sigma_\pm^3, \quad (4.23)$$

where the subscript 0 refers to evaluation at $\sigma_\pm = 0$. Now, defining the angle between k^μ and ℓ^μ as θ , which is assumed to be small, and writing $d^\mu = k^\mu - \ell^\mu = (0, \mathbf{d})$ (where

$|\mathbf{d}| \simeq \theta$), and using the gauge conditions, we have:

$$k_\mu X_-^\mu = m\omega_L \left[-\frac{1}{2}\theta^2 \sigma_- + \frac{1}{2}\mathbf{n} \cdot \mathbf{a}'' \sigma_-^2 - \frac{1}{6}(\mathbf{a}''^2 - \mathbf{d} \cdot \mathbf{a}''') \sigma_-^3 \right], \quad (4.24)$$

together with a similar expression involving \mathbf{b} and σ_+ . In the last bracket, the $\mathbf{d} \cdot \mathbf{a}'''$ term is subdominant, being of order $\mathcal{O}(\theta|\mathbf{a}''|^2)$.

The two integrals in the energy momentum therefore take the form:

$$I^\mu = \int [k^\mu - d^\mu + \ddot{X}^\mu \sigma] \exp \left[-\frac{i m \omega_L}{12} (-3\theta^2 \sigma + 3\theta |\ddot{X}| \sigma^2 \cos \beta - |\ddot{X}|^2 \sigma^3) \right], \quad (4.25)$$

where β is the angle between \mathbf{d} and \mathbf{a}'' . As Damour and Vilenkin pointed out, the first k^μ term is a pure gauge, however, when $d^\mu \neq 0$, it cannot be gauged away, as the product $k^\mu d_\mu \neq 0$, but the trace reversed $\bar{h}_{\mu\nu}$ must be tracefree. However, since correcting for this term simply introduces a subdominant term with the same waveform as the main part of the perturbation, like DV, we simply focus on the main part of the integral and compute the main contribution to the waveform. Thus, rewriting

$$u = \left(\frac{m\omega_L}{12} \ddot{X}^2 \right)^{1/3} \sigma, \quad \varepsilon = \left(\frac{m\omega_L}{12\ddot{X}} \right)^{1/3} \theta, \quad (4.26)$$

the relevant part of the integral becomes

$$I = \left(\frac{12}{m\omega_L \ddot{X}^2} \right)^{2/3} \ddot{X} \int du (u - \varepsilon) \exp [i ((u - \varepsilon)^3 + \varepsilon^3 + 3\varepsilon u^2 (1 - \cos \beta))]. \quad (4.27)$$

For $\varepsilon \ll 1$, this integral is well approximated by the $\varepsilon = 0$ value:

$$I_\pm^\mu = \left(\frac{12}{m\omega_L \ddot{X}_\pm^2} \right)^{2/3} \frac{i}{\sqrt{3}} \Gamma \left(\frac{2}{3} \right) \ddot{X}_\pm^\mu, \quad (4.28)$$

and for $\varepsilon > 1$, the integral rapidly tends to zero due to the oscillatory behaviour of the term proportional to $(1 - \cos \beta)$. Thus DV obtain the logarithmic cusp waveform:

$$h^{cusp}(f, \theta) \sim \frac{G\mu L^{2/3}}{r|f|^{1/3}} H[\theta_m - \theta], \quad (4.29)$$

where H is the Heaviside step function, and θ_m is the critical value of θ for which the integral drops to zero:

$$\theta_m = \left(\frac{12\ddot{X}}{m\omega_L} \right)^{1/3} \simeq \left(\frac{2}{Lf} \right)^{1/3}, \quad (4.30)$$

using $\ddot{X} \sim 2\pi/L$, and $f = m\omega_L/2\pi$.

To transform this to the cosmological setting, one essentially replaces f with $(1+z)f$, where z is the redshift at the time of emission of the cusp GWB, and we must replace r by the physical distance

$$a_0 r = a_0 \int_{t_e}^{t_0} \frac{dt}{a} = \int_0^z \frac{dz}{H} = (1+z)D_A(z), \quad (4.31)$$

where $D_A(z)$ is the angular diameter distance at redshift z .

Damour and Vilenkin next use the one scale model of a string network, which assumes the network can be characterised by a single length scale, [153], by writing

$$L \sim \alpha t \quad , \quad n_L(t) \sim 1/(\alpha t^3), \quad (4.32)$$

for the length and number density of the string network at cosmological time t . Here $\alpha \sim \Gamma G\mu$ is a numerically determined constant, [154, 132, 155, 156, 157, 158, 159], presumed to represent the rate of energy loss from string loops via gravitational radiation. As in DV, we will take $\Gamma \sim 50$, however, see [160, 161, 162] for more recent work and discussion on this issue.

Finally, DV estimate the rate of GWB's observed around frequency f coming from the spacetime volume in redshift interval dz :

$$d\dot{N} \sim \frac{\nu(z)}{(1+z)} \frac{\pi\theta_m^2(z)D_A(z)^2}{(1+z)H(z)} dz, \quad (4.33)$$

where the first factor of $(1+z)$ comes from the redshift of time between emission and observation, $\nu(z)$ is the number of cusp events per unit spacetime volume, and the final part is the measure of the spacetime volume within the beaming cone at redshift z ,

where the beaming cone angle at redshift z is simply given by

$$\theta_m(z) = \left(\frac{2}{(1+z)fL(z)} \right)^{1/3}. \quad (4.34)$$

The number of cusp events is given by

$$\nu \sim \mathcal{C} \frac{n_L}{PT_L} \sim \frac{2\mathcal{C}}{P\alpha^2 t^4}, \quad (4.35)$$

where \mathcal{C} is the average number of cusps per loop period, $T_L = L/2 \sim \alpha t/2$, and P is the reconnection probability of the strings. As we observed at the beginning of this chapter, classical strings almost always commute, thus in four spacetime dimensions, $P \sim 1$.

The final step of the DV argument is to integrate (4.33) to find the rate

$$\dot{N} = \int_0^{z_*} \frac{d\dot{N}}{d \ln z} d \ln z \sim \frac{d\dot{N}(z_*)}{d \ln z}, \quad (4.36)$$

and then substituting in a fiducial frequency and desired rate to find the redshift which dominates the signal. Evaluating the gravitational wave at this redshift and frequency then gives the amplitude (see appendix A for details of the interpolation method).

We have reviewed the formation and some features of cosmic strings in this chapter, particularly the production of gravitational wave bursts from cusps on cosmic string loops. In the next chapter, we consider the formation of higher dimensional cosmic strings and revisit the Damour-Vilenkin argument, concentrating on the effect additional dimensions could have on the GWB signal coming from cosmic string cusps.

Chapter 5

Gravitational wave bursts from cosmic string cusps in extra dimensions

5.1 Introduction

If we consider strings in extra dimensions, the natural assumption to make is that we are talking about string theory, a theory motivated by the search for a consistent theory of quantum gravity and which can unify gravity with the other fundamental forces, [28]. As mentioned briefly in chapter 1, in string theory, point particles are replaced with one dimensional strings, which live naturally in 10 dimensions and can take the form of closed loops or open segments with endpoints.

It is usually thought that these fundamental strings are microscopic in size - of order the Planck length - and thus possess a tension of order the Planck scale, if the theory is to explain quantum gravity, [28]; their direct detection is thus far beyond the reach of current experiments. If this is the case, we will not be able to observe these strings as cosmic strings, since it is not possible to stretch them to the necessary astrophysical sizes, [163]. However, it is possible that in models with large or warped extra dimensions (discussed in chapter 1), the tension of the string is reduced and observable ‘fundamental’ cosmic strings - F-strings - could be formed in these models, [164, 165].

String theories can also contain higher dimensional objects known as D-branes, [166]: surfaces on which open strings can end. These represent a wonderful opportunity to embed the phenomenological ADD model, [33, 34], discussed in section 1.2, in a string

theory setting, [48], where the open strings attached to the D-branes are thought to encode the SM gauge forces, while gravity is related to closed string loops which can propagate throughout the full higher dimensional spacetime, [35]. One possible early universe consequence of this embedding is the creation of (higher dimensional) cosmic strings via a mechanism known as brane inflation, [48, 49, 167]. As the name suggests, the main purpose of this mechanism is the production of inflation - an important part of the present early universe paradigm, [168, 169] - in these stringy models.

The brane inflation scenario associates the inflationary potential with an attractive potential between a brane and anti-brane, related to the inter-brane separation in the extra dimensions, [48]. This potential has been found to be relatively flat at large distances, [48], (due to weak brane-brane interactions), allowing slow roll inflation to take place before a critical inter-brane separation is reached, at which point the potential becomes steep, the slow roll conditions break down and inflation ends when the branes collide and annihilate, reheating the universe in the process, [167, 170]. Tachyonic fields can be created as inflation ends, [171, 172], which then roll down their potential, forming defects; it has been shown that the only defects copiously produced will be cosmic strings, [167, 171, 170, 173]. In this setting, the cosmic strings are thought of as Dp -branes, with $p - 1$ dimensions compactified, [167, 172], and are thus usually known as D-strings. In the rest of this chapter, we will explore how the formation of cusps is affected when considered in the context of these higher dimensional cosmic strings.

In order to compute the gravitational waveform of the cusp GWB with extra dimensions, there are several features we need to consider. First, there is the motion of the string in the extra dimensions, as pointed out by Avgoustidis and Shellard, [174], which causes the strings to appear to slow down in our noncompact space dimensions. The existence of extra dimensions also has an impact on the reconnection probability resulting in the reconnection probability of strings formed in higher dimensional theories being reduced when compared to classical strings, as strings which appear to meet in 3 dimensions could be missing each other in the extra dimensions, [165]. This leads to an enhancement of the number density of loops in the string network, [150, 167, 175], however, more detailed simulations indicate that this result may be modified, [176]. Next, there is the impact of this motion on the formation of cusps: as we will see, the effect of extra degrees of freedom allows the left and right moving modes to misalign in momentum space, thus avoiding an exact cusp in a similar way to avoiding intercommutation. Finally, there is the gravitational aspect of the extra dimensions. Since these strings are formed in brane inflation scenarios, we will assume that the flux stabilisation procedure

that prevents dangerous cosmological moduli evolution also prevents the strings from exciting internal degrees of freedom. Thus, we can use the normal 4D gravitational propagator in calculating the gravitational radiation from a cusp.

5.2 Wave form in extra dimensions

5.2.1 String kinematics with extra dimensions

We begin with an overview of string solutions in $4+n$ dimensions. As with 4 dimensions, these can be expressed in the Kibble-Turok notation

$$\mathbf{R} = \frac{1}{2}[\mathbf{A}(\sigma_-) + \mathbf{B}(\sigma_+)] , \quad (5.1)$$

where we use upper case to denote the full $(3+n)$ dimensional spatial vectors, and lower case the noncompact dimensions. As before, $|\mathbf{A}'|^2 = |\mathbf{B}'|^2 = 1$, hence \mathbf{A}' and \mathbf{B}' trace out closed curves on a unit S^{2+n} . Unlike in 3 space dimensions, where two curves on an S^2 will generically cross, these curves will generically miss each other. This means that the probability of an exact cusp with extra dimensions is precisely zero. However, from the calculation of the GWB waveform (see eqn. (4.29)), it is clear that the power is radiated not exclusively from the cusp, but from a region in which the extrinsic curvature of the worldsheet is significant (we will see shortly how the beaming cone opening angle defines this).

We therefore generalise the exact cusp to a ‘near cusp event’ (NCE) for which

$$|\mathbf{A}' - \mathbf{B}'| = 2\Delta , \quad (5.2)$$

where $\Delta \ll 1$ is a parameter measuring how close to an exact cusp (EC) we are. We can visualise the near cusp event as a rounded cusp, as indicated in figure 5.1.

In order to estimate the probability of near cusp formation, we first assume an even measure in parameter space (we will discuss alternative possibilities later). Each loop carries left and right moving waves of harmonics of the fundamental frequency mode $2\pi/L$, the wave vectors of which are constrained by the gauge restriction (4.15). These can be represented in terms of the rotation group $SO(n+3)$, [177], and thus the parameter space of the loop is simply parameterised by a set of angles.

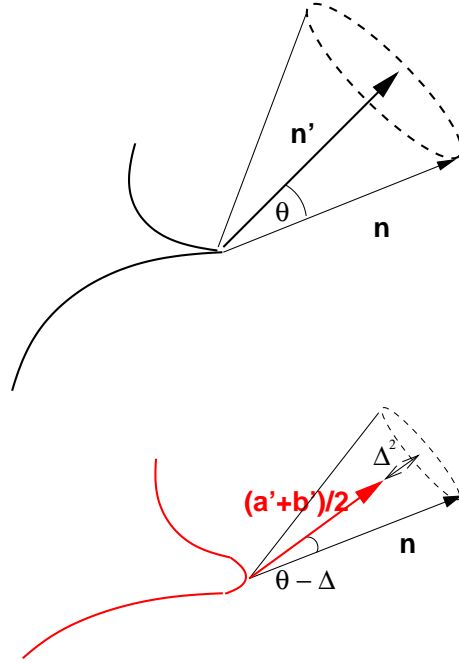


Figure 5.1: A sketch of a near cusp event as opposed to an exact cusp. The rounding of the cusp is indicated, as is the narrowing of the beaming cone.

We estimate the probability of NCE's as $g(\Delta)^q$, where q is the codimension in parameter space of the subspace formed by loops which contain exact cusps, and g is a function which relates a shift in a parameter to a change in $|\mathbf{A}' - \mathbf{B}'|$. q can be readily computed from the condition for a cusp:

$$\mathbf{A}' = \mathbf{B}' . \quad (5.3)$$

This is a set of $n + 3$ equations, however, as $|\mathbf{A}'| = |\mathbf{B}'| = 1$, this results in $n + 2$ constraints. Of these, two are used to fix the values of σ_{\pm} at the cusp, hence n constraints in parameter space remain. Thus, the codimension of the exact cusp space is precisely the number of extra dimensions $q = n$. Explicit loop solutions with one extra dimension were modelled in order to determine the form of the function g , [3]; this was found to be $g(\Delta) = g_0\Delta$, where $g_0 \simeq 1$.

The outcome of our analysis is therefore that the number of NCE's with $|\mathbf{A}' - \mathbf{B}'|_{\min} \leq 2\Delta$ in a generic loop is $\mathcal{N}(\Delta) \simeq \Delta^n$ (since all loops have $|\mathbf{A}' - \mathbf{B}'| \leq 2$ at all points on their trajectory). This argument of course simply refers to the cusps in the full higher dimensional loop motion, and not those loops which are close to our 3 dimensional loops; it also makes no reference to any warping of any of the spacetime dimensions. In addition,

it assumes an exact Nambu description, i.e. an exactly zero width string. The strings will in general have finite width, and we expect that should the string width become a significant fraction of the internal dimension size, then the motion in the internal dimension will be irrelevant. Note however, that because these strings are basically classical objects, there is no quantisation of the motion in the internal directions.

5.2.2 The gravitational waveform

We now compute the waveform for a NCE with parameter Δ . The main difference between the EC and the NCE is that the velocity $\dot{X}^\mu = (1, (\mathbf{a}' + \mathbf{b}')/2)$ is now no longer necessarily null, and that the individual left and right moving velocities need not be aligned. In other words, in evaluating the integral (4.25), we no longer have “ $\varepsilon = 0$ ”, since there are additional phase terms coming from the misalignment of \mathbf{a}' and \mathbf{b}' , as well as from the fact that \dot{X}_\pm^μ is no longer null.

Define

$$\boldsymbol{\delta} = \frac{1}{2}(\mathbf{a}' - \mathbf{b}') \tag{5.4}$$

$$\mathbf{n}' = \frac{(\mathbf{a}' + \mathbf{b}')}{|\mathbf{a}' + \mathbf{b}'|}, \tag{5.5}$$

to be the separation vector of \mathbf{a}' and \mathbf{b}' at the NCE, and the direction vector of the NCE respectively. Then writing $\mathbf{A}' = (\mathbf{a}', \mathbf{a})$, $\mathbf{B}' = (\mathbf{b}', \mathbf{b})$, shows that $|\mathbf{a}'|^2 = 1 - a^2$, and $|\mathbf{b}'|^2 = 1 - b^2$ (with $a = |\mathbf{a}|$ etc.). A quick check of (4.23), (4.24) then indicates that the gravitational integral (4.25) will be damped unless $a, b \ll 1$. While modelling with compact extra dimensions indicates no particular restrictions on the parameter space, the expectation is that either warping of extra dimensions, or some other kinematic consequence of cosmological expansion, will lead to the trajectories being somehow close to the four dimensional behaviour (although [178] indicates this may not be the case). We will therefore take $a, b \ll 1$ from now on. Under these assumptions, expansion of $\boldsymbol{\delta}$ and \mathbf{n}' gives generically that $a^2 \sim b^2 = \mathcal{O}(\Delta^2) = \mathcal{O}(\delta)$. Thus in orders of magnitude

$$\mathbf{a}' = \frac{1}{2}|\mathbf{a}' + \mathbf{b}'|\mathbf{n}' + \boldsymbol{\delta} \simeq \left(1 - \frac{\Delta^2}{2}\right)\mathbf{n}' + \boldsymbol{\delta} \tag{5.6}$$

$$\mathbf{b}' = \frac{1}{2}|\mathbf{a}' + \mathbf{b}'|\mathbf{n}' - \boldsymbol{\delta} \simeq \left(1 - \frac{\Delta^2}{2}\right)\mathbf{n}' - \boldsymbol{\delta}. \tag{5.7}$$

Finally, estimating $\mathbf{n}'\cdot\mathbf{a}'' \sim \mathbf{n}'\cdot\mathbf{b}'' = \mathcal{O}(\Delta)|\ddot{X}|$ we find (making the same approximations as DV) the expression

$$k_\mu X_-^\mu = -\frac{1}{2}(\theta^2 + \Delta^2) \sigma_- + \frac{1}{2}(\theta + \Delta) |\ddot{X}| \sigma_-^2 - \frac{1}{6} \ddot{X}^2 \sigma_-^3, \quad (5.8)$$

with a similar expression involving X_+ and σ_+ .

Thus we find that the waveform of the NCE is the same as that of the EC, with the proviso that the cone opening angle is now decreased to

$$\theta_\Delta = \theta_m - \Delta \simeq \left(\frac{2}{Lf}\right)^{1/3} - \Delta, \quad (5.9)$$

i.e. the (logarithmic) NCE waveform is

$$h^{\text{NCE}} \sim \frac{G\mu L^{2/3}}{r|f|^{1/3}} H[\theta_\Delta - \theta]. \quad (5.10)$$

Notice that (5.9) provides a high frequency cutoff to the waveform,

$$f_\Delta = 1/(\Delta^3 T_L), \quad (5.11)$$

therefore our long frequency ‘tail’ to the waveform is curtailed at some (high) Δ -dependent frequency. However, what is more relevant cosmologically is the combination of the impact of this cutoff of the beaming cone area and the effect of the lowering of the number of NCE’s.

Cosmologically, we need to calculate the GWB event rate, \dot{N} , for near cusp events, however, for a general network there will be a range of NCE’s with different Δ values, up to and including the cutoff value when the GWB beaming cone closes off. We clearly need to integrate over these options to obtain the net effect of *all* possible NCE’s. We therefore write

$$\frac{d\dot{N}_{\text{NCE}}}{dzd\Delta} \sim \frac{\mathcal{C}(\Delta)n_L(z)}{PT_L(z)} \frac{\pi(\theta_m(z) - \Delta)^2 D_A(z)^2}{(1+z)^2 H(z)}, \quad (5.12)$$

where $\mathcal{C}(\Delta)$ is the local probability density of NCE’s for the network. In four spacetime dimensions, a loop with continuous momentum functions always has a cusp, which would correspond to $\mathcal{C}(\Delta) = \delta(\Delta)$ in an integration of (5.12) (where $\delta(\Delta)$ is now the Dirac δ -function). For extra dimensions, assuming that the loops are spread evenly in the

parameter space of solutions, we get

$$\mathcal{C}(\Delta) = \mathcal{N}'(\Delta) = n\Delta^{n-1}, \quad (5.13)$$

and hence the Δ integral yields

$$\int_0^{\theta_m} \mathcal{C}(\Delta) (\theta_m(z) - \Delta)^2 d\Delta = \frac{2\theta_m(z)^{n+2}}{(n+1)(n+2)}, \quad (5.14)$$

where the integral is saturated by $\theta_m < 1$. Note that for the fiducial frequency $f \sim 150$ Hz, corresponding to the LIGO experiment, $\theta_m \sim 10^{-4} \rightarrow 10^{-2}$ as $G\mu \sim 10^{-6} \rightarrow 10^{-12}$ respectively (the analogous LISA values are $\theta_m \sim 10^{-3} \rightarrow 10^{-1}$), and since θ_m varies as $(1+z)^{1/6}$, it remains small until extremely high redshifts ($(1+z_{\text{rec}})^{1/6} \simeq 3$).

Gathering together these different effects, we therefore arrive at the expression for the GWB rate:

$$\frac{d\dot{N}_{\text{NCE}}}{dz} = \frac{2\theta_m(z)^{n+2}}{(n+1)(n+2)} \frac{n_L(z)}{PT_L(z)} \frac{\pi D_A(z)^2}{(1+z)^2 H(z)}. \quad (5.15)$$

Figures 5.2 and 5.3 show the gravitational wave amplitudes for the cosmic string cusp bursts for the characteristic frequencies of the LIGO and LISA detectors, in the form presented by DV, [150], for varying values of n . The plots are presented first by calculating the amplitude in exactly the way DV did, by using interpolating functions (appendix A), and also neglecting Ω_Λ . However, the dotted data curves also show an exact redshift integration, keeping the precise values of the angular diameter and cosmological time for the concordance cosmology ($\Omega_r = 4.6 \times 10^{-5}$, $\Omega_m = 0.28$, $\Omega_\Lambda = 1 - \Omega_m - \Omega_r$) and integrating out numerically in redshift space for different values of $G\mu$.

An alternative way of presenting the GWB information is to instead compute the expected detection rate of events with amplitudes greater than (or equal to) a given amplitude. As explained in the papers of Siemens et al., [179, 180], the one scale model used by DV, in which all loops are taken to have essentially the same length, (4.32), does not capture the full dynamical range of the cosmic string network which will have loops, in theory, at all scales. They therefore recomputed the rate in order to take into account the dependence not only on redshift, but also on length scales, which they encoded in

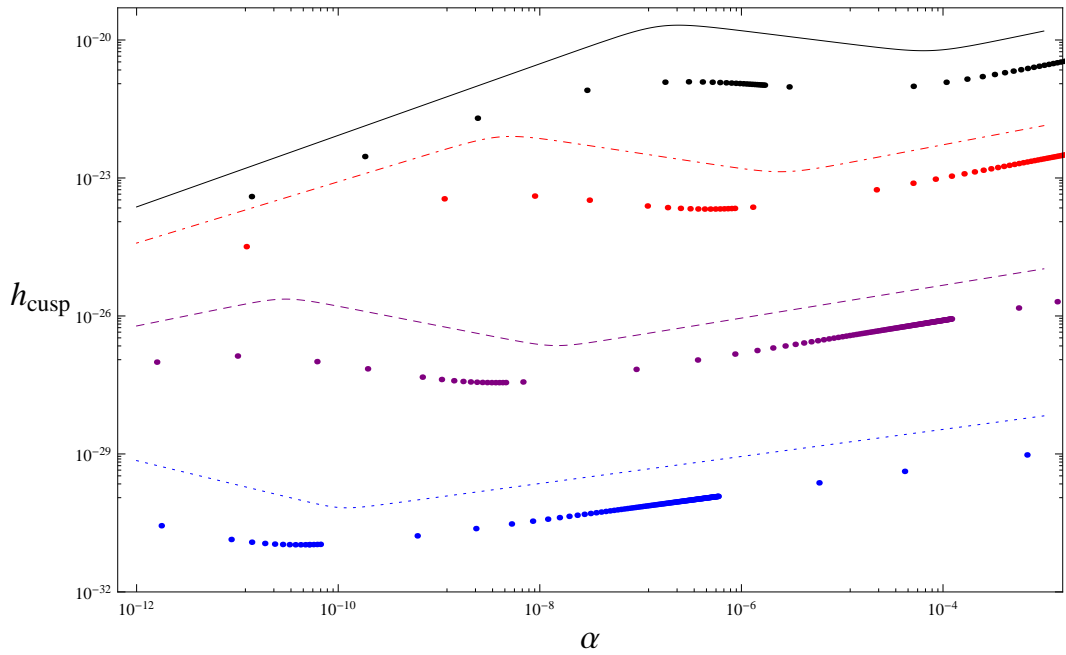


Figure 5.2: Log log plots of the gravitational wave amplitude of bursts as a function of α for the LIGO frequency $f = 150$ Hz, and a detection rate of 1 per year. The lines (solid or dotted/dashed) represent the graphs obtained using the DV interpolating functions, allowing for a direct comparison with [150]. The sets of individual dots correspond to the exact numerical redshift integrations, where we used the exact functions $t(z)$, $D_A(z)$, for the concordance cosmology. The plots are colour coded, from the black, DV result at the top, through red (dot-dash) for $n = 1$, purple (dashed) for $n = 3$, and blue (dotted) for $n = 6$ and all have an intercommutation probability of $P = 10^{-3}$.

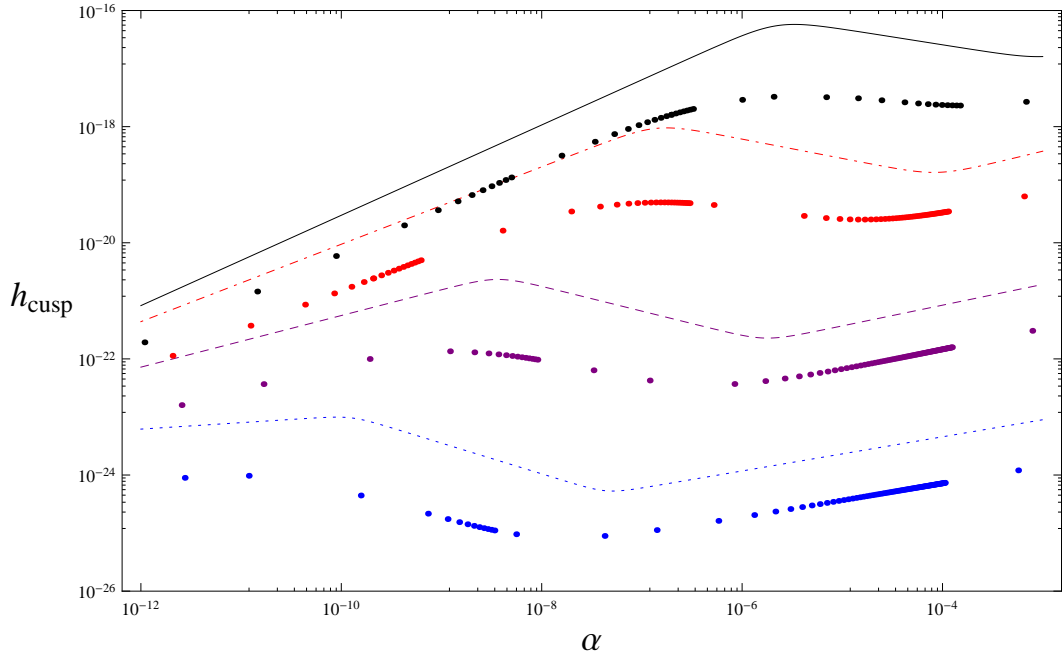


Figure 5.3: A similar plot to figure 5.2, but for the LISA frequency, $f = 3.9$ mHz. Again the lines represent the graphs obtained using the DV interpolating functions, while the sets of individual dots correspond to the exact numerical integrations. The same colour coding as the previous plot applies.

the amplitude of the cusp waveform, A , found by considering

$$h^{cusp} = A|f|^{-1/3}, \quad (5.16)$$

(in the logarithmic representation of DV), and comparing with (4.29), or in the extra dimensional case, (5.10), resulting in a rate per redshift interval dz and amplitude interval, dA , rather than the rate per redshift interval obtained by DV. However, on using the one scale model, (4.32), where amplitudes are directly associated with redshifts, the amplitude dependence is effectively integrated out and the generalised expression found in [179] reduces to (4.33), the expression used by DV and hence to (5.15) in the extra dimensional case. The results in [179] are therefore presented as a rate plot against the string parameter α , calculated by integrating $d\dot{N}$ out to redshift values corresponding to the chosen amplitude (we use their value of $A = 10^{-21}\text{s}^{-1/3}$ only) at various values of α :

$$\frac{\varphi_t^{2/3}(z)}{(1+z)^{1/3}\varphi_r(z)} = \frac{50AH_0^{-1/3}}{\alpha^{5/3}}, \quad (5.17)$$

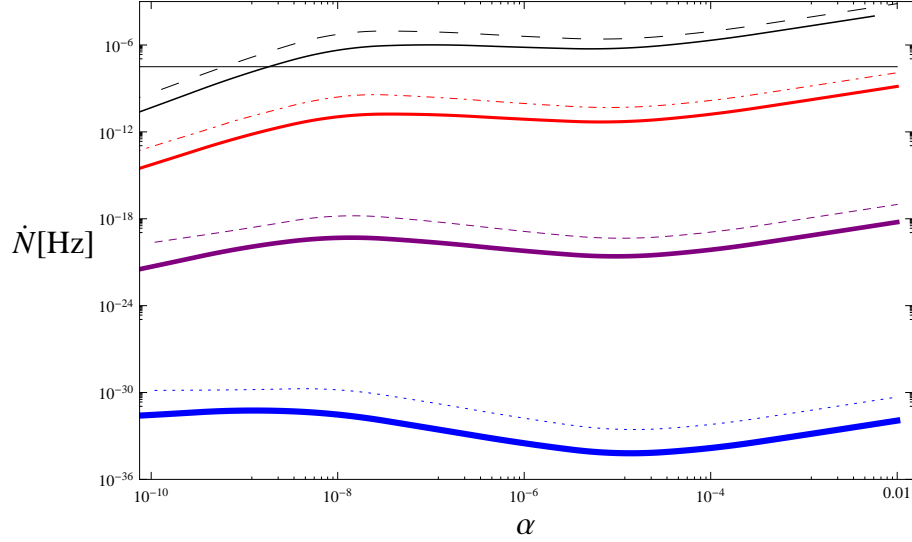


Figure 5.4: A similar plot to that of figure 5.2 (LIGO), but in this case showing the expected rate at an amplitude of $10^{-21} s^{-1/3}$, using the method of [179]. The plots are colour coded as in figure 5.2 except in this case the thick solid lines are now the numerical integration results. From top to bottom: the 3D $P = 10^{-3}$ result, and the extra dimension plots with $n = 1$, $n = 3$, and $n = 6$ respectively. The horizontal black line indicates a rate of one event per year.

where $\alpha \sim 50G\mu$ as usual, and φ_t , φ_r are either the DV interpolating functions, or are related to the exact functions $t(z)$, $D_A(z)$ (c.f. appendix A and [179]). This equation relating the redshift and amplitude is easily found from the expression for the cusp waveform derived in [50].

Figures 5.4 and 5.5 show the rates calculated for the 3D and extra dimensional cases using this alternative approach for both the LIGO and LISA frequencies.

5.3 Discussion

It is clear on examining our results in the previous section, that the motion of the string in the extra dimensions has a significant impact on gravitational emission from cusps. That extra dimensions should have an effect is not unreasonable, since they can be viewed as additional degrees of freedom living on the string, [181, 182, 183], for example, superconducting cosmic strings, [184], can be represented as a dimensional reduction of standard five dimensional KK theory, [181, 182, 183]. For these cosmic strings, the currents round off cusps in much the same way as we have described here, [185], and

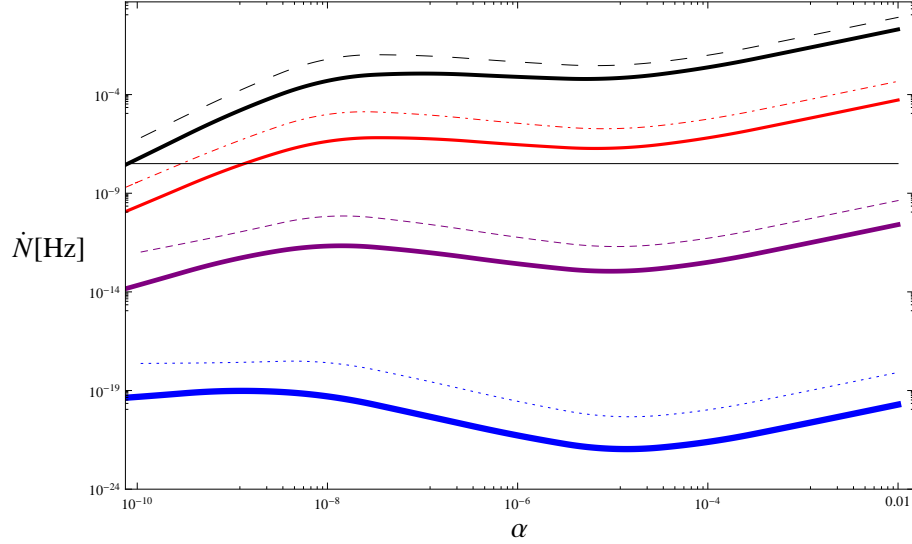


Figure 5.5: A similar plot to that of figure 5.3 (LISA), but in this case showing the expected rate at an amplitude of $10^{-21} s^{-1/3}$, using the method of [179]. The plots are colour coded as in figure 5.3 and again the thick solid lines are the numerical integration results. From top to bottom: the 3D $P = 10^{-3}$ result, and the extra dimension plots with $n = 1$, $n = 3$, and $n = 6$ respectively. The horizontal black line again indicates a rate of one event per year.

also alter the balance between the energy and tension of the string, [186], which has a clear gravitational impact. This naturally raises the concern that we may not be able to distinguish between extra fields living on a cosmic string, and extra dimensions in which the string is moving. This would certainly be the case if one was observing a string and a single GWB. However, our calculation was for the expected signal from a cosmological network of strings, which depends not only on the GWB waveform, but also on the properties of the network. Superconducting string networks have not been as well explored as those of standard cosmic strings, [187, 188], with the main focus being on the different physics induced by the long range electromagnetic interactions. However, as superconducting strings have similar intercommutation properties to standard cosmic strings, [189], it is likely that the network is more similar to the usual cosmic strings than that of the cosmic superstrings. Thus, while the individual GWB waveforms will be similar, the expected rates and signals we have calculated for the cosmological networks are indeed specific to extra dimensions.

It is perhaps a little surprising that the effect of extra dimensions can be so dramatic. We therefore now examine our assumptions carefully, raising below a series of critiques together with a discussion of their validity and resolution.

The basic reason for the suppression of the signal is the distribution over the near cusp parameter Δ . In the previous section, we used a uniform distribution in solution space, however we would expect the allowed parameter space of the string to be constrained in some way by the presence of compact extra dimensions. Since these strings form from the collision of a brane and anti-brane, it seems likely that they have significant initial momentum in the extra dimensions, thus we see no reason to curtail our solution space in this way. The main objection to having total freedom of the internal modes is that by wrapping back and forth across the extra dimension(s) the string has more opportunity to self intersect, thus curtailing the additional freedom in that direction.

The effect of self intersections on the extra dimensions was modelled in [3]. It was found that the introduction of an additional dimension resulted in the measure of the solution set allowing for self intersections becoming zero as it did in the case of exact cusp formation: once again, the argument used is a parametric one. A string will self intersect if

$$\mathbf{A}(\tau - \sigma) + \mathbf{B}(\tau + \sigma) = \mathbf{A}(\tau - \sigma') + \mathbf{B}(\tau + \sigma') \quad (5.18)$$

for some τ, σ, σ' . Thus, there are three dynamical variables and $3 + n$ constraints. In 3D, it is therefore possible to satisfy these constraints simultaneously and we see how the subspace of self intersecting loops can be of nonzero measure in parameter space. With extra dimensions however, satisfying (5.18) necessarily requires a constraint on parameter space, hence the subspace with self intersections will be of lower dimension. Even compactifying the extra dimensions does not change this argument, unless we take into account the finite width of the string. Essentially, if we take the string to have zero width, then it can easily miss itself even when winding back and forth across the extra dimensions many times. However, with finite width, the self intersection probability now becomes nonzero, and of order $\mathcal{O}(w/R)^n$ (where w is the string width, and R the size of the extra dimension). This therefore suggests that we introduce this ratio in a finite width correction to the GWB measure.

As we mentioned during our initial discussion, warping of the extra dimensions could also provide some significant dynamical effect. The results of Avgoustidis, [178], indicate that warping is not as dramatic a trapping force as initially suspected, however, any confinement of strings could be significant, and a detailed modelling of this effect is necessary. For now, we model a restriction in the extra dimensional motion by a restriction in Δ . Instead of allowing Δ to range over the full unit interval, we restrict $\Delta \in [0, \Delta_0]$.

Thus we must renormalise \mathcal{C} :

$$\mathcal{N}(\Delta_0) = \int_0^{\Delta_0} \mathcal{C}(\Delta) d\Delta = 1 \quad \Rightarrow \quad \mathcal{C}(\Delta) = \frac{n}{\Delta_0^n} \Delta^{n-1}, \quad (5.19)$$

and the relevant Δ integral (5.14) becomes

$$\int_0^{\min\{\Delta_0, \theta_m\}} \mathcal{C}(\Delta) (\theta_m(z) - \Delta)^2 d\Delta = \theta_m(z)^2 \mathcal{F}_n \left[\frac{\theta_m}{\Delta_0} \right], \quad (5.20)$$

where

$$\mathcal{F}_n[x] = \frac{2x^n}{(n+1)(n+2)} H[1-x] + \left(1 - \frac{2n}{(n+1)x} + \frac{n}{(n+2)x^2} \right) H[x-1]. \quad (5.21)$$

A reasonable value for Δ_0 might be to use the one parameter ratio that does impact on the loop families and motion: the ratio of string width to the size of the extra dimension. The Nambu action is only a good approximation when the width of the string is small compared to scales of physical interest. This is rarely a problem in cosmology, as the string width is set by the inflationary scale, and the size of the universe rapidly becomes large. As far as the extra dimensions are concerned however, these are stabilised at a couple of orders of magnitude above the string scale, hence while the Nambu action is a good approximation, we might expect some corrections to show up due to parameter restriction from self intersection or excessive winding as already discussed. We therefore expect this parameter to be related to the probability of intercommutation, which can be viewed as arising because of the strings ‘missing’ each other in the internal dimensions.

To test this alternate expression, we took values of $\Delta_0 = 0.1, 0.01, 0.001$, and 10^{-4} . These values were motivated by a limiting sensible ratio w/R , and the value of P . From (5.20), we see that the effect of Δ_0 is to cut off the integral as θ_m grows. For $\theta_m < \Delta_0$, the dependence of the rate on $\theta_m(z)$ remains that of the previous section, however, as θ_m grows, the functional dependence shifts towards the $\theta_m(z)^2$ form of the 3D result. From the expression for $\theta_m(z)$, (4.34), we see that this is proportional to $(G\mu)^{-1/3}$, hence the rates converge to the 3D value sooner for smaller $G\mu$.

Figure 5.6 shows the effect of the Δ_0 parameter on the event rate at an amplitude cutoff of $10^{-21} s^{-1/3}$ and frequency $f = 150$ Hz for Δ_0 ranging from $10^{-1} - 10^{-4}$ as indicated. Note that once we use this more complicated expression (5.20), the use of the interpolating function approximation becomes too unwieldy, and the rates had to be calculated by direct integration. Figure 5.7 shows the effect of the rate on the number

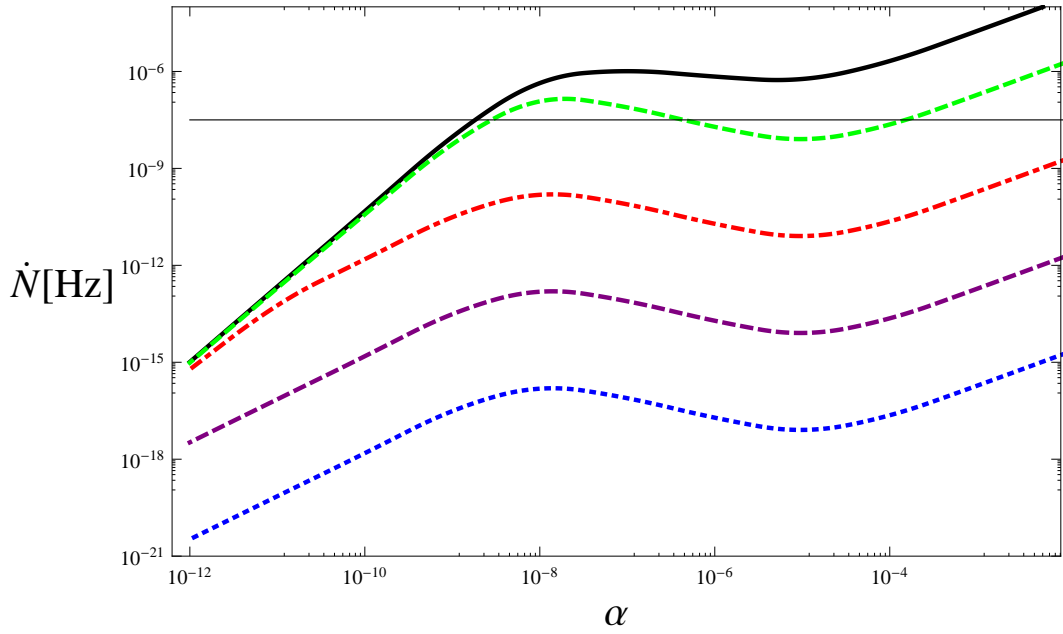


Figure 5.6: A plot of the dependence of the rate on Δ_0 with the number of extra dimensions fixed at three for $f = 150$ Hz (LIGO). From top to bottom, the solid black line indicates the 3D result, $\Delta_0 = 10^{-4}$ in dashed green, $\Delta_0 = 10^{-3}$ in dot-dash red, $\Delta_0 = 10^{-2}$ in dashed purple, and $\Delta_0 = 10^{-1}$ in dotted blue respectively. The horizontal black line indicates a rate of one event per year.

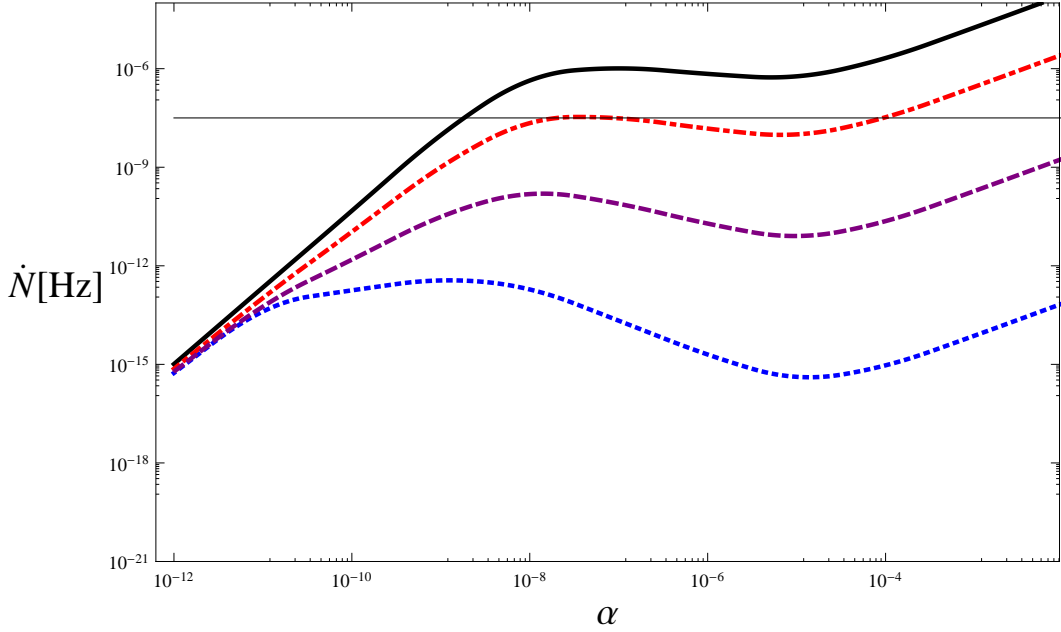


Figure 5.7: A recomputation of the rate plot at $f = 150$ Hz (LIGO) with the new nearcusp measure (5.20) fixing $\Delta_0 = 10^{-3}$, and allowing n to vary. From top to bottom, $n = 0, 1, 3$ and 6 respectively. The horizontal black line indicates a rate of one event per year.

of extra dimensions, fixing $\Delta_0 = 10^{-3}$ and allowing n to vary as indicated for the LIGO detector. Here we see that for all n the plots converge on the 3D result at $\alpha \sim 10^{-11}$ but for $\alpha \sim 10^{-8}$ for example, the rate drops by roughly an order of magnitude per dimension. However, as we can see from the LISA plots (figures 5.8, 5.9), the value at which the plots converge on the 3D value is frequency dependent: in figure 5.9, the plots converge at $\alpha \sim 10^{-8}$ and the drop with the number of extra dimensions is much less significant. Nevertheless, a positive detection therefore could potentially tell us the number of extra dimensions.

We briefly mention frequencies outside the LIGO and LISA cases from the point of view of the methods discussed in this chapter. As we have noticed, the GWB amplitudes are frequency dependent and on checking the high (100 MHz) frequencies discussed by Cruise, [148, 149], the amplitude was found to be low enough that a cusp signal of this frequency would not be observed even before the extra damping effect of the extra dimensions was taken into account. Finally in the case of nHz frequencies (which are investigated using pulsar timing experiments as mentioned earlier), an order of magnitude calculation of θ_m , eqn. (4.34), found that for $\alpha \sim 10^{-9}$, θ_m is of order unity. This re-

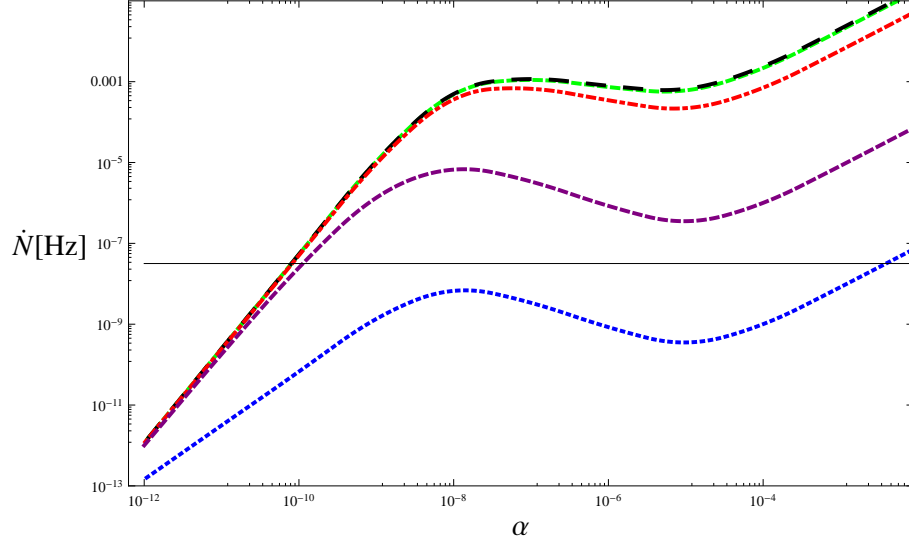


Figure 5.8: A plot of the dependence of the rate on Δ_0 with the number of extra dimensions fixed at three for $f = 3.9$ mHz (LISA). From top to bottom, the large dashed black line indicates the 3D result, $\Delta_0 = 10^{-4}$ in dashed green (coincident with the black line), $\Delta_0 = 10^{-3}$ in dot-dash red, $\Delta_0 = 10^{-2}$ in dashed purple and $\Delta_0 = 10^{-1}$ in dotted blue respectively. As before, the horizontal black line indicates a rate of one event per year.

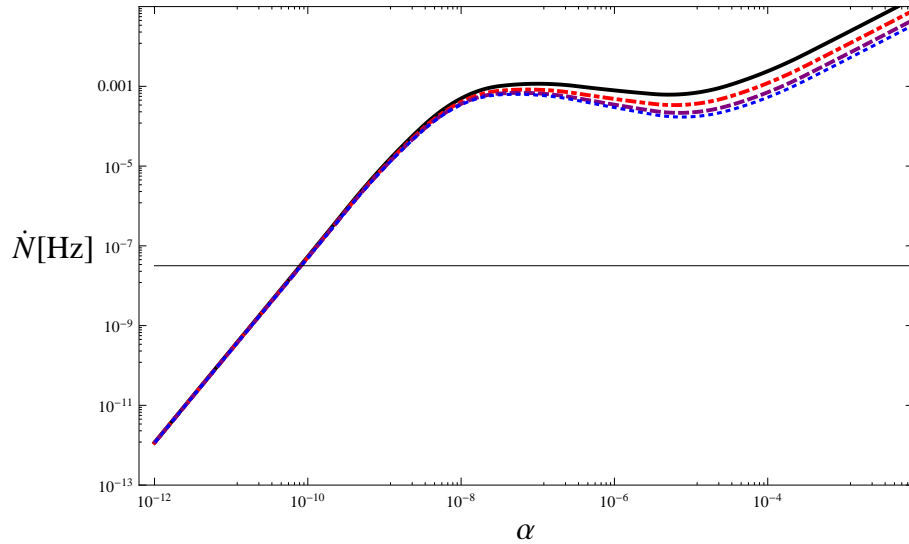


Figure 5.9: A recomputation of the rate plot with the new nearcusp measure (5.20) at $f = 3.9$ mHz (LISA), fixing $\Delta_0 = 10^{-3}$ and varying n as before. The colour coding is done as for figure 5.7 and $\Delta_0 = 10^{-3}$ as before. As always, the horizontal black line indicates a rate of one event per year.

sults in the approximation of the integral in eqn. (4.27) breaking down in the parameter region in which we are interested, invalidating the method at these frequencies.

To sum up: in this chapter we have discussed the effect that motion in extra dimensions has on the computation of the gravitational wave burst signal from cusp events on cosmic string loops. We find a significant effect, even after taking into account finite width effects and the size of the extra dimension. However we have also seen from the comparison of LIGO and LISA results, that the frequency at which the GWB is observed is an important factor. While further work is required to get better control of the approximations being used, it does seem that motion in internal dimensions is important. Finally, if the string tension lies in an appropriate (albeit frequency dependent) range then the possibility arises that a positive detection by gravitational radiation would not only confirm the general brane inflation scenario, but could provide a means of determining the number of (effective) extra dimensions.

Chapter 6

Gravitational wave bursts from kinks in extra dimensions

6.1 Introduction

As we have seen in the previous chapter, the existence of extra dimensions has a significant effect on the gravitational wave bursts emitted by cusps on cosmic string loops. Contrary to previous expectations, [167, 150, 172], the gravitational radiation is not enhanced by the lowering of the intercommutation probability in extra dimensions, but is in fact suppressed by other competing factors. In this chapter we consider kinks - the other main source of gravitational wave bursts from cosmic string loops - and the effect of extra dimensions on the GWB signal they produce.

Kinks are formed when there is a discontinuity in the tangent vector to the string, which occurs whenever the string intercommutes and reconnects, as the segments on either side of the crossing point will have different velocities, [190, 191, 192, 193]; they are thought to be ubiquitous on cosmic strings. Cosmic string loops possess kinks, not only because they are formed by self-intersections, but also because kinks could already be present on the segment of string cut off to form the loop, [194, 192, 193]. Unlike cusps, which only occur at certain points on string loops and are therefore transient events, kinks can persist on strings and travel around a cosmic string loop as it oscillates, [190, 191]. However, they can be smoothed out, (or in the case of an infinite string, removed via loop formation), which can occur as a result of stretching due to the expansion of the universe, or through the backreaction of gravitational radiation, [190, 157, 193].

Returning to the Kibble-Turok formalism reviewed in section 4.2, [151, 121], we recall that the solution to the string equation of motion is given by $X^\mu = (\tau, \mathbf{r}(\tau, \sigma))$, where \mathbf{r} is written as in eqn. (4.14) and the vectors \mathbf{a}' and \mathbf{b}' are constrained by the gauge conditions, (4.10) and (4.11), to lie on a unit sphere (see eqn. (4.15)). Kinks, unlike cusps, which occur whenever the vectors \mathbf{a}' and \mathbf{b}' intersect, form when one of \mathbf{a}' , \mathbf{b}' or one of their derivatives has a discontinuity. As well as being ubiquitous on cosmic strings, kinks can also prevent the formation of cusps on cosmic string loops, even in 3D (where, as we showed in chapter 4 they are generic), as a discontinuity on either \mathbf{a}' or \mathbf{b}' allows the curves to miss each other if they were to otherwise intersect at that point.

Kinks, like cusps, emit bursts of gravitational radiation whose signal was calculated in the 3D case by Damour and Vilenkin, [50], in a similar manner to cusp GWB's and the kink signal was found to be the weaker of the two. However, given that kinks can prevent cusp formation, it is possible that if the number of kinks increases, the number of cusps correspondingly shrinks and the GWB's emitted from kinks could become important despite their smaller size. Because of this, as well as the significant reduction in cusp formation in higher dimensional theories, it is important that the effects of the extra dimensions on kink GWB's are explored.

6.2 Kinks in 3D

We begin with a review of the method used by Damour and Vilenkin, [50], to calculate the kink GWB in 3D, highlighting in particular the differences with the cusp calculation reviewed in chapter 4. In order to obtain the gravitational waveform of the kink GWB, we begin, as before, with the linearised Einstein equations (4.6), whose solution in the far field approximation is given as before by eqn. (4.20). As we continue to use the Nambu action, the energy momentum tensor of the string is that used in [50], whose Fourier transform can be factorised as

$$T^{\mu\nu}(\mathbf{k}, \omega) = \frac{\mu}{L} \int_0^L d\sigma_+ \int_0^L d\sigma_- \dot{X}_+^{(\mu} \dot{X}_-^{\nu)} e^{-\frac{i}{2}(k \cdot X_+ + k \cdot X_-)}, \quad (6.1)$$

where once again we write $X_+^\mu = (\sigma_+, \mathbf{b}(\sigma_+))$, $X_-^\mu = (\sigma_-, \mathbf{a}(\sigma_-))$, a dot denotes a derivative with respect to the argument of X_\pm^μ , $k^\mu = \frac{4\pi m}{L}(1, \mathbf{n}) = m\omega_L(1, \mathbf{n})$ is the null wave vector and ω_L is the frequency of the fundamental mode of the string loop as in chapter 4.

To calculate the energy momentum for the kink, we require a discontinuity in one of the integrals

$$I_{\pm}^{\mu} = \int_0^L d\sigma_{\pm} \dot{X}_{\pm}^{\mu} e^{-\frac{i}{2}k \cdot X_{\pm}}, \quad (6.2)$$

while the other must contain a saddle point (or near saddle point) $k \cdot \dot{X} = 0$ in order to prevent the waveform (4.20) from decaying too rapidly; as discussed in [50], high mode numbers m of the frequency, $\omega_m = m\omega_L$, only contribute to the GWB component of the gravitational wave emission from string loops because of the slower rate of decay of the integrals (6.2) as $m \rightarrow \infty$, which occurs only if they contain either a saddle point in the phase $\phi = k \cdot X$, or a discontinuity in \dot{X} . We choose the discontinuity to be on the \mathbf{a}' curve and thus contained in the I_- integral.

The saddle point integral, I_+ , is computed as in chapter 4, but where we now take the direction vector $\ell^{\mu} = \dot{X}_+^{\mu} = (1, \mathbf{n}')$ to be parallel to some direction of the curve \mathbf{b}' , rather than an intersection of the curves as happens for the cusp. We define the angle between k^{μ} and ℓ^{μ} to be θ , which, as in the case of the cusp, is assumed to be small, and write as before, $d^{\mu} = k^{\mu} - \ell^{\mu} = (0, \mathbf{d})$ (where $|\mathbf{d}| \simeq \theta$). Then, as in section 4.3, we find that

$$I_+^{\mu} = \int [k^{\mu} - d^{\mu} + \ddot{X}_+^{\mu} \sigma_+] \exp \left[-\frac{im\omega_L}{12} (-3\theta^2 \sigma_+ + 3\theta |\ddot{X}_+|^{\mu} \sigma_+^2 \cos \beta - |\ddot{X}_+|^2 \sigma_+^3) \right] d\sigma_+. \quad (6.3)$$

The I_- integral containing the discontinuity, however, requires a slightly different approach. We follow [50] and take \dot{X}_-^{μ} to have a discontinuity at $\sigma_- = \sigma_-^{disc}$ whilst assuming that \dot{X}_-^{μ} jumps from $\dot{X}_-^{\mu}(\sigma_-^{disc} - 0) = n_1^{\mu}$ to $\dot{X}_-^{\mu}(\sigma_-^{disc} + 0) = n_2^{\mu}$, where n_1^{μ} and n_2^{μ} are both null vectors.

We write the integral as

$$\begin{aligned} I_-^{\mu} = & \int_{\sigma_0}^{\sigma_-^{disc} - \epsilon} d\sigma_- \dot{X}_-^{\mu} e^{-\frac{i}{2}(k \cdot X_+ + k \cdot X_-)} + \int_{\sigma_-^{disc} - \epsilon}^{\sigma_-^{disc} + \epsilon} d\sigma_- \dot{X}_-^{\mu} e^{-\frac{i}{2}(k \cdot X_+ + k \cdot X_-)} \\ & + \int_{\sigma_-^{disc} + \epsilon}^{\sigma_0 + L} d\sigma_- \dot{X}_-^{\mu} e^{-\frac{i}{2}(k \cdot X_+ + k \cdot X_-)}, \end{aligned} \quad (6.4)$$

where ϵ is an arbitrary small parameter, introduced to separate out the discontinuity from the rest of the integral (i.e. the middle term of (6.4)), which will be allowed to go to zero at the end of the calculation. The first and third terms then cover the remainder

of the integration range on either side of the discontinuity. We note that these terms in (6.4) now no longer contain the discontinuity, which has been localised to the middle term of the expression, and will not have a saddle point, except in the special cases where the wavevector k^μ is parallel or close to n_1^μ or n_2^μ . If k is parallel, or close to (i.e. within an angle θ of) either of these null vectors, it follows that the wavevector falls within the beaming cone of a cusp, as we saw in chapter 4. This results in a ‘cusp-like’ contribution being added to the waveform, which would be expected to dominate the kink contribution coming from the second null vector, in the vicinity of the intersection. However, as we wish to explore the behaviour of a generic kink, we assume that we are not dealing with one of these special cases. It thus follows that neither the first nor third term in eqn. (6.4) fulfils the conditions necessary to slow their decay and they can therefore be neglected when the high frequency modes contributing to the kink GWB are considered: eqn. (6.4) can therefore be evaluated as

$$\begin{aligned} I_-^\mu &= \int_{\sigma_-^{disc-\epsilon}}^{\sigma_-^{disc+\epsilon}} d\sigma_- \dot{X}^\mu e^{-\frac{i}{2}(k \cdot X_+ + k \cdot X_-)} \\ &= \int_{\sigma_-^{disc-\epsilon}}^{\sigma_-^{disc}} d\sigma_- \dot{X}^\mu e^{-\frac{i}{2}(k \cdot X_+ + k \cdot X_-)} + \int_{\sigma_-^{disc}}^{\sigma_-^{disc+\epsilon}} d\sigma_- \dot{X}^\mu e^{-\frac{i}{2}(k \cdot X_+ + k \cdot X_-)}. \end{aligned} \quad (6.5)$$

The leading order terms then become

$$\begin{aligned} I_-^\mu &\simeq \int_{\sigma_-^{disc-\epsilon}}^{\sigma_-^{disc}} n_1^\mu e^{-\frac{im\omega_L}{2} \hat{k} \cdot n_1 \sigma_-} - \int_{\sigma_-^{disc}}^{\sigma_-^{disc+\epsilon}} n_2^\mu e^{-\frac{im\omega_L}{2} \hat{k} \cdot n_2 \sigma_-} \\ &= n_1^\mu \left(-\frac{2}{im\omega_L k \cdot n_1} \right) e^{-\frac{im\omega_L}{2} k \cdot n_1 \sigma_-} \Big|_{\sigma_-^{disc-\epsilon}}^{\sigma_-^{disc}} - n_2^\mu \left(-\frac{2}{im\omega_L \hat{k} \cdot n_2} \right) e^{-\frac{im\omega_L}{2} \hat{k} \cdot n_2 \sigma_-} \Big|_{\sigma_-^{disc}}^{\sigma_-^{disc+\epsilon}}, \end{aligned} \quad (6.6)$$

and we find that

$$I_- \simeq \frac{2i}{m\omega_L} \left(\frac{n_1^\mu}{\hat{k} \cdot n_1} - \frac{n_2^\mu}{\hat{k} \cdot n_2} \right), \quad (6.7)$$

where $\hat{k} = (1, \mathbf{n})$, so that $m\omega_L \hat{k}^\mu = k^\mu$.

If we now consider the combination of $I_+^{(\mu} I_-^{\nu)}$ which appears in the waveform,

$$\begin{aligned} I_+^{(\mu} I_-^{\nu)} &\sim \left[\int [k^{(\mu} - d^{(\mu} + \ddot{X}_+^{(\mu} \sigma_+)] e^{-\frac{im\omega_L}{12} (-3\theta^2 \sigma_+ + 3\theta |\ddot{X}_+|^2 \sigma_+^2 \cos \beta - |\ddot{X}_+|^2 \sigma_+^3)} d\sigma_+ \right] \\ &\quad * \left[\frac{2i}{m\omega_L} \left(\frac{n_1^\nu}{k \cdot n_1} - \frac{n_2^\nu}{k \cdot n_2} \right) \right], \end{aligned} \quad (6.8)$$

it is easy to see that the first k^μ term can once again be gauged using, [50]:

$$h'_{\mu\nu} = h_{\mu\nu} + k_\mu \xi_\nu + k_\nu \xi_\mu - \eta_{\mu\nu}(k\xi) . \quad (6.9)$$

Reparameterising using eqn. (4.26), we find that

$$T^{\mu\nu} \sim \left(\frac{12}{m\omega_L \dot{X}_+^2} \right)^{2/3} \frac{2i}{m\omega_L} \ddot{X}_+^{(\mu} \int du (u - \varepsilon) e^{i((u-\varepsilon)^3 + \varepsilon^3 + 3\varepsilon u^2(1-\cos\beta))} \left(\frac{n_1^\nu}{\hat{k} \cdot n_1} - \frac{n_2^\nu}{\hat{k} \cdot n_2} \right) , \quad (6.10)$$

where the solution to the I_+ integral is as in [50] and eqn. (4.27). The waveform is then related to the I_\pm integrals as, [50]:

$$h^{\mu\nu}(f) = \frac{2G\mu|f|}{r} I_+^{(\mu} I_-^{\nu)} , \quad (6.11)$$

yielding the logarithmic kink waveform, [50]:

$$h^{kink}(f, \theta) \sim \frac{G\mu L^{1/3}}{r|f|^{2/3}} H[\theta_m - \theta] . \quad (6.12)$$

In a similar manner to the cusp calculation, the waveform (6.12) is transformed to a cosmological setting by replacing f by $(1+z)f$, where z is now the redshift at the time of emission of the kink burst, and r by the physical distance (4.31). Using the one scale model, (4.32), as before, the rate of GWB's from kinks observed in the spacetime volume in redshift interval dz around a frequency f can be calculated from

$$d\dot{N}_k = \frac{2\nu_k(z)}{1+z} \frac{\pi\theta_m D_A(z)^2}{(1+z)H(z)} dz , \quad (6.13)$$

where the number of kink events on a loop ν_k is analogous to (4.35), with the average number of cusps \mathcal{C} replaced by the average number of kinks \mathcal{K} . The main contrast with the cusp rate (4.33) is in the dependence on the angle θ_m , eqn. (4.30), the critical value of the angle for which the integral I_+ drops to zero. Due to the mobile and persistent nature of a kink on a string loop, the emission is not beamed in a cone like the cusp, but is instead radiated in a one dimensional 'fan-like' set of directions, [50], which arise from the occurrence of saddle points; the inclusion of the angle θ_m , so that the observation direction is slightly offset from the direction of the emission, results in the 1D 'line' of emission from the kink being widened so that a strip is swept out on the surface of

the unit sphere and the volume factor becomes $\theta_m/2$, [195]. The amplitude of the kink GWB's is then calculated from the rate, found from (6.13), in the same way as the cusp case.

6.3 Kinks in higher dimensions

We have seen in the previous chapter, how one of the main differences in looking at cusps in extra dimensions is the fundamental change in behaviour of 2D curves moving on the surface of a $2 + n$ -sphere rather than a 2-sphere, which results in intersections, which had been generic, becoming extremely rare. A kink, however, does not require the curves to intersect, nor will the appearance of the discontinuity depend on the number of dimensions in which the string moves; kink formation will thus be unaffected by the inclusion of extra dimensions.

This is not to say that the presence of extra dimensions will have no effect on the GWB's emitted by kinks. As was the case in the previous chapter, (and [150, 167, 175]), motion in higher dimensions affects the intercommutation probability of strings, reducing it, as strings miss each other in the extra dimensions, which in turn affects the network density and leads to an enhancement of the kink amplitude. Furthermore, the inclusion of the saddle point integral, I_+ , affects the kink GWB as it did the cusp, as we demonstrated in chapter 5, showing how the inclusion of higher dimensions and the definition of the near cusp event brought about a decrease in the radiation cone of the cusp, (eqns. (5.8)-(5.10)). While eqn. (5.2) has no relevance for kink formation in the extra dimensions, the higher dimensional vector \mathbf{B}' can still be written in terms of its 3D and extra dimensional components, $\mathbf{B}' = (\mathbf{b}', b)$, so that we may write $|\mathbf{b}'|^2 = 1 - b^2$, as before. As we discussed in section 5.2.2, the saddle point integrals - in this case, I_+ only - will damp too quickly unless we take the extra dimensional component, $b \ll 1$. Combining this with the estimation of $\mathbf{n}' \cdot \mathbf{b}'' = \mathcal{O}(b)|\ddot{X}|$, in a similar manner to the approach used in chapter 5, we find that the exponent of I_+ can now be written as

$$k_\mu X_+^\mu = -\frac{1}{2}(\theta^2 + b^2) \sigma_+ + \frac{1}{2}(\theta + b) |\ddot{X}_+| \sigma_+^2 - \frac{1}{6} \ddot{X}_+^2 \sigma_+^3, \quad (6.14)$$

and we find once again that the angle θ_m narrows as a result of the inclusion of extra dimensions, thus affecting the kink GWB signal. We can therefore see that, as in the cusp case, the extra dimensional (logarithmic) kink waveform is the same as the 3D

waveform, eqn. (6.12), with a reduced beaming angle:

$$h^{kink}(f, \theta) \sim \frac{G\mu L^{1/3}}{r|f|^{2/3}} H[\theta_b - \theta], \quad (6.15)$$

where

$$\theta_b = \theta_m - b \simeq \left(\frac{2}{Lf}\right)^{1/3} - b. \quad (6.16)$$

As always, we wish to calculate the event rate of these higher dimensional kink GWB's occurring on a string network. Unlike the case of cusps discussed in chapter 5, since the mechanism which produces kinks is unchanged by the inclusion of extra dimensions, we assume that the average number of kinks in a loop, \mathcal{K} , is unchanged and will not depend on the number of extra dimensions, (unlike eqn. (5.13)). However, as before, the string network will possess kinks with a range of different θ_b values; we therefore write

$$\frac{d\dot{N}_k}{dz db} \sim \frac{2\mathcal{K}n_L(z)}{PT_L(z)} \frac{\pi(\theta_m(z) - b) D_A(z)^2}{(1+z)^2 H(z)}. \quad (6.17)$$

Integrating over b thus yields

$$\int_0^{\theta_m} (\theta_m - b) = \frac{\theta_m^2}{2}, \quad (6.18)$$

and we can write our kink GWB rate as

$$\frac{d\dot{N}_k}{dz} \sim \frac{\mathcal{K}\theta_m^2 n_L(z)}{PT_L(z)} \frac{\pi D_A(z)^2}{(1+z)^2 H(z)}. \quad (6.19)$$

Figures 6.1 and 6.2 show the 3D gravitational wave amplitude for the cosmic string kink burst calculated by DV, [50], along with our higher dimensional result, for the characteristic frequencies of the LIGO and LISA gravitational wave detectors. We present the amplitudes as in the previous chapter: calculated using the DV interpolating functions (see appendix A) and neglecting Ω_Λ , while also including the results of an exact numerical integration performed for the concordance cosmology ($\Omega_r = 4.6 \times 10^{-5}$, $\Omega_m = 0.28$, $\Omega_\Lambda = 1 - \Omega_m - \Omega_r$).

In figures 6.3 and 6.4 the alternative method of Siemens et al., [179], is used, and we present our results from the kink GWB's in terms of an expected detection rate

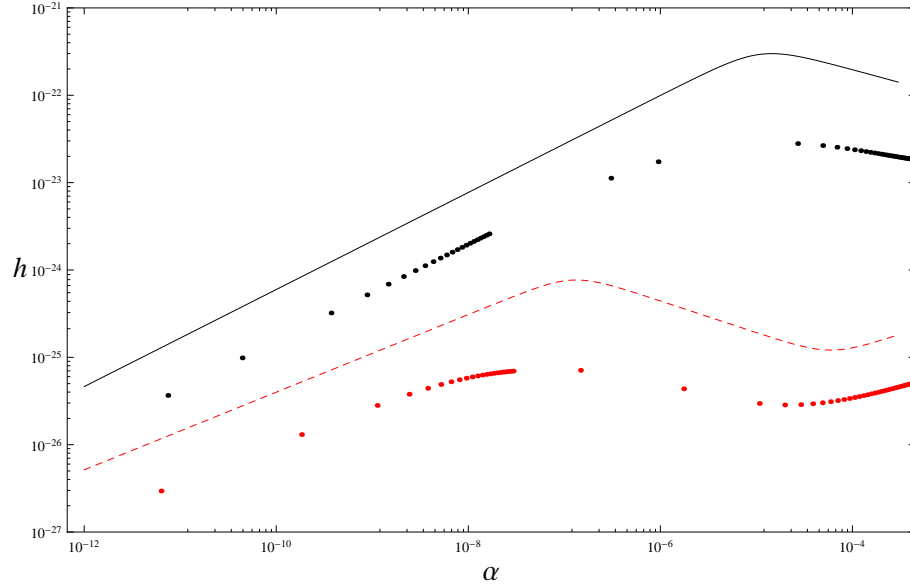


Figure 6.1: Log log plots of gravitational wave amplitudes of bursts as a function of α for $f = 150$ Hz (LIGO) and a detection rate of 1 per year. From top to bottom: the DV kink, (black, solid) and the extra dimensional kink, (red, dashed). Both have an intercommutation probability of $P = 10^{-3}$. The sets of individual dots correspond to the exact numerical redshift integrations as before.

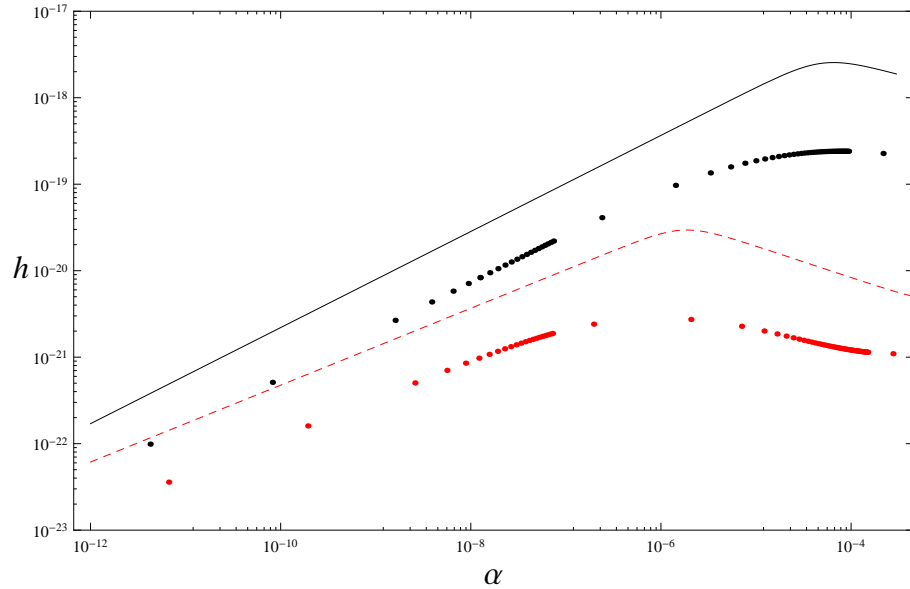


Figure 6.2: Log log plots of gravitational wave amplitudes of bursts as a function of α for $f = 3.9$ mHz (LISA) and a detection rate of 1 per year. From top to bottom: the DV kink, (black, solid) and the extra dimensional kink, (red, dashed). Both have an intercommutation probability of $P = 10^{-3}$. The sets of individual dots correspond to the exact numerical redshift integrations as before.

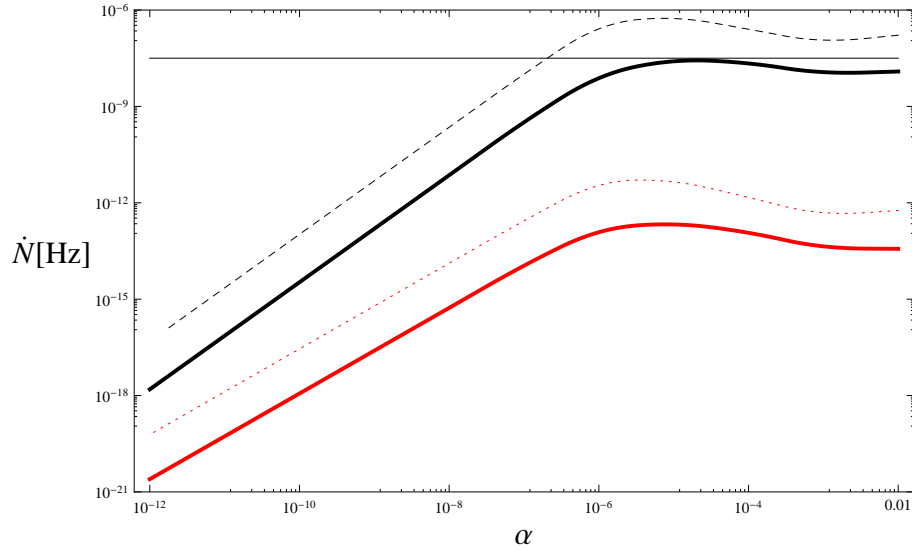


Figure 6.3: A similar plot to that of figure 6.1 (LIGO) but in this case showing the expected rate at an amplitude of $10^{-21} \text{ s}^{-1/3}$, using the method of [179]. The plots are colour coded as before, except in this case, the thick solid lines are now the numerical integration results. From top to bottom: the DV kink, (black, solid) and the extra dimensional kink, (red, dashed). Both have an intercommutation probability of $P = 10^{-3}$. The horizontal black line indicates a rate of one event per year.

at a given amplitude. In this case, the amplitude of the kink waveform is found by comparison with

$$h^{kink} = A|f|^{-2/3}, \quad (6.20)$$

so that the redshift values used for the integration at various values of $G\mu$ are found from

$$\frac{\varphi_t^{1/3}(z)}{(1+z)^{2/3}\varphi_r(z)} = \frac{50AH_0^{-2/3}}{\alpha^{4/3}}, \quad (6.21)$$

where we once again use $A = 10^{-21} \text{ s}^{-1/3}$ (c.f. Siemens et al., [179]), $\alpha \sim 50G\mu$ and φ_t, φ_r are either the DV interpolating functions or related to the exact functions $t(z), D_A(z)$ as before. Figures 6.5 and 6.6 show the DV and extra dimensional kink amplitudes along with the 3D cusp result from [50] for comparison purposes.

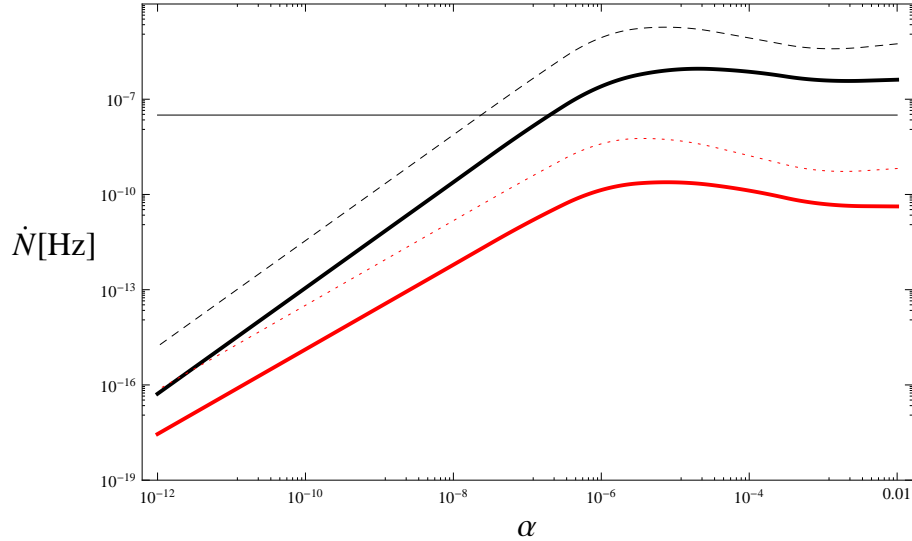


Figure 6.4: A similar plot to that of figure 6.2 (LISA) but in this case showing the expected rate at an amplitude of $10^{-21} \text{ s}^{-1/3}$, using the method of [179]. The plots are colour coded as before, except in this case, the thick solid lines are now the numerical integration results. From top to bottom: the DV kink, (black, solid) and the extra dimensional kink, (red, dashed). Both have an intercommutation probability of $P = 10^{-3}$. The horizontal black line indicates a rate of one event per year.

6.4 Discussion

Once again, we find that the motion of the string in higher dimensions has a noticeable effect on the GWB signal produced by kinks on the string loop, suppressing it with respect to the usual 3D signal, as we found previously on calculating the cusp signal. There is one striking difference, however, with the cusp calculation performed in the last chapter, namely that the suppression of the kink signal does not depend on the number of extra dimensions in which the string is moving.

Although, as observed by Damour and Vilenkin, [50], (and can be seen in figures 6.5 and 6.6), the 3D kink signal is at least an order of magnitude lower than the cusp signal in the case of both frequencies studied before the extra dimensions are taken into account, and would be unlikely to be observed by LIGO, though the LISA signal is more promising. The more ubiquitous nature of kinks on a string loop in extra dimensions when compared to cusps or NCE's, makes the kink amplitude an important signal, particularly if the number of extra dimensions is large. However, when taken in conjunction with the extra dimensional cusp results, the kink amplitude adds an

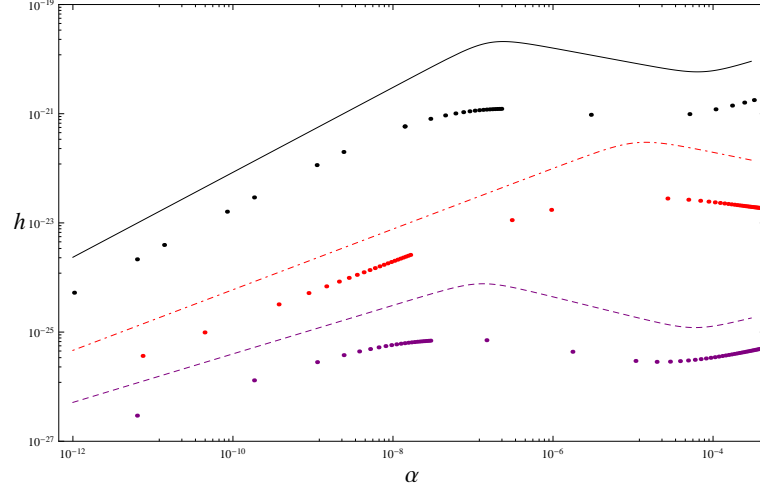


Figure 6.5: Log log plots of gravitational wave amplitudes of bursts as a function of α for $f = 150$ Hz (LIGO) and a detection rate of 1 per year. From top to bottom, the DV cusp, (black, solid), the DV kink, (red, dotdashed) and the extra dimensional kink, (purple, dashed). All have an intercommutation probability of $P = 10^{-3}$. The sets of individual dots correspond to the exact numerical redshift integrations as before.

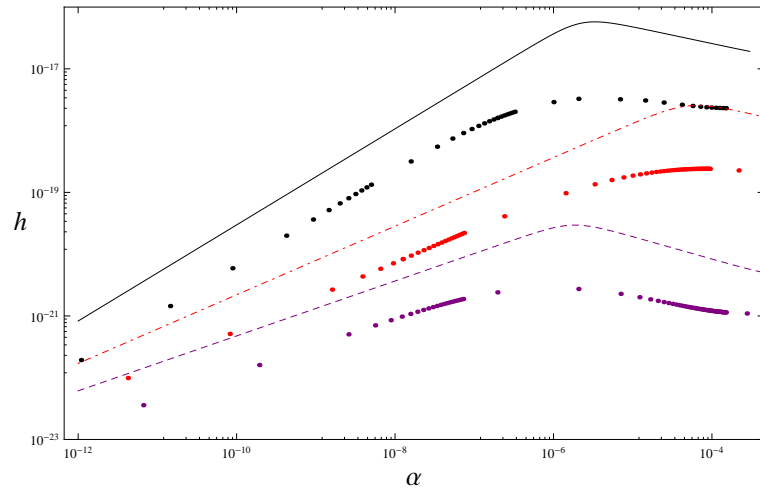


Figure 6.6: Log log plots of gravitational wave amplitudes of bursts as a function of α for $f = 3.9$ mHz (LISA) and a detection rate of 1 per year. From top to bottom, the DV cusp, (black, solid), the DV kink, (red, dotdashed) and the extra dimensional kink, (purple, dashed). All have an intercommutation probability of $P = 10^{-3}$. The sets of individual dots correspond to the exact numerical redshift integrations as before.

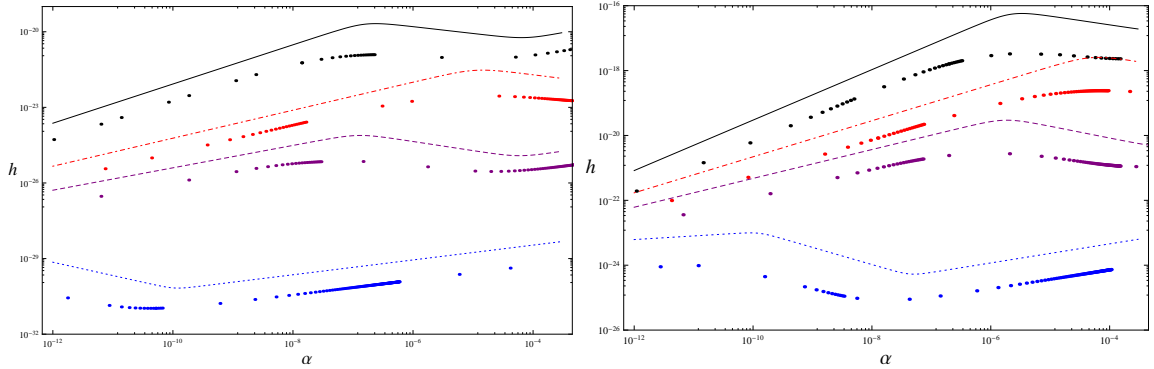


Figure 6.7: Log log plots of gravitational wave amplitudes of bursts as a function of α for $f = 150$ Hz (LIGO) on the left and $f = 3.9$ mHz (LISA) on the right with a detection rate of 1 per year. From top to bottom, the DV cusp, (black, solid), the DV kink, (red, dotdashed), the extra dimensional kink, (purple, dashed) and the extra dimensional cusp with $n = 6$, (blue, dotted). All have an intercommutation probability of $P = 10^{-3}$. The sets of individual dots correspond to the exact numerical redshift integrations as before.

element of ambiguity to the conclusions drawn in the last chapter, as the kink signal sits in between the $n = 1$ and $n = 3$ cusp amplitudes,

Nevertheless, if we look at the cusp and kink amplitudes in figures 6.1, 5.2 (or the LISA equivalents), we can see that the effect of including increasing numbers of extra dimensions is to shift the maximum of the amplitude to smaller values of α . However it is also evident that the maximum of the 3D kink amplitude occurs at a larger value of α than the corresponding cusp maximum before being shifted and so it is possible that the position of this maximum could allow us to distinguish between cusps and kinks. Furthermore, if the cusp in fact has a modified measure as in eqn. (5.20), which could occur if any restriction is placed on the extra dimensions, the change in the dependence of the rate on the critical angle θ_m from θ_m^2 to θ_m^{n+2} could be used as a distinguishing feature, as the probability of kink formation will not be affected by any restrictions of the string motion in the extra dimensions.

In summary, we find that the gravitational wave burst signal from kinks on cosmic string loops are affected by the motion of the string in extra dimensions, producing a noticeable reduction in the signal despite the reduced intercommutation probability. Although the kink signal is weaker than that of the cusp, its independence of the number of extra dimensions, n , could lead to it being important, particularly if n is large and the detection of such a signal would be a valuable step in confirming the general brane inflation scenario. We note as before, that these effects are dependent on the frequency

at which they are observed; it is evident, (particularly from the rate plots figures 6.3 and 6.4), that there is a much better chance of observing a kink signal at LISA rather than LIGO. We finally observe, as in the cusp case, that the approximation used in this method to find the waveform, (i.e. that $\theta_m \ll 1$), breaks down at nHz frequencies, where the angle $\theta_m \sim \mathcal{O}(1)$ and the integral $I_+ \rightarrow 0$ rapidly.

Chapter 7

Conclusions

The emergence of extra dimensions as a mechanism to modify more standard gravitational models has a historical precedent from the time of Kaluza. Whether introduced for phenomenological reasons or in anticipation of string theory, the addition of extra dimensions to a theoretical framework is becoming more widespread, and it is therefore worth examining their observational consequences. In this thesis we considered the observable effects extra dimensions could have on various aspects of cosmology: in chapter 3 we considered the asymmetric brane model, [46, 47], and its cosmological implications, while the effects on gravitational wave bursts from cosmic string cusps and kinks were considered in chapters 5 and 6.

We began by discussing braneworlds, which confine the standard model forces to a four dimensional surface, while allowing gravity to propagate in all dimensions; these models can produce both short and long range modifications of gravity. In particular, the large scale modifications have been thought of as a possible method of inducing late time acceleration in the universe without the use of a cosmological constant. This has been most widely studied in the context of the DGP model. However, underlying problems with this model prompted us to consider whether an alternative model could replicate the promising results of the DGP model, while avoiding its problems. The cosmological equations derived from the asymmetric brane model, which can produce long range modifications of gravity, were also shown to reduce to the standard 4D results over a range of scales, which can be chosen appropriately to satisfy observational constraints. To facilitate comparisons with the DGP model, we showed how the asymmetric equations of motion could be viewed as a generalisation of the DGP cosmological equations and reparameterised in order to express the asymmetric contribution in terms of a single new parameter. We then investigated the qualitative effect of this new parameter with

type Ia supernovae and the cosmic microwave background. Baryon acoustic oscillation (BAO) data were included simply for reference and we did not add to the debate on the suitability of this quantity for models with non-standard evolution. We found that the inclusion of the new parameter worsened agreement with the data, as different datasets had opposing effects on the parameter space. Furthermore, it was shown, [73], that the asymmetric model contains ghosts and so, both phenomenologically and fundamentally, the model was ruled out as a sensible alternative to the concordance cosmology.

We then changed direction slightly to consider the consequences of extra dimensions in the early universe, in particular studying the behaviour of cosmic string loops in higher dimensional models. Cosmic strings are topological defects formed by phase transitions in the early universe; higher dimensional cosmic strings can also arise in models of brane inflation, [48, 49, 167], where the attractive potential between a brane and anti-brane can produce slow roll inflation. If these cosmic strings self intersect, they can create loops due to the intercommutation properties of the string. It was shown by Damour and Vilenkin that features of these string loops, known as cusps and kinks, can produce high frequency beamed bursts of gravitational radiation, which could provide a highly distinctive signal for gravitational wave detectors. We investigated the effect on cusps and kinks and the gravitational wave bursts they emit if the string moves in a higher dimensional spacetime. Cusp formation was found to be substantially affected by the inclusion of extra dimensions, the main reason being the gauge conditions, which require the string solutions to move on the surface of a $(2 + n)$ -sphere. As the string curves are two dimensional and cusp formation requires the left and right moving halves of the string to intersect, the inclusion of any extra dimensions changes a cusp from a generic event to a very rare occurrence. In consequence, we introduced the concept of a near cusp event, where a cusp is almost formed, and found that these events can still produce gravitational wave bursts. The distribution of near cusp events was shown to play a part in altering the extra dimensional signal and we discussed the possible effects of warping and other methods of restricting the extra dimensions. We also discussed how these events and their distribution resulted in a suppression of the signal dependent on the number of extra dimensions, despite an enhancement effect from a decrease in the intercommutation probability. These alterations in the cusp amplitude could lead to predictions for the number of extra dimensions (although unlikely due to the frequency dependence and the narrow range of α values where the signals would be distinct).

Next we considered the analogous effects on gravitational radiation emitted from kinks. We found that the presence of extra dimensions also leads to a suppression of the

kink signal, however, the effect is not as pronounced as in the case of cusps. As kinks are formed as a result of the discontinuity in the tangent vector to the string, which occurs whenever there is an intercommutation, whether between two strings or as a result of a self intersection, their formation is not affected by the movement of the string loops in higher dimensions. In particular, this means the probability of kink formation does not change with the addition of higher dimensions, unlike cusps, and we found that the suppression of the kink signal was not dependent on the number of extra dimensions.

We have shown that higher dimensional models can have an impact on cosmological observations. While our results have not produced evidence of a ‘smoking gun’ for extra dimensions, we have seen some intriguing hints and can be assured that further study of the effects arising from extra dimensions will be rewarding. At a time when the LHC is beginning to probe higher energy scales and increasing numbers of experiments are mapping our universe (Planck, Herschel, LIGO, planned LISA etc.), these extra dimensional effects, if observed, could offer an unparalleled insight into the fundamental nature of the universe.

Appendix A

The Damour-Vilenkin interpolating functions

Damour and Vilenkin, [50], used interpolating functions of redshift for the time

$$t(z) = \int_z^\infty \frac{dz'}{(1+z')H(z')}, \quad (\text{A.1})$$

the physical distance

$$a_0 r = a_0 \int_0^z \frac{dz'}{H(z')}, \quad (\text{A.2})$$

related to the angular diameter distance, $D_A(z)$, and the volume element

$$dV(z) = \frac{4\pi r^2}{(1+z)^3 H(z)} dz, \quad (\text{A.3})$$

where the Hubble parameter for a flat universe is given by

$$H(z) = H_0(\Omega_m(1+z)^3 + \Omega_r(1+z)^4 + \Omega_\Lambda)^{1/2}. \quad (\text{A.4})$$

These interpolating functions are given by, [50, 179]:

$$t(z) = t_0(1+z)^{-3/2}(1+z/z_{eq})^{-1/2} \quad (\text{A.5})$$

$$a_0 r(z) = t_0 \frac{z}{(1+z)} \quad (\text{A.6})$$

$$dV(z) = t_0^3 10^2 z^2 (1+z)^{-13/2} (1+z/z_{eq})^{-1/2}. \quad (\text{A.7})$$

If we substitute these expressions into eqn. (4.33) (taking an extra factor of z into account because of the logarithmic derivative in eqn. (4.36)), we find, neglecting factors of 2 and using the interpolating functions along with eqn. (4.34) for θ_m ,

$$\dot{N} \sim 10^2 \mathcal{C} P^{-1} t_0^{-1} \alpha^{-8/3} (ft_0)^{-2/3} z^3 (1+z)^{-7/6} (1+z/z_{eq})^{11/6}. \quad (\text{A.8})$$

If we then rewrite this as

$$\dot{N} \sim 10^2 \mathcal{C} P^{-1} t_0^{-1} \alpha^{-8/3} (ft_0)^{-2/3} y, \quad (\text{A.9})$$

where

$$y = z^3 (1+z)^{-7/6} (1+z/z_{eq})^{11/6}, \quad (\text{A.10})$$

then rearranging eqn. (A.9) yields

$$y = 10^{-2} (\dot{N} P / \mathcal{C}) t_0 \alpha^{8/3} (ft_0)^{2/3}. \quad (\text{A.11})$$

In order to rewrite the redshift in terms of this new quantity y , we consider eqn. (A.10) in 3 redshift regimes, $z < 1$, $1 < z < z_{eq}$ and $z > z_{eq}$, and approximate:

$$z < 1 : y \sim z^3 \implies z \sim y^{1/3} \quad (\text{A.12})$$

$$1 < z < z_{eq} : y \sim z^3 z^{-7/6} \implies z \sim y^{6/11} \quad (\text{A.13})$$

$$z > z_{eq} : y \sim z^3 z^{-7/6} z^{11/6} z_{eq}^{-11/6} \implies z \sim y^{3/11} y_{eq}, \quad (\text{A.14})$$

where $y_{eq} \equiv z_{eq}^{11/6}$. We reassemble the expression for z in the same way and find

$$\begin{aligned} z &\sim y^{1/3} (1+y)^{6/11-1/3} (1+y/y_{eq})^{3/11-6/11} \\ \implies z &\sim y^{1/3} (1+y)^{7/33} (1+y/y_{eq})^{-3/11}. \end{aligned} \quad (\text{A.15})$$

If we now recall the expression for the amplitude of a single cusp, eqn. (4.29), and rewrite it using the interpolating functions (with the use of the one scale model (4.32)), we find

$$h^{cusp} \sim G \mu \alpha^{2/3} (ft_0)^{-1/3} z^{-1} (1+z)^{-1/3} (1+z/z_{eq})^{-1/3}. \quad (\text{A.16})$$

Expanding this expression in the 3 redshift regions used above and replacing each one with the appropriate expression in terms of y ,

$$z < 1 \implies h \sim z^{-1} \sim y^{-1/3} \quad (\text{A.17})$$

$$1 < z, z_{eq} \implies h \sim z^{-1} z^{-1/3} \sim y^{-24/33} \quad (\text{A.18})$$

$$z > z_{eq} \implies h \sim z^{-1} z^{-1/3} z^{-1/3} \sim y^{-5/11}, \quad (\text{A.19})$$

which when reassembled as before and combined with eqn. (A.11) yield an expression for the amplitude of cusps produced in a string network with a rate of \dot{N} :

$$h^{cusp} \sim G\mu\alpha^{2/3}(ft_0)^{-1/3}y^{-1/3}(1+y)^{-13/33}(1+y/y_{eq})^{3/11}. \quad (\text{A.20})$$

This method (and the same interpolating functions (A.5), (A.6) and (A.7)) can also be used to find the interpolating function expression for the amplitude in the extra dimensional case:

$$h_{ed}^{cusp} \sim G\mu\alpha^{2/3}(ft_0)^{-1/3}y^{-1/3}(1+y)^{(-13+n)/(33+3n)}(1+y/y_{eq})^{3/(11+n)}, \quad (\text{A.21})$$

where in this case, we use eqn. (5.15) for the rate, finding that

$$y_{ed} = 10^{-2}(\dot{N}P/C)(n+1)(n+2)t_0\alpha^{(8+n)/3}(ft_0)^{(2+n)/3}, \quad (\text{A.22})$$

and $y_{eq} \equiv z_{eq}^{(11+n)/6}$.

In the case of the kinks, as we saw in chapter 6, the dependence of the rate - eqns. (6.13), (6.19) - on the angle θ_m changes, however, we can still use the above method to derive the interpolating formalism. The 3D kink rate is found to be, [50]:

$$h^{kink} \sim G\mu\alpha^{1/3}(ft_0)^{-2/3}y^{-1/3}(1+y)^{-11/30}(1+y/y_{eq})^{3/10}, \quad (\text{A.23})$$

where

$$y^{kink} = 10^{-2}(\dot{N}P/K)t_0\alpha^{7/3}(ft_0)^{1/3}, \quad (\text{A.24})$$

and $y_{eq} \equiv z_{eq}^{5/3}$, while the extra dimensional expression for the kink GWB amplitude is given by

$$h_{ed}^{kink} \sim G\mu\alpha^{1/3}(ft_0)^{-2/3}y^{-1/3}(1+y)^{-10/33}(1+y/y_{eq})^{3/11}, \quad (\text{A.25})$$

where

$$y_{ed}^{kink} = 0.02(\dot{N}P/\mathcal{K})t_0\alpha^{8/3}(ft_0)^{2/3}, \quad (\text{A.26})$$

and $y_{eq} \equiv z_{eq}^{11/6}$.

Bibliography

- [1] E. O’Callaghan, R. Gregory, and A. Pourtsidou, “The Cosmology of Asymmetric Brane Modified Gravity,” *JCAP* **0909** (2009) 020, [arXiv:0904.4182](#) [[astro-ph.CO](#)].
- [2] E. O’Callaghan, S. Chadburn, G. Geshnizjani, R. Gregory, and I. Zavala, “Effect of Extra Dimensions on Gravitational Waves from Cosmic Strings,” *Phys. Rev. Lett.* **105** (2010) 081602, [arXiv:1003.4395](#) [[hep-th](#)].
- [3] E. O’Callaghan, S. Chadburn, G. Geshnizjani, R. Gregory, and I. Zavala, “The effect of extra dimensions on gravity wave bursts from cosmic string cusps,” *JCAP* **1009** (2010) 013, [arXiv:1005.3220](#) [[hep-th](#)].
- [4] E. Komatsu *et al.*, “Seven-Year Wilkinson Microwave Anisotropy Probe (WMAP) Observations: Cosmological Interpretation,” [arXiv:1001.4538](#) [[astro-ph.CO](#)].
- [5] D. Larson *et al.*, “Seven-Year Wilkinson Microwave Anisotropy Probe (WMAP) Observations: Power Spectra and WMAP-Derived Parameters,” [arXiv:1001.4635](#) [[astro-ph.CO](#)].
- [6] **Supernova Search Team** Collaboration, A. G. Riess *et al.*, “Observational Evidence from Supernovae for an Accelerating Universe and a Cosmological Constant,” *Astron. J.* **116** (1998) 1009–1038, [arXiv:astro-ph/9805201](#).
- [7] **Supernova Search Team** Collaboration, A. G. Riess *et al.*, “Type Ia Supernova Discoveries at $z \leq 1$ From the Hubble Space Telescope: Evidence for Past Deceleration and Constraints on Dark Energy Evolution,” *Astrophys. J.* **607** (2004) 665–687, [arXiv:astro-ph/0402512](#).
- [8] **Supernova Cosmology Project** Collaboration, S. Perlmutter *et al.*, “Measurements of Omega and Lambda from 42 High-Redshift Supernovae,” *Astrophys. J.* **517** (1999) 565–586, [arXiv:astro-ph/9812133](#).
- [9] **ESSENCE** Collaboration, W. M. Wood-Vasey *et al.*, “Observational Constraints on the Nature of the Dark Energy: First Cosmological Results from

- the ESSENCE Supernova Survey,” *Astrophys. J.* **666** (2007) 694–715, arXiv:astro-ph/0701041.
- [10] A. G. Riess *et al.*, “New Hubble Space Telescope Discoveries of Type Ia Supernovae at $z > 1$: Narrowing Constraints on the Early Behavior of Dark Energy,” *Astrophys. J.* **659** (2007) 98–121, arXiv:astro-ph/0611572.
- [11] **Supernova Cosmology Project** Collaboration, M. Kowalski *et al.*, “Improved Cosmological Constraints from New, Old and Combined Supernova Datasets,” *Astrophys. J.* **686** (2008) 749–778, arXiv:0804.4142 [astro-ph].
- [12] **The 2dFGRS** Collaboration, S. Cole *et al.*, “The 2dF Galaxy Redshift Survey: Power-spectrum analysis of the final dataset and cosmological implications,” *Mon. Not. Roy. Astron. Soc.* **362** (2005) 505–534, arXiv:astro-ph/0501174.
- [13] **SDSS** Collaboration, M. Tegmark *et al.*, “Cosmological Constraints from the SDSS Luminous Red Galaxies,” *Phys. Rev.* **D74** (2006) 123507, arXiv:astro-ph/0608632.
- [14] J. L. Feng, “Dark Matter Candidates from Particle Physics and Methods of Detection,” arXiv:1003.0904 [astro-ph.CO].
- [15] R. Bernabei *et al.*, “New results from DAMA/LIBRA,” *Eur. Phys. J.* **C67** (2010) 39–49, arXiv:1002.1028 [astro-ph.GA].
- [16] **CDMS II** Collaboration, “Dark Matter Search Results from the CDMS II Experiment,” *Science* **327** (2010) 1619–1621.
- [17] **XENON** Collaboration, J. Angle *et al.*, “First Results from the XENON10 Dark Matter Experiment at the Gran Sasso National Laboratory,” *Phys. Rev. Lett.* **100** (2008) 021303, arXiv:0706.0039 [astro-ph].
- [18] **CoGeNT** Collaboration, C. E. Aalseth *et al.*, “Results from a Search for Light-Mass Dark Matter with a P- type Point Contact Germanium Detector,” arXiv:1002.4703 [astro-ph.CO].
- [19] J. R. Brownstein and J. W. Moffat, “The Bullet Cluster 1E0657-558 evidence shows Modified Gravity in the absence of Dark Matter,” *Mon. Not. Roy. Astron. Soc.* **382** (2007) 29–47, arXiv:astro-ph/0702146.
- [20] R. R. Caldwell, R. Dave, and P. J. Steinhardt, “Cosmological Imprint of an Energy Component with General Equation-of-State,” *Phys. Rev. Lett.* **80** (1998) 1582–1585, arXiv:astro-ph/9708069.
- [21] S. M. Carroll, V. Duvvuri, M. Trodden, and M. S. Turner, “Is Cosmic Speed-Up Due to New Gravitational Physics?,” *Phys. Rev.* **D70** (2004) 043528, arXiv:astro-ph/0306438.

- [22] S. M. Carroll, A. De Felice, V. Duvvuri, D. A. Easson, M. Trodden, and M. S. Turner, “The cosmology of generalized modified gravity models,” *Phys. Rev.* **D71** (2005) 063513, [arXiv:astro-ph/0410031](#).
- [23] D. A. Easson, “Cosmic Acceleration and Modified Gravitational Models,” *Int. J. Mod. Phys.* **A19** (2004) 5343–5350, [arXiv:astro-ph/0411209](#).
- [24] M. Milgrom, “A Modification of the Newtonian dynamics as a possible alternative to the hidden mass hypothesis,” *Astrophys. J.* **270** (1983) 365–370.
- [25] J. D. Bekenstein, “Relativistic gravitation theory for the MOND paradigm,” *Phys. Rev.* **D70** (2004) 083509, [arXiv:astro-ph/0403694](#).
- [26] K. Freese and M. Lewis, “Cardassian Expansion: a Model in which the Universe is Flat, Matter Dominated, and Accelerating,” *Phys. Lett.* **B540** (2002) 1–8, [arXiv:astro-ph/0201229](#).
- [27] V. F. Cardone, A. Troisi, and S. Capozziello, “Unified dark energy models: A phenomenological approach,” *Phys. Rev.* **D69** (2004) 083517, [arXiv:astro-ph/0402228](#).
- [28] J. Polchinski, *String Theory*, vol. 1 and 2. Cambridge University Press, 1998.
- [29] O. Klein, “Quantum Theory and Five Dimensional Theory of Relativity,” *Zeits. Phys.* **37** (1926) 895.
- [30] T. Kaluza, “On the Problem of Unity in Physics,” *Sitzungsber. Preuss. Akad. Wiss. Berlin (Math. Phys.)* **K1** (1921) 966–972.
- [31] J. M. Overduin and P. S. Wesson, “Kaluza-Klein gravity,” *Phys. Rept.* **283** (1997) 303–380, [arXiv:gr-qc/9805018](#).
- [32] P. S. Wells, “Experimental tests of the standard model,” *Eur. Phys. J.* **C33** (2004) s5–s20.
- [33] N. Arkani-Hamed, S. Dimopoulos, and G. R. Dvali, “The hierarchy problem and new dimensions at a millimeter,” *Phys. Lett.* **B429** (1998) 263–272, [arXiv:hep-ph/9803315](#).
- [34] N. Arkani-Hamed, S. Dimopoulos, and G. R. Dvali, “Phenomenology, astrophysics and cosmology of theories with sub-millimeter dimensions and TeV scale quantum gravity,” *Phys. Rev.* **D59** (1999) 086004, [arXiv:hep-ph/9807344](#).
- [35] I. Antoniadis, N. Arkani-Hamed, S. Dimopoulos, and G. R. Dvali, “New dimensions at a millimeter to a Fermi and superstrings at a TeV,” *Phys. Lett.* **B436** (1998) 257–263, [arXiv:hep-ph/9804398](#).
- [36] D. J. Kapner, T. S. Cook, E. G. Adelberger, J. H. Gundlach, B. R. Heckel, C. D. Hoyle, and H. E. Swanson, “Tests of the gravitational inverse-square law below

- the dark-energy length scale,” *Phys. Rev. Lett.* **98** (2007) 021101, [arXiv:hep-ph/0611184](#).
- [37] E. G. Adelberger, B. R. Heckel, and A. E. Nelson, “Tests of the gravitational inverse-square law,” *Ann. Rev. Nucl. Part. Sci.* **53** (2003) 77–121, [arXiv:hep-ph/0307284](#).
- [38] A. A. Geraci, S. J. Smullin, D. M. Weld, J. Chiaverini, and A. Kapitulnik, “Improved constraints on non-Newtonian forces at 10 microns,” *Phys. Rev.* **D78** (2008) 022002, [arXiv:0802.2350 \[hep-ex\]](#).
- [39] L. Randall and R. Sundrum, “A large mass hierarchy from a small extra dimension,” *Phys. Rev. Lett.* **83** (1999) 3370–3373, [arXiv:hep-ph/9905221](#).
- [40] L. Randall and R. Sundrum, “An alternative to compactification,” *Phys. Rev. Lett.* **83** (1999) 4690–4693, [arXiv:hep-th/9906064](#).
- [41] R. Maartens and K. Koyama, “Brane-World Gravity,” [arXiv:1004.3962 \[hep-th\]](#).
- [42] T. Shiromizu, K.-i. Maeda, and M. Sasaki, “The Einstein equations on the 3-brane world,” *Phys. Rev.* **D62** (2000) 024012, [arXiv:gr-qc/9910076](#).
- [43] C. Csaki, M. Graesser, C. F. Kolda, and J. Terning, “Cosmology of one extra dimension with localized gravity,” *Phys. Lett.* **B462** (1999) 34–40, [arXiv:hep-ph/9906513](#).
- [44] J. Garriga and T. Tanaka, “Gravity in the brane-world,” *Phys. Rev. Lett.* **84** (2000) 2778–2781, [arXiv:hep-th/9911055](#).
- [45] G. R. Dvali, G. Gabadadze, and M. Porrati, “4D gravity on a brane in 5D Minkowski space,” *Phys. Lett.* **B485** (2000) 208–214, [arXiv:hep-th/0005016](#).
- [46] A. Padilla, “Cosmic acceleration from asymmetric branes,” *Class. Quant. Grav.* **22** (2005) 681–694, [arXiv:hep-th/0406157](#).
- [47] A. Padilla, “Infra-red modification of gravity from asymmetric branes,” *Class. Quant. Grav.* **22** (2005) 1087–1104, [arXiv:hep-th/0410033](#).
- [48] G. R. Dvali and S. H. H. Tye, “Brane inflation,” *Phys. Lett.* **B450** (1999) 72–82, [arXiv:hep-ph/9812483](#).
- [49] S. H. S. Alexander, “Inflation from D - anti-D brane annihilation,” *Phys. Rev.* **D65** (2002) 023507, [arXiv:hep-th/0105032](#).
- [50] T. Damour and A. Vilenkin, “Gravitational wave bursts from cusps and kinks on cosmic strings,” *Phys. Rev.* **D64** (2001) 064008, [arXiv:gr-qc/0104026](#).
- [51] T. Damour and A. Vilenkin, “Gravitational wave bursts from cosmic strings,” *Phys. Rev. Lett.* **85** (2000) 3761–3764, [arXiv:gr-qc/0004075](#).

- [52] G. R. Dvali and G. Gabadadze, “Gravity on a brane in infinite-volume extra space,” *Phys. Rev.* **D63** (2001) 065007, [arXiv:hep-th/0008054](#).
- [53] C. de Rham *et al.*, “Cascading gravity: Extending the Dvali-Gabadadze-Porrati model to higher dimension,” *Phys. Rev. Lett.* **100** (2008) 251603, [arXiv:0711.2072 \[hep-th\]](#).
- [54] I. I. Kogan, S. Mouslopoulos, A. Papazoglou, G. G. Ross, and J. Santiago, “A three three-brane universe: New phenomenology for the new millennium?,” *Nucl. Phys.* **B584** (2000) 313–328, [arXiv:hep-ph/9912552](#).
- [55] I. I. Kogan and G. G. Ross, “Brane universe and multigravity: Modification of gravity at large and small distances,” *Phys. Lett.* **B485** (2000) 255–262, [arXiv:hep-th/0003074](#).
- [56] V. Sahni and Y. Shtanov, “Braneworld models of dark energy,” *JCAP* **0311** (2003) 014, [arXiv:astro-ph/0202346](#).
- [57] R. Gregory, V. A. Rubakov, and S. M. Sibiryakov, “Opening up extra dimensions at ultra-large scales,” *Phys. Rev. Lett.* **84** (2000) 5928–5931, [arXiv:hep-th/0002072](#).
- [58] R. Gregory, V. A. Rubakov, and S. M. Sibiryakov, “Gravity and antigravity in a brane world with metastable gravitons,” *Phys. Lett.* **B489** (2000) 203–206, [arXiv:hep-th/0003045](#).
- [59] C. Charmousis, R. Gregory, and A. Padilla, “Stealth Acceleration and Modified Gravity,” *JCAP* **0710** (2007) 006, [arXiv:0706.0857 \[hep-th\]](#).
- [60] Y.-S. Song, I. Sawicki, and W. Hu, “Large-Scale Tests of the DGP Model,” *Phys. Rev.* **D75** (2007) 064003, [arXiv:astro-ph/0606286](#).
- [61] S. Rydbeck, M. Fairbairn, and A. Goobar, “Testing the DGP model with ESSENCE,” *JCAP* **0705** (2007) 003, [arXiv:astro-ph/0701495](#).
- [62] R. Maartens and E. Majerotto, “Observational constraints on self-accelerating cosmology,” *Phys. Rev.* **D74** (2006) 023004, [arXiv:astro-ph/0603353](#).
- [63] V. Barger, Y. Gao, and D. Marfatia, “Accelerating cosmologies tested by distance measures,” *Phys. Lett.* **B648** (2007) 127–132, [arXiv:astro-ph/0611775](#).
- [64] M. Fairbairn and A. Goobar, “Supernova limits on brane world cosmology,” *Phys. Lett.* **B642** (2006) 432–435, [arXiv:astro-ph/0511029](#).
- [65] O. Elgaroy and T. Multamaki, “On using the CMB shift parameter in tests of models of dark energy,” [arXiv:astro-ph/0702343](#).

- [66] Y. Wang and P. Mukherjee, “Robust Dark Energy Constraints from Supernovae, Galaxy Clustering, and Three-Year Wilkinson Microwave Anisotropy Probe Observations,” *Astrophys. J.* **650** (2006) 1, [arXiv:astro-ph/0604051](#).
- [67] C. Charmousis, R. Gregory, N. Kaloper, and A. Padilla, “DGP spectroscopy,” *JHEP* **10** (2006) 066, [arXiv:hep-th/0604086](#).
- [68] R. Gregory, N. Kaloper, R. C. Myers, and A. Padilla, “A New Perspective on DGP Gravity,” *JHEP* **10** (2007) 069, [arXiv:0707.2666 \[hep-th\]](#).
- [69] V. A. Rubakov and M. E. Shaposhnikov, “Extra Space-Time Dimensions: Towards a Solution to the Cosmological Constant Problem,” *Phys. Lett.* **B125** (1983) 139.
- [70] V. A. Rubakov and M. E. Shaposhnikov, “Do We Live Inside a Domain Wall?,” *Phys. Lett.* **B125** (1983) 136–138.
- [71] K. Akama, “An early proposal of ‘brane world’,” *Lect. Notes Phys.* **176** (1982) 267–271, [arXiv:hep-th/0001113](#).
- [72] W. Israel, “Singular hypersurfaces and thin shells in general relativity,” *Nuovo Cim.* **B44S10** (1966) 1.
- [73] K. Koyama, A. Padilla, and F. P. Silva, “Ghosts in asymmetric brane gravity and the decoupled stealth limit,” *JHEP* **03** (2009) 134, [arXiv:0901.0713 \[hep-th\]](#).
- [74] P. Bowcock, C. Charmousis, and R. Gregory, “General brane cosmologies and their global spacetime structure,” *Class. Quant. Grav.* **17** (2000) 4745–4764, [arXiv:hep-th/0007177](#).
- [75] C. Deffayet, “Cosmology on a brane in Minkowski bulk,” *Phys. Lett.* **B502** (2001) 199–208, [arXiv:hep-th/0010186](#).
- [76] C. Deffayet, G. R. Dvali, and G. Gabadadze, “Accelerated universe from gravity leaking to extra dimensions,” *Phys. Rev.* **D65** (2002) 044023, [arXiv:astro-ph/0105068](#).
- [77] Z.-K. Guo, Z.-H. Zhu, J. S. Alcaniz, and Y.-Z. Zhang, “Constraints on the DGP Model from Recent Supernova Observations and Baryon Acoustic Oscillations,” *Astrophys. J.* **646** (2006) 1, [arXiv:astro-ph/0603632](#).
- [78] **WMAP** Collaboration, J. Dunkley *et al.*, “Five-Year Wilkinson Microwave Anisotropy Probe (WMAP) Observations: Likelihoods and Parameters from the WMAP data,” *Astrophys. J. Suppl.* **180** (2009) 306–329, [arXiv:0803.0586 \[astro-ph\]](#).

- [79] **WMAP** Collaboration, D. N. Spergel *et al.*, “Wilkinson Microwave Anisotropy Probe (WMAP) three year results: Implications for cosmology,” *Astrophys. J. Suppl.* **170** (2007) 377, [arXiv:astro-ph/0603449](#).
- [80] **WMAP** Collaboration, D. N. Spergel *et al.*, “First Year Wilkinson Microwave Anisotropy Probe (WMAP) Observations: Determination of Cosmological Parameters,” *Astrophys. J. Suppl.* **148** (2003) 175–194, [arXiv:astro-ph/0302209](#).
- [81] C. Deffayet, S. J. Landau, J. Raux, M. Zaldarriaga, and P. Astier, “Supernovae, CMB, and gravitational leakage into extra dimensions,” *Phys. Rev.* **D66** (2002) 024019, [arXiv:astro-ph/0201164](#).
- [82] J. R. Bond, G. Efstathiou, and M. Tegmark, “Forecasting Cosmic Parameter Errors from Microwave Background Anisotropy Experiments,” *Mon. Not. Roy. Astron. Soc.* **291** (1997) L33–L41, [arXiv:astro-ph/9702100](#).
- [83] **WMAP** Collaboration, E. Komatsu *et al.*, “Five-Year Wilkinson Microwave Anisotropy Probe (WMAP) Observations: Cosmological Interpretation,” *Astrophys. J. Suppl.* **180** (2009) 330–376, [arXiv:0803.0547 \[astro-ph\]](#).
- [84] **SDSS** Collaboration, D. J. Eisenstein *et al.*, “Detection of the Baryon Acoustic Peak in the Large-Scale Correlation Function of SDSS Luminous Red Galaxies,” *Astrophys. J.* **633** (2005) 560–574, [arXiv:astro-ph/0501171](#).
- [85] W. J. Percival *et al.*, “Measuring the Baryon Acoustic Oscillation scale using the SDSS and 2dFGRS,” *Mon. Not. Roy. Astron. Soc.* **381** (2007) 1053–1066, [arXiv:0705.3323 \[astro-ph\]](#).
- [86] J. Dick, L. Knox, and M. Chu, “Reduction of Cosmological Data for the Detection of Time-varying Dark Energy Density,” *JCAP* **0607** (2006) 001, [arXiv:astro-ph/0603247](#).
- [87] Y. Wang, “Clarifying Forecasts of Dark Energy Constraints from Baryon Acoustic Oscillations,” [arXiv:0904.2218 \[astro-ph.CO\]](#).
- [88] **HST** Collaboration, W. L. Freedman *et al.*, “Final Results from the Hubble Space Telescope Key Project to Measure the Hubble Constant,” *Astrophys. J.* **553** (2001) 47–72, [arXiv:astro-ph/0012376](#).
- [89] E. V. Linder, “Cosmic growth history and expansion history,” *Phys. Rev.* **D72** (2005) 043529, [arXiv:astro-ph/0507263](#).
- [90] H. Wei, “Growth Index of DGP Model and Current Growth Rate Data,” *Phys. Lett.* **B664** (2008) 1–6, [arXiv:0802.4122 \[astro-ph\]](#).

- [91] K. Koyama, “Are there ghosts in the self-accelerating brane universe?,” *Phys. Rev. D* **72** (2005) 123511, arXiv:hep-th/0503191.
- [92] A. Higuchi, “Forbidden Mass Range For Spin-2 Field Theory In De Sitter Space-Time,” *Nucl. Phys. B* **282** (1987) 397.
- [93] R. Gregory, “The three burials of Melquiades DGP,” *Prog. Theor. Phys. Suppl.* **172** (2008) 71–80, arXiv:0801.1603 [hep-th].
- [94] C. Deffayet, G. Gabadadze, and A. Iglesias, “Perturbations of self-accelerated universe,” *JCAP* **0608** (2006) 012, arXiv:hep-th/0607099.
- [95] G. Dvali, “Predictive Power of Strong Coupling in Theories with Large Distance Modified Gravity,” *New J. Phys.* **8** (2006) 326, arXiv:hep-th/0610013.
- [96] M. A. Luty, M. Porrati, and R. Rattazzi, “Strong interactions and stability in the DGP model,” *JHEP* **09** (2003) 029, arXiv:hep-th/0303116.
- [97] V. A. Rubakov, “Strong coupling in brane-induced gravity in five dimensions,” arXiv:hep-th/0303125.
- [98] A. Nicolis and R. Rattazzi, “Classical and quantum consistency of the DGP model,” *JHEP* **06** (2004) 059, arXiv:hep-th/0404159.
- [99] K. Koyama and K. Koyama, “Brane induced gravity from asymmetric compactification,” *Phys. Rev. D* **72** (2005) 043511, arXiv:hep-th/0501232.
- [100] T. M. Davis *et al.*, “Scrutinizing exotic cosmological models using ESSENCE supernova data combined with other cosmological probes,” *Astrophys. J.* **666** (2007) 716, arXiv:astro-ph/0701510.
- [101] G. B. Arfken and H. J. Weber, *Mathematical Methods for Physicists*. Harcourt Academic Press, fifth ed., 2001.
- [102] V. Sahni, “Dark matter and dark energy,” *Lect. Notes Phys.* **653** (2004) 141–180, arXiv:astro-ph/0403324.
- [103] V. Sahni and A. Starobinsky, “Reconstructing Dark Energy,” *Int. J. Mod. Phys. D* **15** (2006) 2105–2132, arXiv:astro-ph/0610026.
- [104] M. Ishak, A. Upadhye, and D. N. Spergel, “Probing cosmic acceleration beyond the equation of state: Distinguishing between dark energy and modified gravity models,” *Phys. Rev. D* **74** (2006) 043513, arXiv:astro-ph/0507184.
- [105] A. Vilenkin and E. Shellard, *Cosmic Strings and Other Topological Defects*. Cambridge University Press, 2000.
- [106] M. E. Peskin and D. V. Schoeder, *An Introduction to Quantum Field Theory*. Westview Press, 1995.

- [107] T. W. B. Kibble, “Topology of Cosmic Domains and Strings,” *J. Phys.* **A9** (1976) 1387–1398.
- [108] M. B. Hindmarsh and T. W. B. Kibble, “Cosmic strings,” *Rept. Prog. Phys.* **58** (1995) 477–562, [arXiv:hep-ph/9411342](#).
- [109] A. Vilenkin, “Cosmic Strings and Domain Walls,” *Phys. Rept.* **121** (1985) 263.
- [110] J. Goldstone, “Field Theories with Superconductor Solutions,” *Nuovo Cim.* **19** (1961) 154–164.
- [111] A. Vilenkin, “Cosmic Strings,” *Phys. Rev.* **D24** (1981) 2082–2089.
- [112] A. Vilenkin, “Gravitational Field of Vacuum Domain Walls and Strings,” *Phys. Rev.* **D23** (1981) 852–857.
- [113] M. R. Anderson, *The Mathematical Theory of Cosmic Strings*. Institute of Physics Publishing, 2003.
- [114] D. Forster, “Dynamics of Relativistic Vortex Lines and their Relation to Dual Theory,” *Nucl. Phys.* **B81** (1974) 84.
- [115] E. P. S. Shellard, “Cosmic String Interactions,” *Nucl. Phys.* **B283** (1987) 624–656.
- [116] K. J. M. Moriarty, E. Myers, and C. Rebbi, “Dynamical Interactions Of Flux Vortices In Superconductors,” *Phys. Lett.* **B207** (1988) 411.
- [117] R. A. Matzner, “Interaction of U(1) Cosmic Strings: Numerical Intercommutation,” *Comput. Phys.* **2** (1988) 51.
- [118] J. Silk and A. Vilenkin, “Cosmic Strings And Galaxy Formation,” *Phys. Rev. Lett.* **53** (1984) 1700–1703.
- [119] A. Vilenkin, “Cosmological Density Fluctuations Produced by Vacuum Strings,” *Phys. Rev. Lett.* **46** (1981) 1169–1172.
- [120] Y. B. Zeldovich, “Cosmological fluctuations produced near a singularity,” *Mon. Not. Roy. Astron. Soc.* **192** (1980) 663–667.
- [121] N. Turok, “Grand Unified Strings and Galaxy Formation,” *Nucl. Phys.* **B242** (1984) 520.
- [122] A. Albrecht, R. A. Battye, and J. Robinson, “The case against scaling defect models of cosmic structure formation,” *Phys. Rev. Lett.* **79** (1997) 4736–4739, [arXiv:astro-ph/9707129](#).
- [123] U.-L. Pen, U. Seljak, and N. Turok, “Power spectra in global defect theories of cosmic structure formation,” *Phys. Rev. Lett.* **79** (1997) 1611–1614, [arXiv:astro-ph/9704165](#).

- [124] M. Wyman, L. Pogosian, and I. Wasserman, “Bounds on cosmic strings from WMAP and SDSS,” *Phys. Rev.* **D72** (2005) 023513, [arXiv:astro-ph/0503364](#).
- [125] R. H. Brandenberger, A. T. Sornborger, and M. Trodden, “Gamma-ray bursts from ordinary cosmic strings,” *Phys. Rev.* **D48** (1993) 940–942, [arXiv:hep-ph/9302254](#).
- [126] V. Berezhinsky, B. Hnatyk, and A. Vilenkin, “Gamma ray bursts from superconducting cosmic strings,” *Phys. Rev.* **D64** (2001) 043004, [arXiv:astro-ph/0102366](#).
- [127] A. Babul, B. Paczynski, and D. Spergel, “Gamma-ray bursts from superconducting cosmic strings at large redshifts,” *Astrophys. J.* **316** (1987) L49–L54.
- [128] C. T. Hill, D. N. Schramm, and T. P. Walker, “Ultrahigh-Energy Cosmic Rays from Superconducting Cosmic Strings,” *Phys. Rev.* **D36** (1987) 1007.
- [129] P. Bhattacharjee, “Cosmic Strings and Ultrahigh-Energy Cosmic Rays,” *Phys. Rev.* **D40** (1989) 3968.
- [130] J. R. Gott, III, “Gravitational lensing effects of vacuum strings: Exact solutions,” *Astrophys. J.* **288** (1985) 422–427.
- [131] W. A. Hiscock, “Exact Gravitational Field of a String,” *Phys. Rev.* **D31** (1985) 3288–3290.
- [132] T. Vachaspati and A. Vilenkin, “Gravitational Radiation from Cosmic Strings,” *Phys. Rev.* **D31** (1985) 3052.
- [133] A. Einstein and N. Rosen, “On gravitational waves,” *J. Franklin. Inst.* **223** (1937) 43–54.
- [134] R. A. Hulse and J. H. Taylor, “Discovery of a pulsar in a binary system,” *Astrophys. J.* **195** (1975) L51–L53.
- [135] J. M. Weisberg and J. H. Taylor, “Gravitational Raditation From An Orbiting Pulsar,” *Gen. Rel. Grav.* **13** (1981) 1–6.
- [136] G. Hobbs, “Gravitational wave detection using high precision pulsar observations,” *Class. Quant. Grav.* **25** (2008) 114032, [arXiv:0802.1309 \[astro-ph\]](#).
- [137] G. Hobbs *et al.*, “The international pulsar timing array project: using pulsars as a gravitational wave detector,” *Class. Quant. Grav.* **27** (2010) 084013, [arXiv:0911.5206 \[astro-ph.SR\]](#).
- [138] F. Acernese *et al.*, “Status of Virgo,” *Class. Quant. Grav.* **25** (2008) 114045.

- [139] F. Acernese *et al.*, “VIRGO and the worldwide search for gravitational waves,” *AIP Conf. Proc.* **751** (2005) 92–100.
- [140] **LIGO Scientific** Collaboration, H. Grote, “The GEO 600 status,” *Class. Quant. Grav.* **27** (2010) 084003.
- [141] **LIGO Scientific** Collaboration, M. Hewitson, “Preparing GEO 600 for gravitational wave astronomy: A status report,” *Class. Quant. Grav.* **22** (2005) S891–S900.
- [142] **LIGO Scientific** Collaboration, B. Abbott *et al.*, “LIGO: The Laser Interferometer Gravitational-Wave Observatory,” *Rept. Prog. Phys.* **72** (2009) 076901, [arXiv:0711.3041 \[gr-qc\]](#).
- [143] **LIGO Scientific** Collaboration, B. P. Abbott *et al.*, “First LIGO search for gravitational wave bursts from cosmic (super)strings,” *Phys. Rev.* **D80** (2009) 062002, [arXiv:0904.4718 \[astro-ph.CO\]](#).
- [144] K. Danzmann, “LISA and ground-based detectors for gravitational waves: An overview,”. Prepared for 2nd International LISA Symposium on Gravitational Waves, Pasadena, CA, 6-9 Jul 1998.
- [145] L. Ju, D. G. Blair, and C. Zhao, “Detection of gravitational waves,” *Rept. Prog. Phys.* **63** (2000) 1317–1427.
- [146] Weber, J. , “Detection and Generation of Gravitational Waves,” *Phys. Rev.* **117** no. 1, (Jan, 1960) 306–313.
- [147] J. Weber, “Evidence for discovery of gravitational radiation,” *Phys. Rev. Lett.* **22** (1969) 1320–1324.
- [148] A. M. Cruise, “An electromagnetic detector for very-high-frequency gravitational waves,” *Class. Quant. Grav.* **17** (2000) 2525–2530.
- [149] A. M. Cruise and R. M. J. Ingley, “A prototype gravitational wave detector for 100-MHz,” *Class. Quant. Grav.* **23** (2006) 6185–6193.
- [150] T. Damour and A. Vilenkin, “Gravitational radiation from cosmic (super)strings: Bursts, stochastic background, and observational windows,” *Phys. Rev.* **D71** (2005) 063510, [arXiv:hep-th/0410222](#).
- [151] T. W. B. Kibble and N. Turok, “Selfintersection of Cosmic Strings,” *Phys. Lett.* **B116** (1982) 141.
- [152] X. Siemens and K. D. Olum, “Gravitational radiation and the small-scale structure of cosmic strings,” *Nucl. Phys.* **B611** (2001) 125–145, [arXiv:gr-qc/0104085](#).

- [153] T. W. B. Kibble, “Evolution Of A System Of Cosmic Strings,” *Nucl. Phys.* **B252** (1985) 227.
- [154] T. Vachaspati, A. E. Everett, and A. Vilenkin, “Radiation From Vacuum Strings And Domain Walls,” *Phys. Rev.* **D30** (1984) 2046.
- [155] C. J. Burden, “Gravitational Radiation From A Particular Class Of Cosmic Strings,” *Phys. Lett.* **B164** (1985) 277.
- [156] T. Vachaspati, “Gravity Of Cosmic Loops,” *Phys. Rev.* **D35** (1987) 1767–1775.
- [157] J. M. Quashnock and D. N. Spergel, “Gravitational Selfinteractions Of Cosmic Strings,” *Phys. Rev.* **D42** (1990) 2505–2520.
- [158] B. Allen and E. P. S. Shellard, “Gravitational radiation from cosmic strings,” *Phys. Rev.* **D45** (1992) 1898–1912.
- [159] B. Allen, P. Casper, and A. Ottewill, “Analytic results for the gravitational radiation from a class of cosmic string loops,” *Phys. Rev.* **D50** (1994) 3703–3712, [arXiv:gr-qc/9405037](#).
- [160] X. Siemens, K. D. Olum, and A. Vilenkin, “On the size of the smallest scales in cosmic string networks,” *Phys. Rev.* **D66** (2002) 043501, [arXiv:gr-qc/0203006](#).
- [161] J. Polchinski and J. V. Rocha, “Cosmic string structure at the gravitational radiation scale,” *Phys. Rev.* **D75** (2007) 123503, [arXiv:gr-qc/0702055](#).
- [162] J. V. Rocha, “Scaling solution for small cosmic string loops,” *Phys. Rev. Lett.* **100** (2008) 071601, [arXiv:0709.3284 \[gr-qc\]](#).
- [163] E. Witten, “Cosmic Superstrings,” *Phys. Lett.* **B153** (1985) 243.
- [164] J. Polchinski, “Introduction to cosmic F- and D-strings,” [arXiv:hep-th/0412244](#).
- [165] M. G. Jackson, N. T. Jones, and J. Polchinski, “Collisions of cosmic F- and D-strings,” *JHEP* **10** (2005) 013, [arXiv:hep-th/0405229](#).
- [166] J. Polchinski, “Dirichlet-Branes and Ramond-Ramond Charges,” *Phys. Rev. Lett.* **75** (1995) 4724–4727, [arXiv:hep-th/9510017](#).
- [167] N. T. Jones, H. Stoica, and S. H. H. Tye, “The production, spectrum and evolution of cosmic strings in brane inflation,” *Phys. Lett.* **B563** (2003) 6–14, [arXiv:hep-th/0303269](#).
- [168] A. H. Guth, “The Inflationary Universe: A Possible Solution to the Horizon and Flatness Problems,” *Phys. Rev.* **D23** (1981) 347–356.
- [169] A. D. Linde, “A New Inflationary Universe Scenario: A Possible Solution of the Horizon, Flatness, Homogeneity, Isotropy and Primordial Monopole Problems,” *Phys. Lett.* **B108** (1982) 389–393.

- [170] N. T. Jones, H. Stoica, and S. H. H. Tye, “Brane interaction as the origin of inflation,” *JHEP* **07** (2002) 051, [arXiv:hep-th/0203163](#).
- [171] G. Shiu, S. H. H. Tye, and I. Wasserman, “Rolling tachyon in brane world cosmology from superstring field theory,” *Phys. Rev.* **D67** (2003) 083517, [arXiv:hep-th/0207119](#).
- [172] G. Dvali and A. Vilenkin, “Formation and evolution of cosmic D-strings,” *JCAP* **0403** (2004) 010, [arXiv:hep-th/0312007](#).
- [173] S. Sarangi and S. H. H. Tye, “Cosmic string production towards the end of brane inflation,” *Phys. Lett.* **B536** (2002) 185–192, [arXiv:hep-th/0204074](#).
- [174] A. Avgoustidis and E. P. S. Shellard, “Cosmic string evolution in higher dimensions,” *Phys. Rev.* **D71** (2005) 123513, [arXiv:hep-ph/0410349](#).
- [175] E. J. Copeland, R. C. Myers, and J. Polchinski, “Cosmic F- and D-strings,” *JHEP* **06** (2004) 013, [arXiv:hep-th/0312067](#).
- [176] A. Avgoustidis and E. P. S. Shellard, “Effect of Reconnection Probability on Cosmic (Super)string Network Density,” *Phys. Rev.* **D73** (2006) 041301, [arXiv:astro-ph/0512582](#).
- [177] D. B. DeLaney and R. W. Brown, “A Product Representation For The Harmonic Series Of A Unit Vector: A String Application,” *Phys. Rev. Lett.* **63** (1989) 474.
- [178] A. Avgoustidis, “Cosmic String Dynamics and Evolution in Warped Spacetime,” *Phys. Rev.* **D78** (2008) 023501, [arXiv:0712.3224 \[hep-th\]](#).
- [179] X. Siemens, J. Creighton, I. Maor, S. Majumdar, K. Cannon, and J. Read, “Gravitational wave bursts from cosmic (super)strings: Quantitative analysis and constraints,” *Phys. Rev.* **D73** (2006) 105001, [arXiv:gr-qc/0603115](#).
- [180] X. Siemens, V. Mandic, and J. Creighton, “Gravitational wave stochastic background from cosmic (super)strings,” *Phys. Rev. Lett.* **98** (2007) 111101, [arXiv:astro-ph/0610920](#).
- [181] N. K. Nielsen, “Dimensional Reduction And Classical Strings,” *Nucl. Phys.* **B167** (1980) 249.
- [182] N. K. Nielsen and P. Olesen, “Dynamical Properties Of Superconducting Cosmic Strings,” *Nucl. Phys.* **B291** (1987) 829.
- [183] J. J. Blanco-Pillado, K. D. Olum, and A. Vilenkin, “Dynamics of superconducting strings with chiral currents,” *Phys. Rev.* **D63** (2001) 103513, [arXiv:astro-ph/0004410](#).
- [184] E. Witten, “Superconducting Strings,” *Nucl. Phys.* **B249** (1985) 557–592.

-
- [185] J. J. Blanco-Pillado and K. D. Olum, “Electromagnetic radiation from superconducting string cusps,” *Nucl. Phys.* **B599** (2001) 435–445, [arXiv:astro-ph/0008297](#).
- [186] I. Moss and S. J. Poletti, “The Gravitational Field Of A Superconducting Cosmic String,” *Phys. Lett.* **B199** (1987) 34–36.
- [187] M. N. Butler, R. A. Malaney, and M. B. Mijic, “On The Evolution Of A Superconducting Cosmic String Network,” *Phys. Rev.* **D43** (1991) 2535–2541.
- [188] K. Dimopoulos and A.-C. Davis, “Cosmological consequences of superconducting string networks,” *Phys. Lett.* **B446** (1999) 238–246, [arXiv:hep-ph/9901250](#).
- [189] P. Laguna and R. A. Matzner, “Numerical simulation of bosonic superconducting string interactions,” *Phys. Rev.* **D41** (1990) 1751–1763.
- [190] D. Garfinkle and T. Vachaspati, “Radiation From Kinky, Cuspless Cosmic Loops,” *Phys. Rev.* **D36** (1987) 2229.
- [191] D. Garfinkle and T. Vachaspati, “Fields Due To Kinky, Cuspless, Cosmic Loops,” *Phys. Rev.* **D37** (1988) 257–262.
- [192] B. Allen and R. R. Caldwell, “Generation of structure on a cosmic string network,” *Phys. Rev. Lett.* **65** (1990) 1705–1708.
- [193] B. Allen and R. R. Caldwell, “Small scale structure on a cosmic string network,” *Phys. Rev.* **D43** (1991) 3173–3187.
- [194] A. C. Thompson, “Dynamics of Cosmic String,” *Phys. Rev.* **D37** (1988) 283–297.
- [195] S. Olmez, V. Mandic, and X. Siemens, “Gravitational-Wave Stochastic Background from Kinks and Cusps on Cosmic Strings,” *Phys. Rev.* **D81** (2010) 104028, [arXiv:1004.0890 \[astro-ph.CO\]](#).